A Study of the Static and Dynamic Properties of Al-Based Al_2O_3 Metal Matrix Composites

BY

SYED HAFEEZ

A Thesis Presented to the

DEANSHIP OF GRADUATE STUDIES

KING FAHD UNIVERSITY OF PETROLEUM & MINERALS

DHAHRAN, SAUDI ARABIA

In Partial Fulfillment of the
Requirements for the Degree of

MASTER OF SCIENCE

In

MECHANICAL ENGINEERING

MAY 2005

KING FAHD UNIVERSITY OF PETROLEUM AND MINERALS
DHAHRAN 31261, SAUDI ARABIA

DEANSHIP OF GRADUATE STUDIES

This thesis, written by **SYED HAFEEZ** under the direction of his Thesis Advisor and approved by his Thesis Committee, has been presented to and accepted by the Dean of Graduate Studies, in partial fulfillment of the requirements for the degree of **MASTER OF SCIENCE IN MECHANICAL ENGINEERING.**

Thesis Committee

Dr. Khalid A Al-Dheylan (Advisor)

Dr. Zafarullah Khan (Member)

Dr. Amro Al-Qutub (Member)

Dr.Faleh Al-.Sulaiman
Department Chairman

Dr. Mohammad A Al-Ohali
Dean of Graduate Studies

Date
4-9-2005

عمادة الدراسات العليا
DEANSHIP OF GRADUATE STUDIES

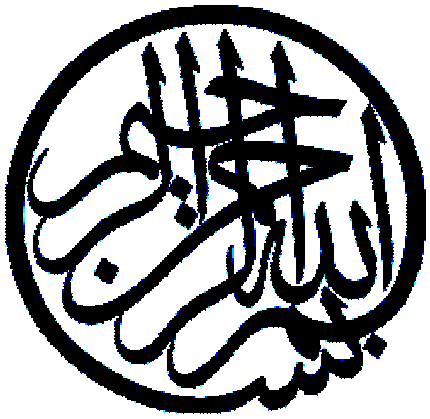

In the Name of Allah, Most Gracious, Most Merciful.

Dedicated to My Beloved Parents, Family Members and Friends whose constant prayers, sacrifice and inspiration led to this wonderful accomplishment

ACKNOWLEDGEMENTS

All praises and thanks are due to Allah (subhana wa taala) for bestowing me with health, knowledge and patience to complete this work. Thereafter, acknowledgement is due to KFUPM for the support given to this research through its tremendous facilities and for granting me the opportunity to pursue graduate studies with financial support.

I acknowledge, with deep gratitude and appreciation, the inspiration, encouragement, valuable time and guidance given to me by my Committee Chairman, Dr. Khaled A.Al-Dheylan. I greatly appreciate dedication, attention and patience provided by him throughout the course of this study.

I am grateful to my Committee members, Dr. Amro Al-Qutub and Dr.Zafarullah Khan for their constructive guidance and technical support. Thanks are due to the laboratory personnel, Mr. Zain, Mr.Hashmi and Mr.Saleh who assisted me in the experimental work and the Department secretaries, Mr. Lateef and Mr.Jameel for their help and assistance.

I owe very deep appreciations to Dr. Anwar Khaleel Shaikh, Director ME workshop and other staff of the ME workshop for their prompt and timely help and technical advice in specimen preparation.

Special thanks are due to my senior colleagues at the University, Mujtaba Hussain, Salman A Gaffar, Abdul Baseer, Mohammad Ahsan, Farrukh Saghir, Ifthekar who were always there to help me in my work. I would also like to thank my friends, Basha, Sami, Baba, Riyaz, Anees, Hameed, Qaiyum, Abbas, Mujahed, Farooq, kashif, Baqtiar, Yousuf, Fareed, Khaleel, Khaliq, Shafeeq, Faheem, Shujath, Gayaz, Shafi, Faisal, Baber, Awes, Atif, Saad, Hasan, Bilal, Khaled, Turki and all others who provided wonderful company and good memories that will last a life time.

Last but not the least I am grateful to my parents, sisters and friends for their extreme moral support, encouragement and patience during the course of my studies at KFUPM as well as throughout my academic career. No personal development can ever take place without the proper guidance of parents. This work is dedicated to my parents for their constant prayers and never ending love.

TABLE OF CONTENTS

LIST OF TABLES

LIST OF FIGURES

THESIS ABSTRACT

NAME:	**SYED HAFEEZ**
TITLE:	**A STUDY OF THE STATIC AND DYNAMIC PROPERTIES OF Al BASED $Al_2 0_3$ METAL MATRIX COMPOSITES.**
DEPARTMENT:	**MECHANICAL ENGINEERING**
DATE:	**24 MAY 2005**

A particle reinforced metal matrix composite (PRMMC) consists of uniformly distributed ceramic particles (approximately of equiaxed geometries) within a metal matrix. Recently, extensive research has been carried out on PRMMC composites with particles size greater than 1 μm; few researchers investigated PRMMC composites with reinforced particles less than 1μm.

The main objective of this study is to determine the strengthening mechanisms of Al-based Al_20_3 metal matrix composites under both static and dynamic loadings. Several samples of these composites with volume contents of 10, 20, and 30 % Al_20_3 were tested and studied. Low-velocity impact test results were compared with the outcome of a finite element model. In order to understand experimentally the influence of Al_20_3 particle clustering on the deformation characteristics and. microstructural effects on the ductility and fracture properties of these composites. The fracture surfaces of tested samples were examined under SEM

The tensile strength and elastic modulus of the composite materials studied increases with increasing volume fraction of the particle reinforcement. Comparison of strengths under tensile (static), flexural (static) and low–velocity impact test loadings was undertaken. There is significant decrease in flexural strength, fracture toughness and fracture impact energy with increasing volume fraction (v_f) of the particle reinforcement. SEM analyses of the fracture surfaces under static tests revealed the main fracture mechanism was due to void nucleation, growth and linking. Stress concentration and triaxial stress state were found to enhance fracture. In low-velocity impact tests, the impact force enlarges the void, which in turn causes fracture rapidly. Low-velocity impact test results were compared with the outcome of a finite element model. Percent error between the low–velocity impact test results and finite element numerical values for Al-based Al_2O_3 PRMMC composites increases with increasing volume fraction of the particle reinforcement.

MASTER OF SCIENCE DEGREE

KING FAHD UNIVERSITY OF PETROLEUM AND MINERALS

Dhahran, Saudi Arabia

ا خلاصة الرسالة

الاسم : **سيد حفيظ**

العنوان: **دراسة الخواص الاستاتيكية و الديناميكية للعنصر الأساسي للألمونيوم (Al_2O_3) مادة المركبات المعدنية**

القسم : **الهندسة الميكانيكية**

التاريخ: **24 مايو 2005م**

الجزء المقوي مادة المركبات المعدنية (PRMMC) تتألف من أجزاء السيراميك المنتظمة الموزعة داخل مادة المعدن. حديثا, عملت بحوث واسعة على مركبات (PRMMC) المواد المقوية ذو أجزاء بمقاسات أكبر من 1 من مليون جزء من المتر; كما قام قليل من الباحثين بدراسة مركبات (PRMMC) ذو أجزاء مقوية بمقاسات أقل من 1 من مليون جزء من المتر.

الهدف الأساسي من هذه الدراسة هو تحديد آلية القوة للعنصر الأساسي لمادة الألمونيوم (Al_2O_3) كأساس للمركبات المعدنية تحت حمولات ساكنة وفعالة. تم اختبار و دراسة العديد من العينات من هذه المركبات التي تحتوي على حجم 10, 20 و 30 % Al_2O_3. لقد قورنت نتائج اختبار التصادم قليل السرعة مع نتيجة مخطط العنصر المحدد (FEM) النظرية. كل هذا لفهم تأثير الجزء المتجمع Al_2O_3 المختبر على خاصية التشويه و تأثير البنية المجهرية على الليونة وخواص انكسار هذه المركبات. لقد تم اختبار عينات السطح المكسور تحت جهاز فحص العينات (SEM) الالكتروني.

قوة التأثير و عامل المرونة لمواد المركب المدروسة تزيد مع تزايد حجم الجزء الكسري من الجزء المقوي. لقد أخذت في الاعتبار مقارنة القوى تحت اختبار التوتر (الساكن), اختبار الثني (الساكن) واختبار حمولة التصادم قليل السرعة. لقد وجد انخفاض هام في قوة الثني, قساوة الانكسار و طاقة انكسار التصادم مع زيادة حجم الجزء الكسري (v_f) من الجزء المقوي. اظهر تحليل عينات السطح المكسور للاختبارات الساكنة تحت جهاز فحص العينات (SEM) بأن آلية الانكسار الأساسي هو بسبب فراغ النواة, التطور والارتباط. لقد وجد أن تركيز الاجتهاد و حالة إجهاد ثلاثي الأبعاد تزيد الانكسار. في اختبار التصادم قليل السرعة, قوة التصادم تكبر الفراغ الذي بالتالي تؤثر على سرعة الانكسار. لقد قورنت نتائج اختبار التصادم قليل السرعة مع نتائج مخطط العنصر المحدد (FEM). يزيد الخطأ جزء من المائة بين نتائج اختبار التصادم قليل السرعة وقيم مخطط العنصر المحدد للعنصر الأساسي للألمونيوم(Al_2O_3) مادة المركبات مع زيادة حجم الجزء الكسري من الجزء المقوي.

هذه الدراسة أعدت لنيل درجة الماجستير في العلوم
جامعة الملك فهد للبترول والمعادن
الظهران - المملكة العربية السعودية

CHAPTER 1

INTRODUCTION

1.1 METAL MATRIX COMPOSITES

A composite is a material that is produced via a physical combination of materials to obtain a new material with unique properties when compared to the monolithic material properties. This definition distinguishes a composite from other multiphase materials, which are produced by bulk processes where one or more phases result from phase transformation ("in-situ" composites).

Reinforcement of a ductile, tough metal with a ceramic material should result in improvement in properties. Composite materials have been of interest to aerospace and defense markets for many decades as they sought to obtain continuous performance improvements. In the 1970s and 1980s, metal matrix composites (MMC) were the focus of substantial attention due to the availability and individual properties of the matrix alloys such as Al and Ti. Ceramics were the reinforcements of choice, since they provide the largest increase in strength and stiffness.

Composites are classified by: (1) their matrix (either polymer, ceramic, or metal), (2) their reinforcement, which includes the chemical nature (oxides, carbides, nitrides), shape (continuous fibers, short fibers, whiskers, particulates), and orientation, (3) their

processing routes. MMCs are composite materials in which one constituent is a metal, forming at least one percolating networks, the other constituent is embedded in this metal matrix and usually serves as the reinforcement. The terms *matrix* and *reinforcement* are often used. The matrix is a percolating "soft" phase (with in general has excellent ductility, formability and thermal conductivity) in which are embedded the "hard" reinforcements (high stiffness and low thermal expansion). The reinforcements can be continuous or discontinuous, aligned, or random.

MMCs are rising as a vital class of materials in the continuing search for improved strength, and stiffness in addition to other desirable properties, which make them competitive compared to monolithic metals [1]. The specific properties obtained in MMCs will depend upon the exact matrix alloy and ceramic selection, the form, size and percentage of the ceramic added, ceramic properties, interface properties and the processing method selected to produce the composite [2-4]. MMC is normally fabricated using a ductile metal (e.g. Al, titanium and nickel) as the matrix, ceramic as the reinforcement (e.g. alumina, SiC, and graphite), which combines the good ductility and toughness of the metal matrix with the high strength, hardness, and elastic modulus of the ceramic reinforcement [5-9].

Most of the related MMC research is aluminum based MMC with ceramic as the reinforcement. Aluminum alloys are chosen because of their low density, wide alloy range, heat treatment capability and processing flexibility. Moreover Al based MMCs offers advantage of lower cost over most other MMCs and has excellent thermal conductivity, high shear strength, nonflammability, and ability to be formed, compared to the unreinforced Al alloys [10-13]. The ceramic reinforcement materials, such as SiC,

B4C, nitrides, and Al_20_3 are in the form of continuous fibers, whiskers, platelets, or particles.

1.2 TYPES OF REINFORCEMENT

Continuous reinforcement: In a continuous fiber reinforced composites the fibres are cylindrical ingredient material produced continuously to form an essentially endless reinforcement in the composite, which is usually delivered on the form of multifilament tows. Each tow consists of many individual fibers of diameters typically in the range of 3 to 30 microns.

Discontinuous reinforcement: a non-percolating constituent of a composite, taking the form of individual elements embedded in the matrix constituent (e.g., particulates, short fibres, whiskers). Preforms produced from discontinuous reinforcements that are mechanically stabilized by a binder or by cold compaction are still considered discontinuous reinforcements. Other reinforcements are known as particulates, roughly equiaxed reinforcement or composite ingredient, usually of aspect less than about 5. Particulates can be either mono- or polycrystalline, can take various geometrical shapes and are typically greater than 1 μm in diameter. Dispersoids are the same as particulates, except that the diameter is less than 1μm, hence, being capable of providing Orowan strengthening. In particle reinforced MMC (PRMMC) composites the particle reinforcement occupies a volume fraction greater than 5% in the material. Where in dispersoid reinforced MMC the dispersoid reinforcement occupies a volume fraction greater than 5% and the distance between particles are less than 1 μm (otherwise, the material is considered to be a dispersion strengthened metal). The other discontinuous reinforcements are the platelet, short fibres, and whiskers.

1.3 CATEGORIES OF MMC

Particle reinforced metal matrix composites (PRMMC) are materials where reinforcement occupies a volume fraction greater than 5% in the material.

The other categories are short fiber reinforced MMC with short fiber as the reinforcement, whereas whisker-reinforced MMC has whisker as the reinforcement. Other forms of MMC include continuous fiber reinforced MMC with reinforcement of continuous fibers.

- **Particle reinforced metal matrix composites**

A particle reinforced metal matrix composite consists of a uniform distribution of strengthening ceramic particles embedded within a metal matrix. These differ from composites containing higher aspect ratio reinforcements significantly. The range of particles reinforcement volume fractions can vary significantly, with commercial products containing 5-75% reinforcement by volume. Even the materials in which the metal matrix is the minor phase on a volume basis are included in the class of materials known as PRMMC composites, since they maintain metallic properties.

PRMMC composites have been under development for more than 30 years and were commercially available in significant quantities for the last decade. In that time, substantial progress has been made on many fronts, most notably in composites with aluminum as the matrix metal. The primary driving force for research and development of PRMMC composites was the need to produce a material with these desirable features characteristic of MMCs without paying the high price of fibers, monofilaments, or whiskers that can be used as reinforcement for a metal. PRMMC composites are produced by a variety of methods, including both solid and liquid state processes.

Much research has been carried out on PRMMC composites due to the combination of high strength to weight ratio, high stiffness, isotropic properties, and the ability to be formed by conventional metal processing techniques, such as rolling, forging, or extrusion [14-18].

In addition, superior engineering properties and low cost raw materials, make PRMMC a candidate for a wide range of performance-driven, and price sensitive applications. However, these improvements have been accompanied by degradation in tensile ductility and toughness compared with conventional Al alloys [3, 7, 18-21].

1.4 OBJECTIVES OF THE STUDY

As have been mentioned, PRMMC materials exhibit higher strength and stiffness, in addition to isotropic behavior at a lower density, when compared to the unreinforced matrix material. PRMMC composites benefit from the ceramic's ability to withstand high velocity impacts and the high toughness from the metal matrix, which helps in preventing total shattering. These factors lead to an excellent balance between cost and mechanical properties, which are appealing for many industrial applications. From the mechanical behavior standpoint, the main drawback of these materials is their low ductility, which is limited by the nucleation, growth, and coalescence of voids created by the ceramic reinforcements; this of course has hindered their use in structural applications. The above factors have acted as the driving force to study the damage and failure processes in PRMMC composites. The mechanical behavior of many materials is quite different under static and dynamic loading. The strength data, which are the main technological requirement, are separated into tension, compression, bend with stiffness

moduli etc. These mechanical properties are helpful in assessing the damage tolerance capability.

The main contribution to the strengthening of PRMMC composites is particle addition; it affects most of the mechanical properties of PRMMC composites. Several particle parameters, which might affect the mechanical properties of PRMMC composites, include volume fraction, size, shape, and distribution of the reinforced particles within the metal matrix. The most important among these parameters is the volume fraction [4]. Consequently, there is a need to determine the effects of volume fraction on the mechanical properties of PRMMC composites.

The main objective of this work is to study the strengthening mechanisms of Al based Al_20_3 metal matrix composites under both static and dynamic loadings. Several samples of these composites with contents of 10, 20, and 30 % volume fractions (v_f) Al_20_3 were tested. Static tensile and flexural strengths, and fracture toughness (K_{Ic}) were determined Low-velocity impact tests were also conducted. To validate Low-velocity impact test results of PRMMC composites a numerical technique was attempted for this study. A finite element model (FEM) was designed and processed to simulate the low-velocity impact tests, using the finite element code ANSYS. Test results were then compared with the outcome of the numerical FEM model.

CHAPTER 2

LITERATURE REVIEW

McDanels [3] evaluated the mechanical properties and stress-strain behavior for several types of discontinuous SiC/Al composites, containing SiC-whiskers, nodules and particulate reinforcement. He studied the effects of type of reinforcement, matrix alloy, and reinforcement content by analyzing the stress-strain curves. The elastic modulus of the composites was found to be isotropic, and independent of type of reinforcement and matrix alloy; it depends only on the vol. % of SiC reinforcement and there was 50-100% increase over the modulus of unreinforced Al alloy as shown in Fig. 2.1. Yield/Ultimate tensile strengths were controlled mainly by matrix alloy, temper conditions and by reinforcement content. The yield and tensile strengths showed 60% increase over those of unreinforced Al alloy. Ductility was dependent upon percent reinforcement and matrix alloy. It increased with increased homogeneity in particle distribution.

Ibrahim et al. [4] reviewed large body of literature in the field of PRMMC composites and presents crossection of views with particular emphasis on strengthening mechanisms under static and dynamic loadings. They observed modulus of elasticity is affected by reinforcement content and increases with an increase in volume fraction of reinforcement.

Aghajanian et al. [22] studied static properties along with thermal resistance of

four Al_20_3-Al composites and durafrax 1542, (a dense sintered Al_20_3 available commercially). All four composites studied were fabricated by directly oxidizing molten Al alloys. Two materials were oxidized in air at 1400K, one is fully oxidized and other partially. Similarly the other two materials were prepared at 1600K. He observed that new composites are stronger in flexure, tougher and more resistant to thermal shocks.

David [23] conducted the tensile and fracture toughness tests on 2014 Al alloy/SiC composite consisting of 15 vol. % SiC particulates. Overall tensile elongations values ranged from 1.6 to 2.4% and fracture toughness values from 18.7 to 29.5 MPa. He observed that tensile ductility and fracture toughness were controlled by two factors namely; deformation characteristics of the matrix and SiC particles distribution. He discovered that the best method for increasing fracture toughness of composites is dispersing uniformly the particles and by increasing ductility of matrix

Vincent et al. [24] fabricated two different types of composites. The approach, referred to as microstructurally toughened composites, consists of segregating the composite into particle-reinforced regions and continuous ductile toughening regions. Composites consisting of SiC particle-reinforced 6061 Al (SiCp/6061) with monolithic 6061 and pure titanium toughening regions were fabricated. He observed the longitudinal tensile properties are same for both types of composites while impact energy for both 10 to 20 times greater than a conventional SiC particle reinforced 6061 Al composite. The titanium toughened composite displaced high transverse tensile strength than 6061 Al toughened composite.

Manoharan and Kamat [25] related the micromechanical event like particle cracking, interface failure, near interface failure to macroscopic fracture properties. He

observed that the damage was nucleated at the ceramic reinforcement then void nucleates which grows and becomes a microcrack. They stated, when a microcrack-macrocrack distance reaches a specific characteristic fracture distance link up occurs by ductile failure of the matrix.

Paul [26] done extensive study on the properties of discontinuous reinforced aluminum (DRA) composites produced by powder metallurgy processing. Fig. 2.2 shows the variation of proportional limit (S_o), yield strength (YS), ultimate tensile strength (UTS) with the vol. % of SiC particles from 15 to 25%. An increase in volume fraction of SiC particles from 15 to 25% produces increase in S_o, UTS, YS. Fig. 2.3 shows Proportional limit, YS, UTS vs particle size, there is increase in these properties with the reduction in particle size except in the range 2 μm to 0.7 μm, where proportional limit decreases. Fig. 2.4 shows Elastic modulus (E) vs vol. % of SiC where E increases as vol. % of SiC increases. He found that there is no change in ductility as the particle size reduces from 10μm to 2 μm only after 0.7 μm does the ductility decreases drastically. He indicated that strength and ductility increased effectively by reducing particle size than by increasing volume fraction. He observed that in DRA composites ductility is an index of cavitations resistance and toughness is an index of coalescence resistance, no exact correlation between ductility and toughness exists.

Zhiru and Ruby [27] studied mechanical properties of 15% SiC particle / A356 with size ranging from 5-10μm and with differing aspect ratio of individual particles, the composite found to have high YS, E, but UTS and ductility were lower than that of pure alloy. The YS and E was 24%, 28% higher than there corresponding YS and E of A356 alloy. The UTS and ductility was 7%, 98% lower than their corresponding UTS and duct-

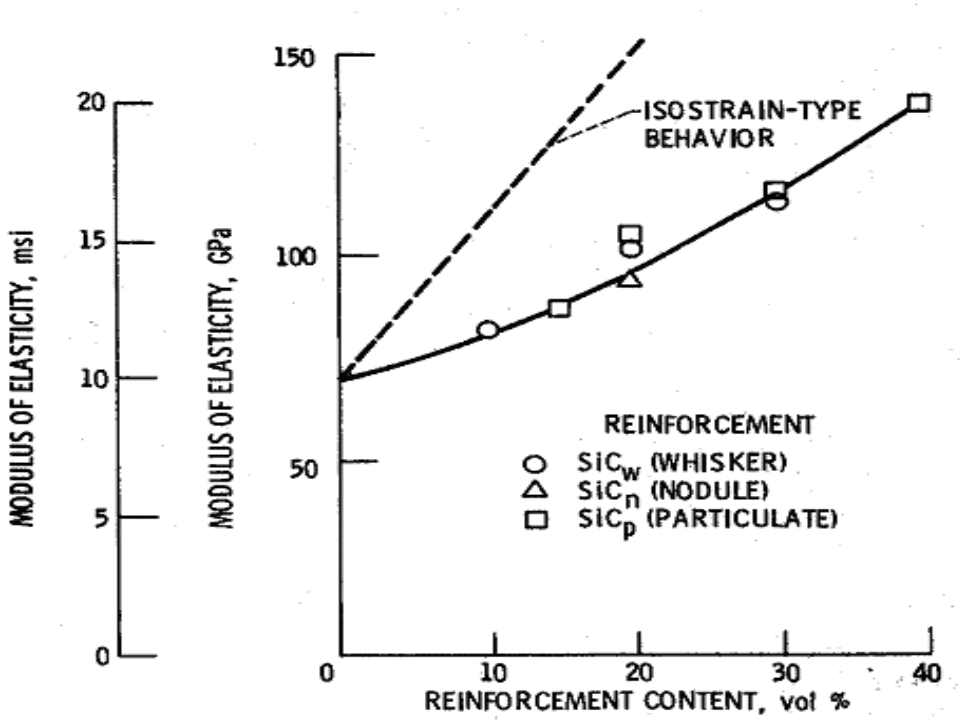

Fig.2.1: Effect of reinforcement content on modulus of elasticity of discontinuous SiC/6061 Al composites [3].

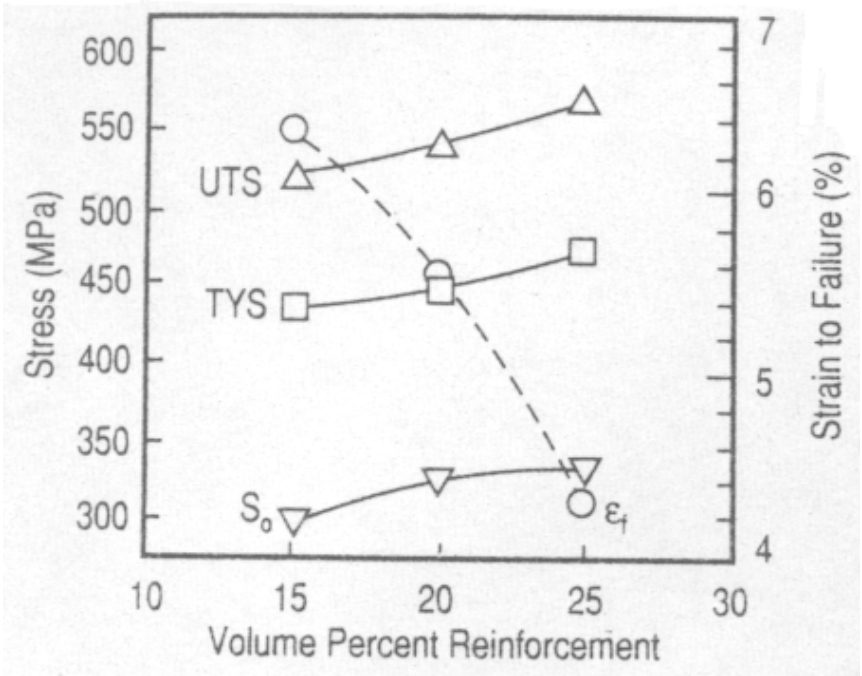

Fig. 2.2: The ultimate tensile strength (UTS), Tensile Yield strength (TYS) proportional limit (S_o) and strain to failure (ε_f) vs. the vol. % reinforcement for 6013/SiC/XXp-T6 DRA composites [26].

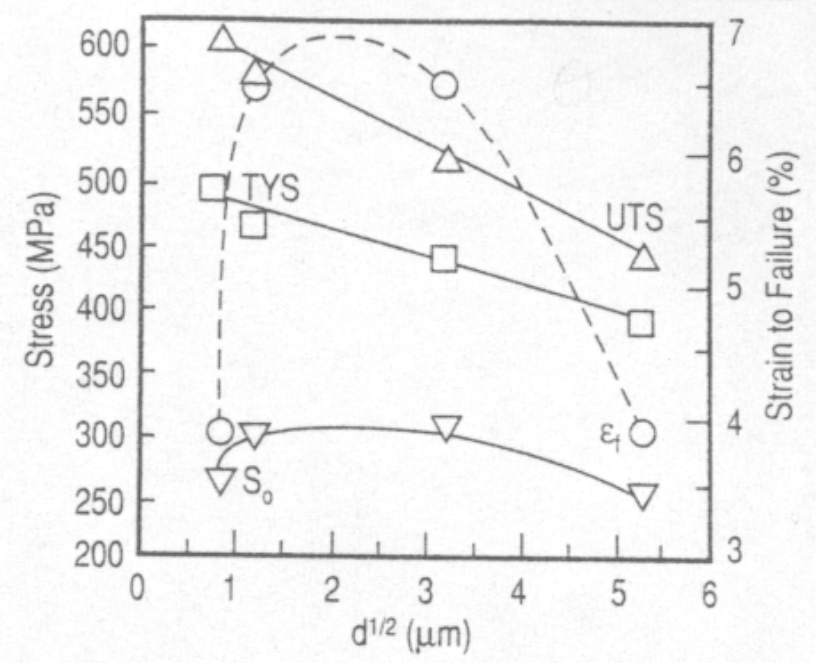

Fig. 2.3: The UTS, TYS, S_o and ε_f vs. the square root of median reinforcement particle diameter (d) for 6013/SiC/20p-T6 DRA composites [26].

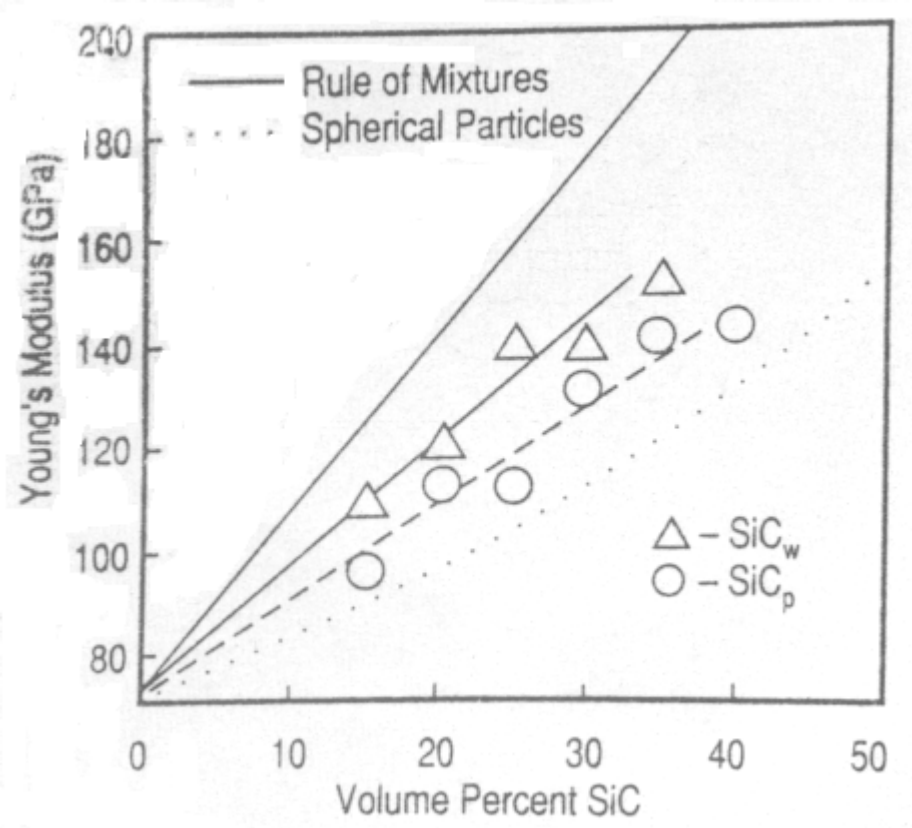

Fig. 2.4: Young's modulus vs. vol. % of SiC_w and SiC_p reinforcement [26].

ility of A356 alloy. The particle distribution found to be affecting strengthening mechanism. He observed that non-uniform particle distribution due to clustering, dentric structure results in stress triaxiality and internal stress which results for special hardening behavior and also earlier particle cracking, void formation and particle interface debonding. This behavior gives rise to less ductility.

Mummery and derby [28] studied fracture processes in a pure Al matrix reinforced with SiC particles of 3 particles sizes (3, 10, 30 μm) and two volume fractions (5, 20%) by conducting tensile tests. He found there is increase in YS, UTS and E as the volume fraction increases but strain to decreases for a given particle size. Fracture found to occur by ductile rupture mechanism. In low volume fraction for a given particle size strain to failure was increased due to increase in void growth strain. Also in low volume fraction large particle PRMMC composites there was increase strain to failure because of hindrance to void elongation caused by increased local constraint around fractured particles. On increasing particle size and/or volume fracture there was transition in fracture mechanism, the fracture mechanism changes from decohesion to particle cracking.

Kim et al. [29] observed that fracture toughness of 6061 Al/SiCp composite decreases from 0.08 to 0.065% as volume fraction increases from 5% to 30%.

Bhattacharya et al. [30] studied the influence of alumina microspheres on mechanical characteristics of an aluminum alloy AA6061 reinforced with alumina microspheres. The reinforcing particles have an average diameter of 20μm and a 25% volume fraction. He observed structure of reinforcing particles influences the material behavior by initiating the fracture. He reported that MMC is stiffer and stronger than

6061 Al alloy, 10% stronger in yield and 25% stiffer. But toughness under impact is poor and energy absorption capacity is only 14% of 6061 Al alloy. He concluded that microsphere is porous and accounted for initiating fracture in composite and also with low decohosive rupture strength. They limit the strength of the material.

Chia et al. [31] investigated the effects of strain rate on the tensile properties of 0%, 10%, 15% and 20% v_f Al_20_3 reinforced 6061 Al alloy composite. He found that composite is more sensitive to strain rate than the unreinforced material and composite has less ductility than Al alloy irrespective of strain rate.

Luster et al. [2] tested 6061/ Al_20_3 composite with volume fraction of 0, 10, and 20 % to find its mechanical properties. The average size of 10 vol. % and 20 vol. % of Al_20_3 in 6061 Al composite is 10 and 20 μm respectively. He carried out tensile test, creep resistance, fatigue tests. The 0.2% YS, stiffness and hardness increased with volume fraction by corresponding decrease in ductility. The increase in YS is 31% for the 10% v_f Al_20_3 composite and 41% for the 20% v_f Al_20_3 composite, compared to a 6061 Al alloy. The increase in E is 22% for the 10% v_f Al_20_3 composite and 36% for the 20% v_f Al_20_3 composite, compared to a 6061 Al alloy. The decrease in ductility is 42% for the 10% v_f Al_20_3 composite and 75% for the 20% v_f Al_20_3 composite, compared to a 6061 Al alloy.

Pestes et al. [32] studied the effect of particle size from 3-165 μm on the fracture toughness of Al-4mg/Al_20_3 PRMMC with volume fraction ranging from 45-54%. Fracture toughness found to be dependent on interparticle spacing provided that particles are below a critical size. Increasing interparticle spacing can increase the toughness either by decreasing volume fraction of particulates or increasing size of the particles.

Kamat et al. [33] performed tension, fracture toughness tests on 2014-O and 2024-O Al alloy reinforced with Al_20_3 having 2 to 20 % volume fraction with different particle sizes. He observed that yield strength increases with decrease in spacing between particles. The fracture toughness increases with increasing spacing between particles provided that the particle size should be less than 15 μm. Fractured occurred by local ductile mechanism, even though microscopically they exhibited limited ductility.

Manoharan and lewandowski [34] studied fracture properties of Al-Si-mg/Si MMC by varying volume fraction and matrix flow properties keeping particle size constant. J_{Ic} found decreasing linearly with an increase in volume fraction of Si particles. Fracture found to occur by fracturing of Si particles ahead of the crack tip, fracture link-up in the matrix.

Hadianford et al. [35] studied fracture toughness of 6061 Al reinforced with 20 % angular particulates. Fracture toughness tests were conducted on compact tension peak-aged specimens and it was 22.8 MPa√m. The dominant fracture mechanism was particle fracture. This particles act as void initiation sites, these voids coalescence and then final fracture occurs. He observed that the smaller particles are less susceptible to fracture than long and elongated particles; hence particle size reduction results in improved toughness.

Park et al. [11] examined the toughness and fracture behavior of 6061 Al alloy reinforced by 20μm of 20 vol. % of polycrystalline microspheres of alumina (COMRAL 85 ^{TM}). Due to reinforcement stiffness increases by 30 % and strength by 10 %. The fracture toughness was reduced with values from 16.7 to 20.4 $MPam^{1/2}$ about one half of the unreinforced alloy. The fracture found to occur by ceramic failure subsequently ductile failure of matrix ligaments.

Hadianford et al. [36] compared fracture toughness values of four 6061 Al reinforced alumina particles. Precracked compact tension and chevron notched short rod. These four reinforced composites were with 10, 15, 20 vol. %, 20 % angular particulate alumina and 20 vol. % Comral-85 alumina microspheres. The average size of particles in 10%, 20% and comral-85 composites were 14.3, 18.7, 17.5 μm respectively. Fracture toughness values obtained from the two sample geometries was in good agreement and he observed that fracture toughness decreases with the increase in volume fraction of reinforcement from 10 to 20%. Fracture toughness values for unreinforced Al alloys are in the range of 25 to 75 $MPam^{1/2}$, whereas reinforced Al matrix are in the range of 7 to 25 $MPam^{1/2}$. 20 vol % angular particulate alumina has 10 to 20% higher toughness than 20% reinforced Comral-85.

Lloyd [10] reviewed large body of literature and he observed that the percent elongation (Fig. 2.5) and fracture toughness decreases with increase in vol. % of reinforcement. The reduction in fracture toughness is most significant from 0-10% and then slightly from higher vol. %. There are many factors like particle distribution, reinforcement inhomogeneity, and residual stress in composite influencing the fracture toughness. The main factor controlling the elastic modulus is the volume fraction of reinforced particles.

Zulfikar et al. [37] carried out finite element simulation to determine the effect of the presence of single particles and particle clusters on the stress distribution at the crack tip. The crack opening stress at the crack tip found to increase due to the presence of particles far away from the crack tip but it decrease as the crack approaches the particles. The plastic deformation in the particles cluster suppressed by cluster of particles and

occurs outside the cluster. In the particles away from crack tip high interface shear stress and vonmises stresses are created due particle clustering whereas highest normal stress region exists at the interface of particles along the crack line. Therefore crack can go around the cluster region or go through cluster region depending upon the stress that predominates.

Sriram et al. [38] undertook the study to evaluate the influence of Al_20_3 particulates on fracture behavior of 6061 Al alloy reinforced with 10% v_f Al_20_3 PRMMC composites. The E and YS of the composite was 13% and 20% more than their corresponding YS and E of unreinforced 6061 Al alloy. Fractography revealed macroscopically brittle appearance whereas microscopically local ductile and brittle mechanisms. Failure of the composite was found to occur by reinforcement cracking and particle-matrix decohesion at the interface.

Srivatsan [39] studied the fracture behavior of 2014 Al alloy reinforced with two different volume fractions of 10 and 15% Al_20_3 in order to understand the affects of reinforcement on microstructure, tensile and quasistatic fracture behavior. He observed that the elastic modulus in 10 and 15 vol. % composites was respectively 10 and 45% more than that of the unreinforced alloy. The tensile strength in the 15 vol. % composite was found to be 2% more than that of the 10 vol. % composite. The tensile fracture surface shows brittle appearance on macroscopic scale and microscopically local ductile and brittle fracture. Fracture of the particles with failure of matrix between particles and decohesion found to occur.

Shi et al. [40] and Song et al. [41] studied the effect of the particulate shape on fracture and ductility of the composite. The composite under study consist of spherical

and angular particulate of 20% v_f Al_20_3 reinforced 6061 Al alloy with 5µm particles size. He observed that spherical particle reinforced composite exhibits lower YS and work hardening rate but a higher ductility compared to angular particle reinforced composite.

Watt [42] created a 3D FEM model to find the effect of particle shape, volume fraction and distribution on stress and strain distributions around and within particles in matrix, which deforming plastically which aimed to find the effect of particle shape, volume fraction, size and particle distribution on ductility of Al/SiCp MMC. He observed that spherically reinforced particles have much less stress. Closely spaced particles develop very large stresses in loading direction. He said spherically reinforced particles have good ductility and large particle should distribute evenly.

Brent et al. [43] conducted flexural, fracture toughness and charpy impact tests on four Al alloys namely, 520, 201, 295, 2214 alloy and each alloy is reinforced with three ceramic powders namely, abrasive grade Al_20_3, high purity Al_20_3 and SiC with 55% volume fraction. It was found that composite reinforced with alumina were stronger and tougher than SiC reinforced composites.

Bonollo et al. [44] studied mechanical and impact behavior of AA6061 reinforced by 20% Al_20_3 of 15µm size and AA 2014 reinforced by 17% Al_20_3 of 15µm particle size. He observed testing temperature and loading speed has a limited influence on the failure mechanism. The presences of particles lower the crack nucleation energies with respect to unreinforced alloy and impact strength is less compared to unreinforced alloy. For AA6061 reinforced by 20% Al_20_3 composite the decrease in impact strength was 91.4% compared to AA6061 whereas for AA 2014 reinforced by 17% Al_20_3 composite it was 80% compared to AA2014.

Davis et al. [45] studied strengthening mechanism by considering the effect of particle size and volume fraction on mechanical properties of 2080 Al reinforced with SiC particles in which tensile measurements were compared with FEM results. Good agreement was noted for fine particles. For coarse particles, there was evidence of particle cracking, which affected the yield strength and elastic modulus values.

Jian et al. [46] used strengthening models to analyze the particle size influence (Fig. 2.6) on strength of PRMMC. When the reinforcement is beyond a critical size then influence of particle on YS is unremarkable. The critical size should be less than 0.5µm in work hardening and Orowan strengthening mechanisms and it is less than 20µm in the case of interaction mechanisms. Also when particle is larger than 5µm again particle size influence on YS is unremarkable.

Long et al. [47] studied the mechanical properties of a 60% vol. %, 12µm SiC particle reinforced Al-Cu 4 mg Ag composite. The abrasive wear resistance, hardness, fatigue, strength, stiffness, flexural strength was improved whereas fracture toughness got reduced compared to matrix alloy. The fracture toughness is about 40-50% of the value of matrix alloy. The tensile strength and E was 163% and 186% more than their corresponding tensile strength and E of matrix alloy.

Hsu-Shen et al. [48] evaluated mechanical properties of composite produced by reciprocating extrusion including strength, ductility, and elastic modulus, wear resistance and coefficient of friction as a function of the volume fraction of Al_20_3. The composites studied were 6061 Al- Al_20_3p in various volume fractions of 0, 5, 10, 20 and 30% with 12.5µm Al_20_3. The composites were fully densified with uniform distribution of Al_20_3. The ductility was smaller compared to 6061 Al but E and YS found to be greater than

6061 Al alloy. The YS and tensile strength values ranged from 310 to 328 MPa, 185 to 265 MPa, 186 to 265 MPa, 178 to 296 MPa, and 177 to 331 MPa for the 5, 10, 20 and 30% v_f $Al_2 0_3$ composites, respectively. The percent elongation for this composites ranged from 15.3% for the 5% v_f $Al_2 0_3$ composite to 9.8% for the 30% v_f $Al_2 0_3$ composite, compared to a value of 18.2% for the 6061 Al alloy.

Park et al. [49] studied the effect of volume fraction of 20 micron micral-20 reinforced 6061 Al. The volume fractions were 0, 5, 10, 15, 20, 25 and 30%. As shown in the Fig. 2.7 the E found to increase with volume fraction whereas ductility decreases linearly. The tensile strength (TS) and YS were better than unreinforced alloy but it decreases with increase in volume fraction (Fig. 2.8), which is interpreted as being due to premature fracture of the particles during loading.

Lihe et al. [50] conducted quasi static and dynamic fracture toughness experiments on 6061 Al alloy reinforced with 15 and 25 vol. % of 9.5μm SiC particles, he observed the fracture toughness of composites decreases drastically due to addition of SiC particles at both quasi static and dynamic cases.

Duwell et al. [51] studied the effect of volume fraction on microstructural parameters (Fig. 2.9) with particle size less than 4 μm of $Al_2 0_3$ and fracture toughness of a 6061 Al alloy using three different test standards, ASTM E399, E1290 and ASTM E1737 (now replaced by E1820). With ASTM E399 fracture toughness is in terms of K_{Ic}, in E1290 it is in terms of critical crack tip opening displacement and in E1820 it is J integral concept, determines fracture toughness at 0.2 mm stable crack growth. According to ASTM 1820 curve shows gradual decrease in fracture toughness, according to ASTM

399 at lower volume fractions steep drop followed by plateau (Fig. 2.10). There was decrease in toughness data for increasing volume fraction in ASTM E1290.

The effect of reinforcement volume fraction on crack opening force and propagation energy by 3-point bend tests was investigated by Xia et al. [52]. For low volume fraction reinforced composites, cracks initiated generally at the particle/matrix interfaces. For high volume fraction reinforced composites cracks initiated from both particle/matrix interfaces and broken particles. As the volume fraction of the reinforcement increases the fracture mode changes from interface debonding to particle cracking.

Vecchia et al. [53] fabricated Al-Al_20_3 composite containing 67% v_f Al_20_3 composite, characterized mechanically by evaluating modulus of rupture, compression, tensile strength, hardness and fracture toughness. The materials have high stiffness, good compression and bending strength but UTS is poor. The increase in toughness of composite (5.3MPa) with respect to ceramic (2.6MPa) is recorded, this is due to plastic deformation of metallic zones. There was crack blunting and subsequent crack propagation.

Ceshini et al. [54] carried tensile test on two particle reinforced metal matrix composite, AA6061/20 vol. % Al_20_3 particles and AA7005/10 vol. % Al_20_3 particles. The average size of particles in the 6061/ Al_20_3 is 35μm and in 7005/ Al2O3 is 17μm. He observed that there was increase in E (38% for 6061/ Al_20_3, 17% for 7005/ Al_20_3) and UTS (17.4% for 6061/ Al_20_3, 5.7% for 7005/ Al_20_3) compared to unreinforced alloys. The tensile elongation (1.7% for 6061/ Al_20_3, 4.2% for 7005/ Al_20_3) found to be much lower compared to unreinforced alloys (12% for AA6061, 13% for AA7005). The particle frac-

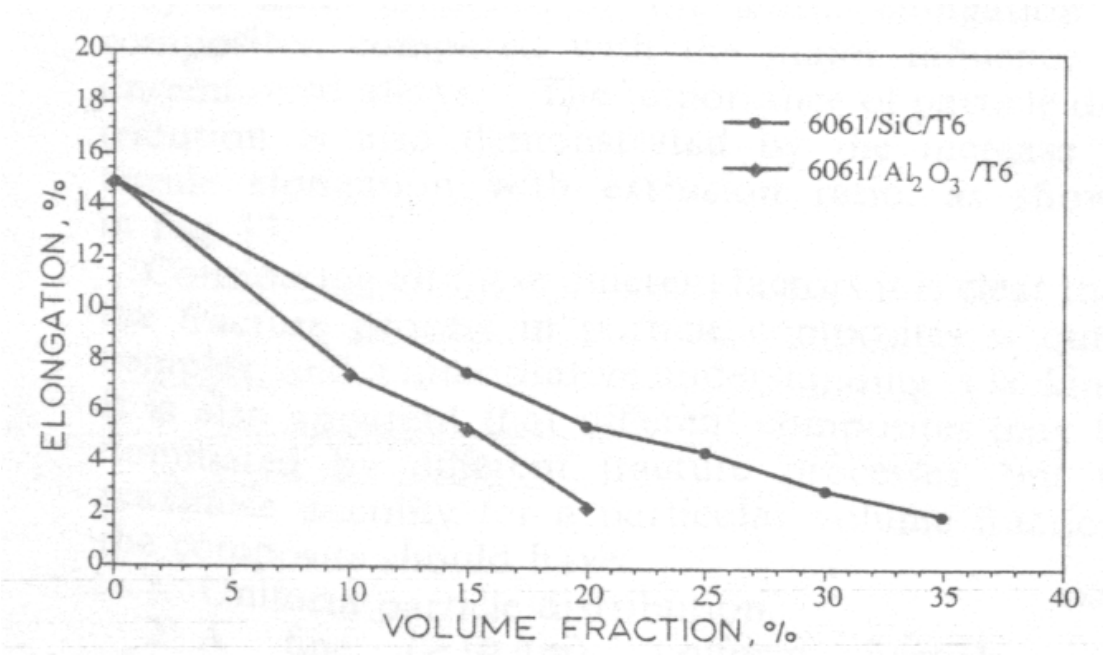

Fig. 2.5: Variation in tensile elongation of 6061 with volume fraction of reinforcement [10]

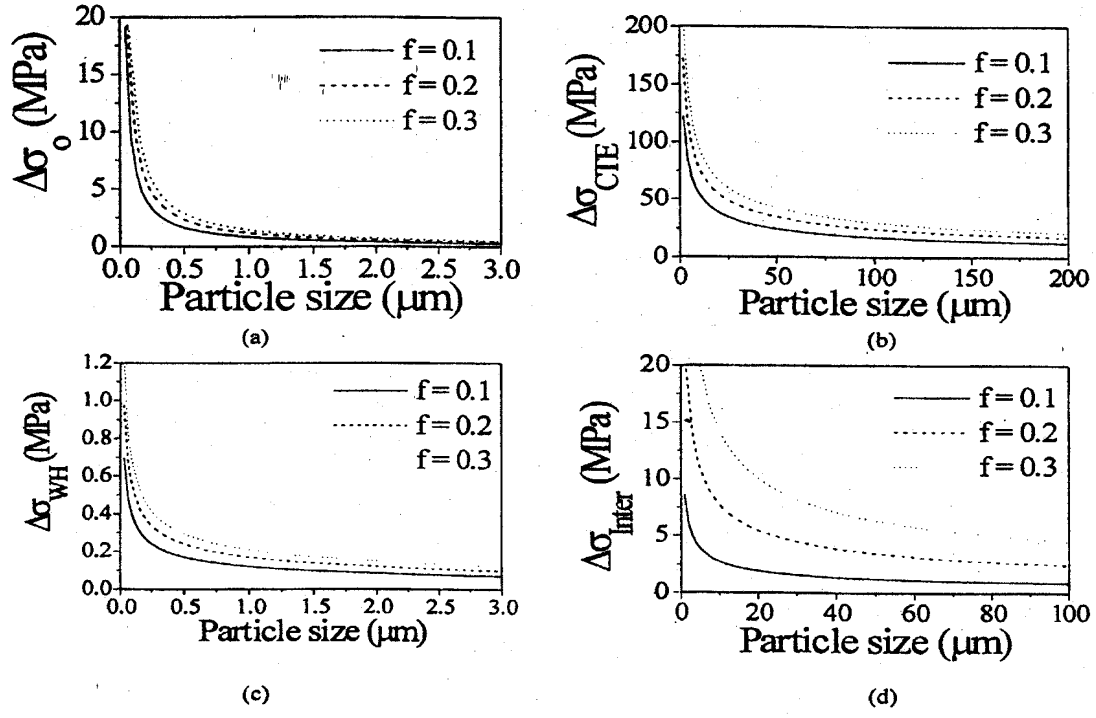

Fig. 2.6: Yield strength increased as a function of particle size due to (a) Orowan process, (b) difference in thermal expansion, (c) effect of work hardening and (d) interaction of the influence of the dislocation density and load transfer mechanism [46].

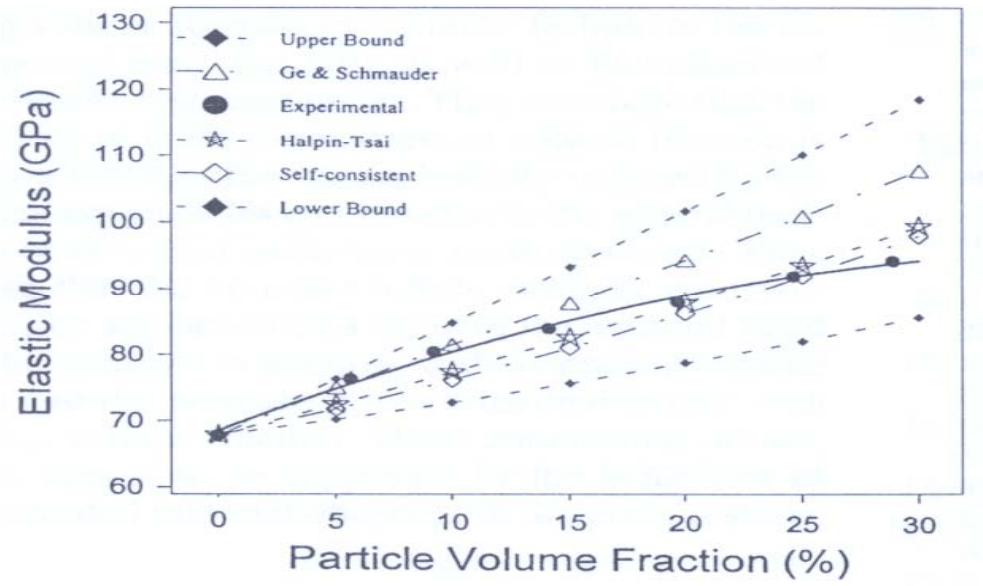

Fig. 2.7: Comparison of elastic moduli with moduli predicted using upper and lower bound, and different models [49].

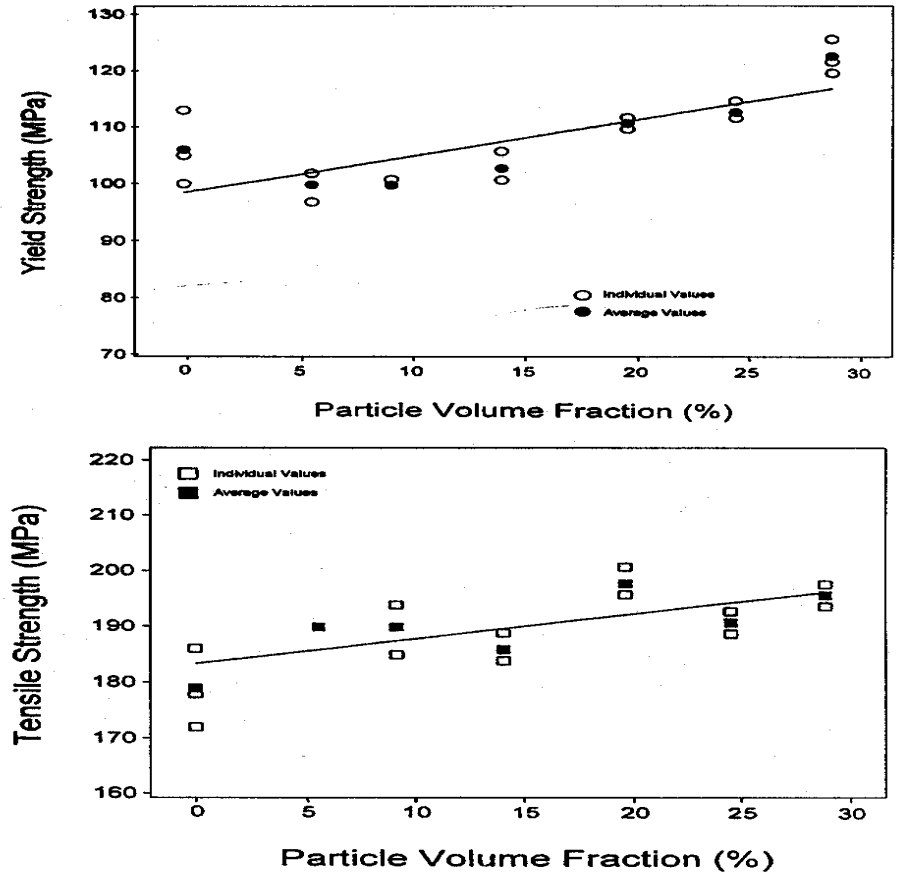

Fig. 2.8: Yield strength and tensile strength (TS) of composites in the as extruded condition [49].

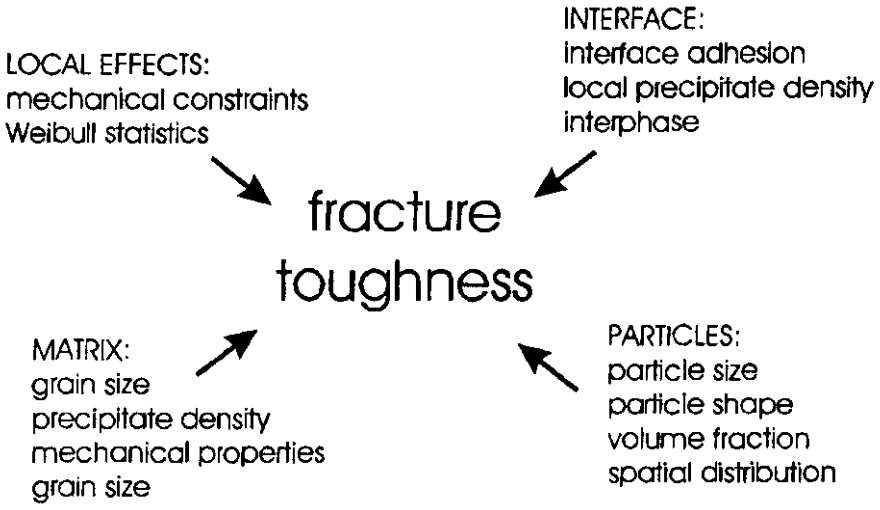

Fig. 2.9: schematic representation of complex relation between microstructural parameters and fracture toughness [51].

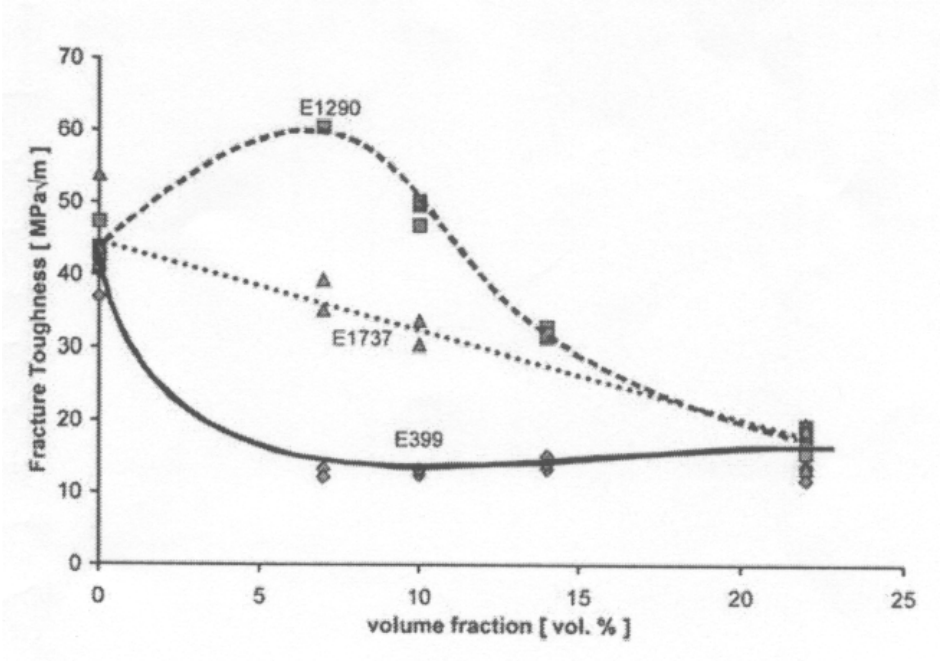

Fig.2.10: Fracture toughness verses volume fraction Al_20_3 for the three test methods [51].

ture was found to be main damage prior to final fracture.

Prewo [55] conducted pendulum impact test on 30% SiC particulate/6061 Al alloy by a charpy impact tester. The samples were notched and unnotched. He observed that SiC particulates/6061 Al alloy are less impact resistant than 6061 Al alloy matrices and it is notch sensitive with 10 times less in impact energy due to a notch. Plasticity limited because the particulate to matrix bond strength is high so there is no large-scale deformation on fracture surface.

Vincent et al. [56] using the microstructural toughening concept, composites were fabricated using a 304 stainless steel toughnening phase within a majority NiAl matrix. Notched impact energy absorption of up to 90 J/cm^2 was measured for these composites compared to 0.8 J/cm^2.

Geiger and walker [57] found that as particles size decreases the strength of Al 6013 with 20% SiC increased. The ductility increases as the particle size decreases, except for finest particles of size 0.7 μm reinforced composite. Hong et al [58] observed increase in compressive strength of Al with 10, 20, and 30 Vol. % SiC particles.

Arsenault et al. [59] studied the 0.5μm 20 vol. %, SiC spherical particles reinforced Al-1100, he observed as the reinforcement content increased proof stress increases. Shanker et al. [60] fabricated a composite containing 43-62 vol. % TaC particles of 0.1-1μm size with the unalloyed Al, resulting in high ductility. Muscat et al. [61] fabricated composite with 0.8 μm TiC of 50-85 vol. % reinforced unalloyed Al PRMMC. He observed that as vol. % of TiC increases the proof stress increased from 250 to 475 MPa and ductility decreased from 5 to 0%.

Redsten et al. [62] investigated the mechanical properties of oxide dispersion strengthened Al containing 25 vol. %, 0.28 μm Al_20_3 particles. He found that the yield strength is low but 0.2% proof stress, UTS were higher about 200 MPa and 330 MPa respectively.

Zhou et al. [63] produced two composites, one with a spheres consisting of Al reinforced by 40 vol. % 0.5 μm Al_20_3 particles, are uniformly distributed in a particle free 6061 Al matrix and other consists of a 4 μm Al_20_3 particles in 6061 Al matrix. The above-mentioned composites have higher E, UTS and hardness then their 6061-matrix alloy but ductility was low. Keeping vol. % constant as particle size decreases from 4 to 0.5 μm it was found that E, UTS, hardness increases significantly with slight increase in ductility. The increase in E was 27.4% for AA6061Al reinforced with 0.5 μm Al_20_3 particles and for 0.9% AA6061Al reinforced with 4 μm Al_20_3 particles. The increase in E was 27.4% for AA6061Al reinforced with 0.5 μm Al_20_3 particles and 0.9% for AA6061Al reinforced with 4 μm Al_20_3 particles when compared to 6061 Al alloy.

Lihe et al. [64] conducted fracture toughness on 6061 Al alloy reinforced with 15 vol. %, fine SiC particles of 0.6μm and 9.5μm. He observed that the toughness of fine 0.6μm SiC particle reinforced composite was 30% higher than that of 9.5μm SiC reinforced composite and it is about one half of the unreinforced 6061 Al alloy. Boundaries between particle clusters and surrounding matrix found to be responsible for the failure mechanism.

It is seen from above that the only few researchers investigated PRMMC composites with reinforced particles less than 1μm [62, 63]. And it is observed that as the particle size decreases the strength increases [28] whereas the decrease in toughness is

less compared to coarse particles. Smaller particles are less susceptible to fracture than long and elongated particles hence submicron particle size results in improved mechanical properties.

Among the mechanical properties, the affect of volume fraction on yield strength, ultimate tensile strength, and elastic modulus is clear. Evaluating toughness (static and dynamic) in MMC is still the subject of debate. There is not even single toughness measurement technique approved as the correct measurement technique for MMCs. Most of the impact damage (toughness) has centered around the use of charpy and izod tests, and instrumented version of these test. The geometry often does not represent to end use application, these test though widely used are not necessarily suited to an understanding of composite material impact response. And frequent impacts are occurred in aircraft structure from bird strikes, runway debris, foreign object damage from ingested birds or combustion debris, ground service equipment, assembly and handling cause by dropping tools. For metals these impacts results in plastic deformation with out leading to catastrophic failures. However in composites repeated low energy impacts leads to failure, with out developing any visible surface damage. In composites localized plasticity, crack blunting; etc contributes to fracture toughness, (K_{Ic}) which no longer represent a simple characteristic of the material toughness. In that fracture toughness is not appropriate and toughness is characterized by measurements of the fracture energy [65] and fracture energy measurement is typically conducted by pendulum impact (or) falling weight impact, quasistatic bend tests.

CHAPTER 3

EXPERIMENTAL METHODS AND PROCEDURES

3.1 MATERIALS

The materials used in this study were composites based on a 6061 Aluminum alloy metal matrix containing 10%, 20%, and 30% vol. fraction of Al_20_3 spherical particles with an average size of 0.7μm, in addition to unreinforced 6061Al alloy. The composite was prepared by powder metallurgy at Fraunhofer Institute Fetigungstenik Materialforschung. First, a blend of 6061 Aluminum powder (< 63μm) and Al_20_3 powder (Average size = 0.7μm) were mechanically alloyed in argon atmosphere using a planetary mill. To reduce welding during milling, 0.5% of weight citric acid was added to the blend. After producing a homogeneous distribution of Al_20_3 with aluminum, the milled powder was compacted by uniaxial pressing at 200 MPa. Then the resultant discs were degassed at 400˚C. The disc was then extruded from a diameter of 76mm to 17mm at 550˚C.

3.2 TESTING PROCEDURES

- **Tensile Testing**

The Instron 8801 material testing system was used to obtain tensile test results. The system is a closed loop servo-hydraulic, dynamic, single axis testing system. The machin

e equipped with a hydraulically actuated self-aligning gripping system. The photograph of testing machine is shown in Fig. 3.1. There are three controlling modes such as Position, Load and Strain. The Capacity of the Machine is ± 100 KN. Displacement is ± 75 mm. Strain is ± 25%. The maximum frequency applied is 100 Hz.

All tensile tests were carried out using specialized software called Series IX, which provided complete machine control, data acquisition, data reduction and analysis capability. Tensile tests were carried out under position control. The software logged position and corresponding load of the test with a constant position increment until fracture occurred. The elastic modulus is obtained by getting the load and position data throughout the test. The maximum stress value just before fracture is selected as the tensile strength and the final actuator position gave the fracture strain.

The standard for tensile testing of PRMMC composites is included in ASTM E 8m [66] "Standard Test Methods for Tension Testing of Metallic Materials" [67]. Cylindrical samples as per ASTM E8m were machined with the stress axis parallel to the extrusion direction. The test samples were smooth and cylindrical in the gauge section with 6.0 mm in diameter and 36 mm in length as shown in Fig. 3.2b. In order to minimize the effects of surface irregularities and finish the entire gauge section of the test sample was mechanically polished by 600 grit SiC paper.

Uniaxial tensile tests were performed on an 8801-test machine at room temperature. An extensometer was fitted to samples to measure the strain to failure (Fig. 3.2b). At least 3 samples were tested to get average value. The crosshead speed of testing for all samples was 3mm/min.

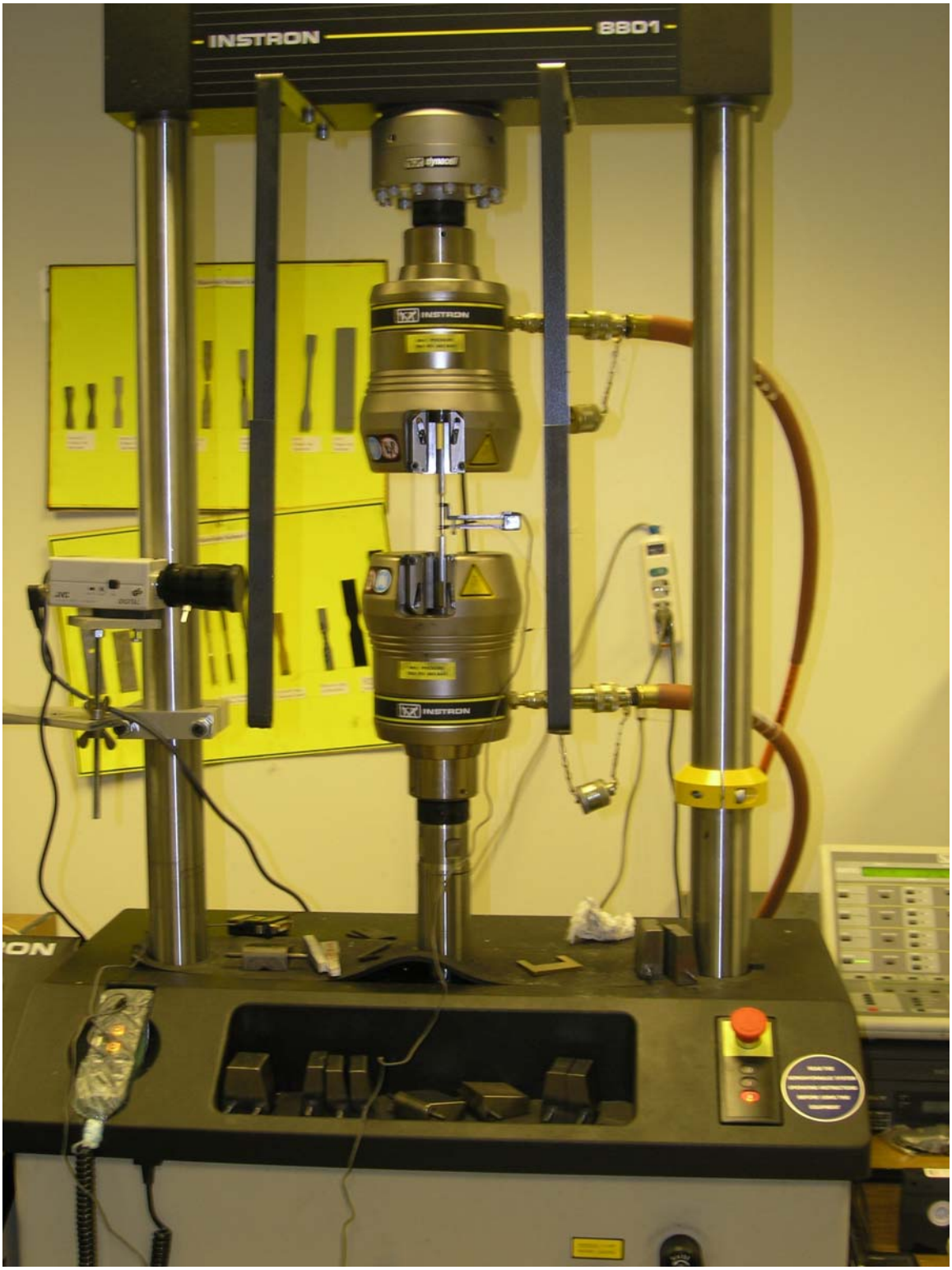

Fig. 3.1: Instron 8801 equipped with Series IX for tensile testing

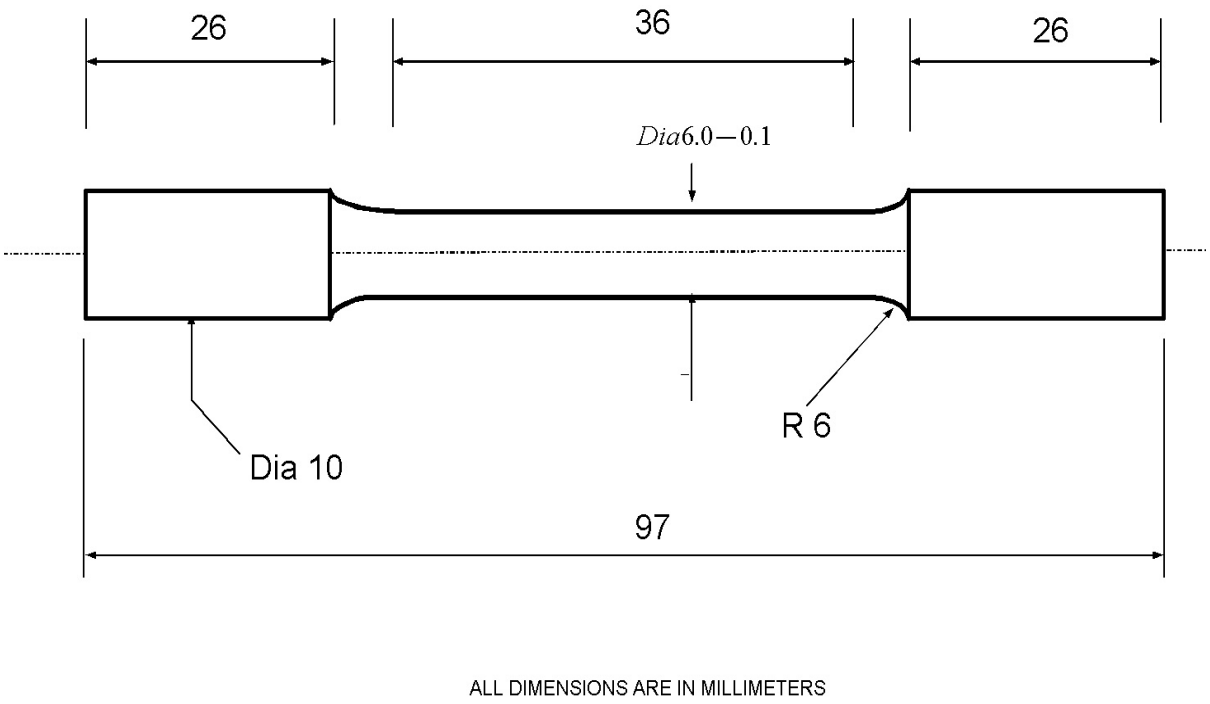

Fig. 3.2a: Tensile sample as per ASTM E 8m standard [67].

Fig. 3.2b: Tensile sample on Instron 8801.

- **Flexural Strength Testing**

A photograph of machine used for flexural strength tests is shown in Fig. 3.3. Flexural strength was determined according to standard C1161-90 "Standard test method for flexural strength of advanced ceramics at ambient temperature" [68]. Rectangular composite samples were placed on a four-point support fixture, such that polished surfaces (l μm finish) of the inner span were loaded in tension. The fracture load (P) for each test was recorded, and the bending strength of the composite (σ_b) was calculated according to (Fig. 3.4).

$$\sigma_b = \frac{3PL}{4bd^2}$$

Where P = break load, L = outer span, b = sample width, and d = sample thickness.

- **Fracture Toughness Testing**

In the present study fracture toughness values (K_{Ic}) for the composites were measured using the modified multiple indentation toughness technique developed by Cook and Lawn (1983). In this technique described by Cook and Lawn (1983) multiple Vickers indentations of proper sizes are introduced on the tensile surface of the inner span of a four-point bend sample. These indentations produce radial cracks of approximately half elliptic shape. Since all indentations (three in the present tests) during bend testing experience the same stress history, the critical crack length at failure can be measured from the remaining intact indentations. The three indentations were aligned in the middle of the tensile surface, 5 mm apart, with the crack arm emanating from the indentation comers perpendicular and parallel to the tensile direction. All samples were indented with Vickers diamond indenters at indentation loads of 10 Kg for the samples,

Fig. 3.3: Instron 5569 equipped with Bluehill for flexural testing

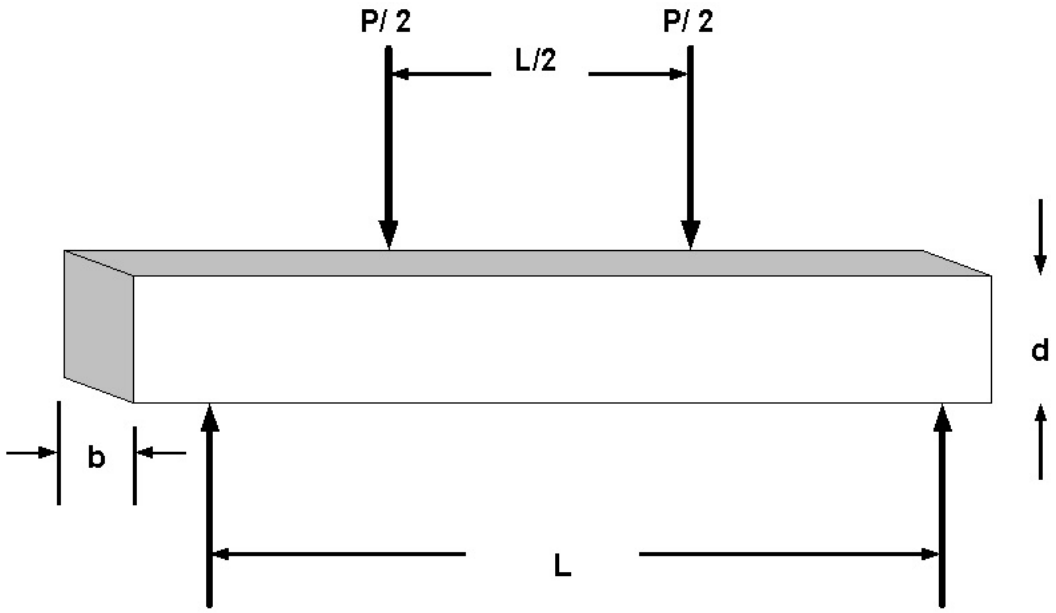

Fig. 3.4a: Flexural sample as per ASTM C1161 standard [68]

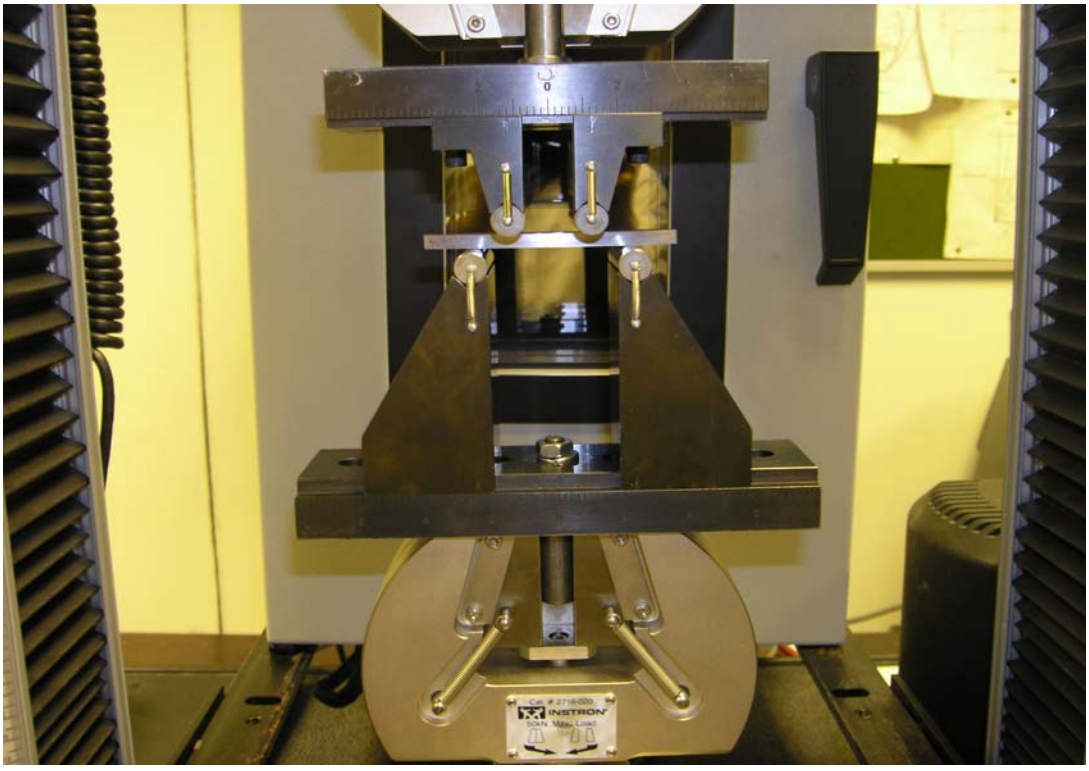

Fig. 3.4b: Flexural sample on Instron 5569

and fractured in four-point bending, under the same conditions as those used for bending strength measurements. After fracture, each sample was visually inspected to ensure that one of the three indentations originated the fracture.

Fig. 3.5 shows typical Vickers indentations of samples. The fracture toughness, K_{Ic}, was calculated according to the following equation (Cook and Lawn, 1983):

$$K_{Ic} = 2.02\ \sigma_m \sqrt{c_m} - 0.68\ \text{MPa}\ \sqrt{m}$$

Where σ_m is maximum stress at failure and c_m is the average crack length of the two remaining indentations.

- **Low Velocity Impact Testing**

The Dynatup 9250G (Fig. 3.6) impact tester was used for low velocity impact tests for this study. The 9250G model is gravity-based system, which generates maximum velocities up to 5 meters per second and impact energies up to 1000 Joules. The ranges of impact energies can be obtained by choosing suitable combinations of crosshead mass and drop height. The contact force is measured with a load transducer located between the cross head and hemispherical tup nose. Instrumented impact test records contain the entire impact event so that the full impact force versus time profile can be analyzed. The Dynatup impulse data acquisition system is the heart of impact testing system. It captures load information at very high speed from impact tests then data is analyzed graphically.

The objective of impact testing is to determine an object's ability to resist high-rate loading, which is measured by the energy absorbed to fracture a test piece at high strain rate. Impact strength along with impact resistance is one of the most commonly

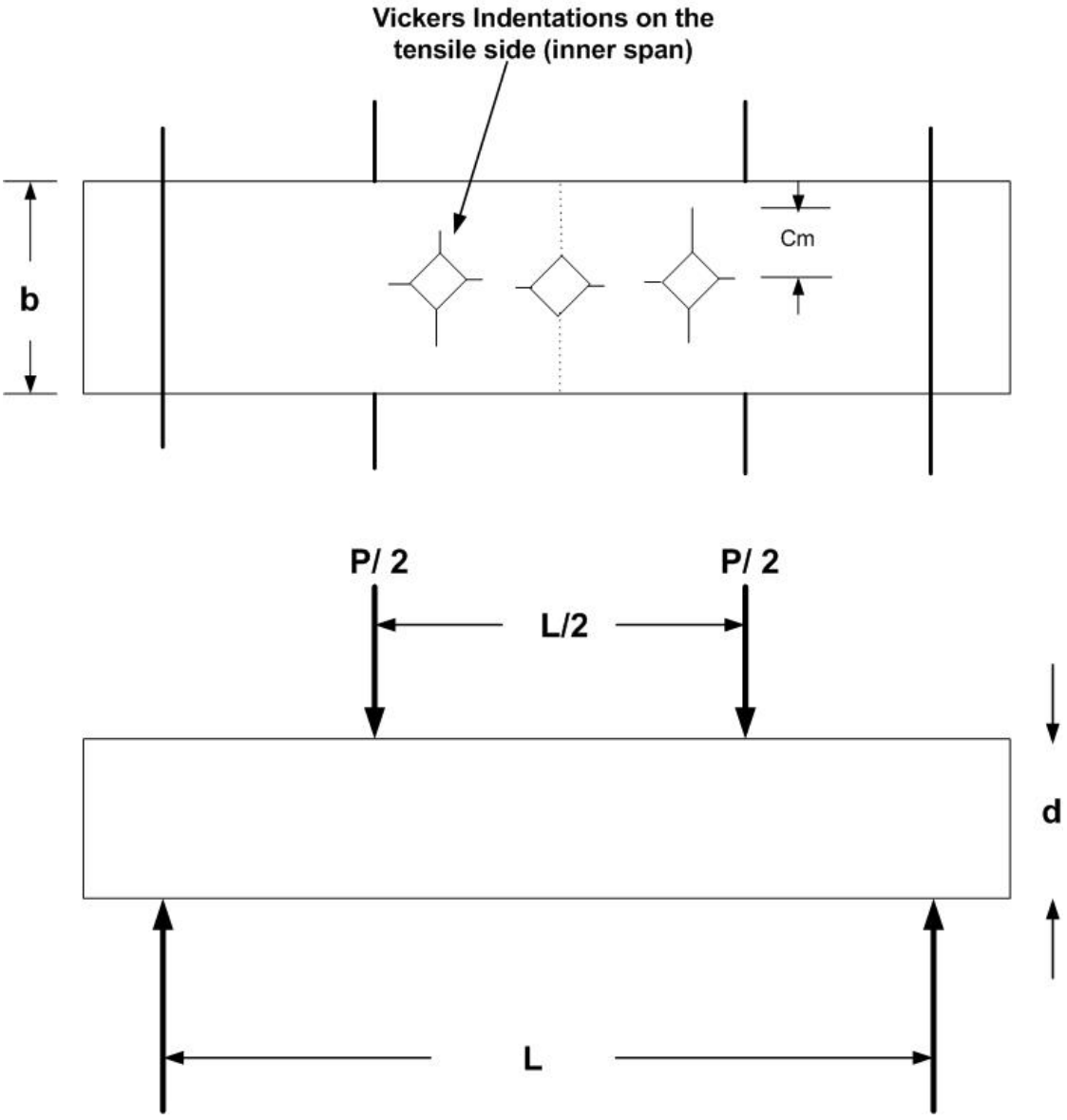

Fig. 3.5: Fracture toughness of Al reinforced with Al_20_3 PRMMC composites.

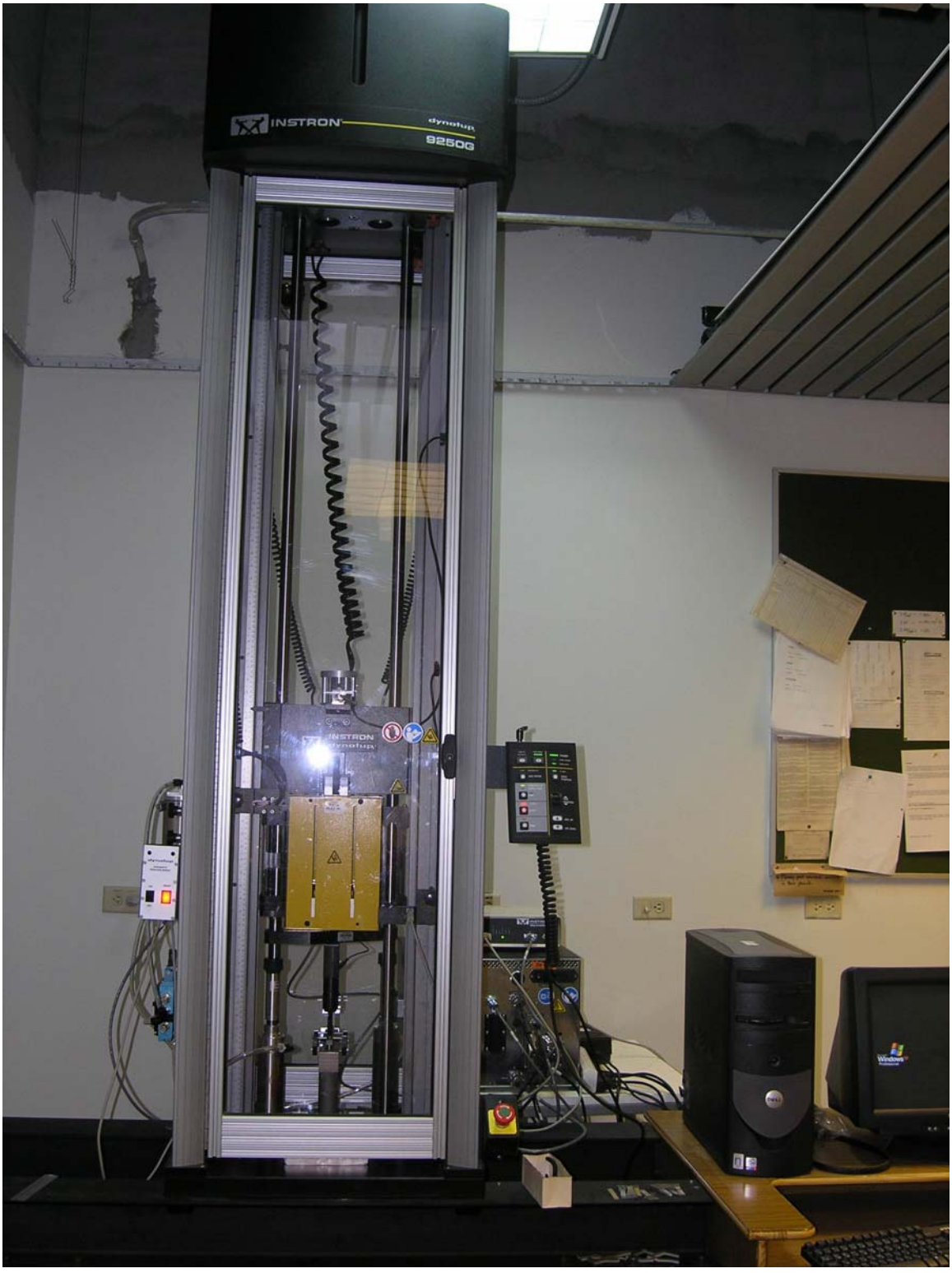

Fig. 3.6: Dynatup 9250G equipped with Impulse for Impact testing

measured properties and to quantify. The impact resistance of a part is, in many applications, a critical measure of service life. More importantly these days, it involves the perplexing problem of product safety and liability.

Drop weight impact testing has been described as an “energy technology”. In this study, low velocity impact tests were conducted using an instrumented drop weight impact testing machine (DYNATUP 9250G) to examine fracture surfaces of the tested specimens. Force/absorbed energy-time plots were generated for each impact test. The samples were cross-sectionally analyzed to record the damage corresponding to each impact energy level.

With the height and weight known, impact energy can be calculated. Since the falling weight either stopped dead on the test sample, or destroyed it completely in passing through, the only results that could be obtained were of a pass/fail nature. It is unidirectional with no preferential direction of failure. Failure can be defined by deformation, crack initiation, or complete fracture, depending on the requirements. Failures originate at the weakest point in the sample and propagate from there. If insufficient energy is delivered to damage the sample, there is option to either maintain that mass and increase the height or vice versa. The force vs time curve can be characterized by the peak force, the energy to peak force, total energy, and displacement to maximum load.

Maximum (peak) load is the highest point in the load-time curve. Often the point of maximum load corresponds to the onset of material damage or complete failure. Energy to maximum load is the energy that the sample has absorbed up to the point of

maximum load. It is the area under the load/deflection curve from the test start to the maximum load point. Total energy is the energy that the sample has absorbed up to the end of the test, when the load reaches zero again. It is the area under the load/deflection curve from the test start to the test end. Deflection to maximum load is the distance the impactor traveled from the point of impact to the point of maximum load.

- **Fracture mechanisms**

The fracture surface morphology of the failed samples was studied using a Joel JSM scanning electron microscope (Fig. 3.7). The magnification range available is 35x to 300,000x, with a resolution of 4nm. The excitation potential can be varied between 1 to 50 kV. A focused electron beam of the smallest possible diameter is scanned across the sample surface. The SEM has a large depth of field, which allows a large amount of the sample to be in focus at one time. The samples were reduced to the appropriate size (for mounting on SEM) by Buehler Isomet^{TM} low speed saw.

Fracture surfaces contain information on the microstructure and the properties of a material, as well as on the conditions during the deformation and fracture.

In order to understand the influence of Al_20_3 particle on the deformation characteristics, the fracture surfaces were examined under SEM, which helps in explaining microstructural effects on the ductility and fracture properties of the 10, 20, and 30% v_f Al_20_3 composites.

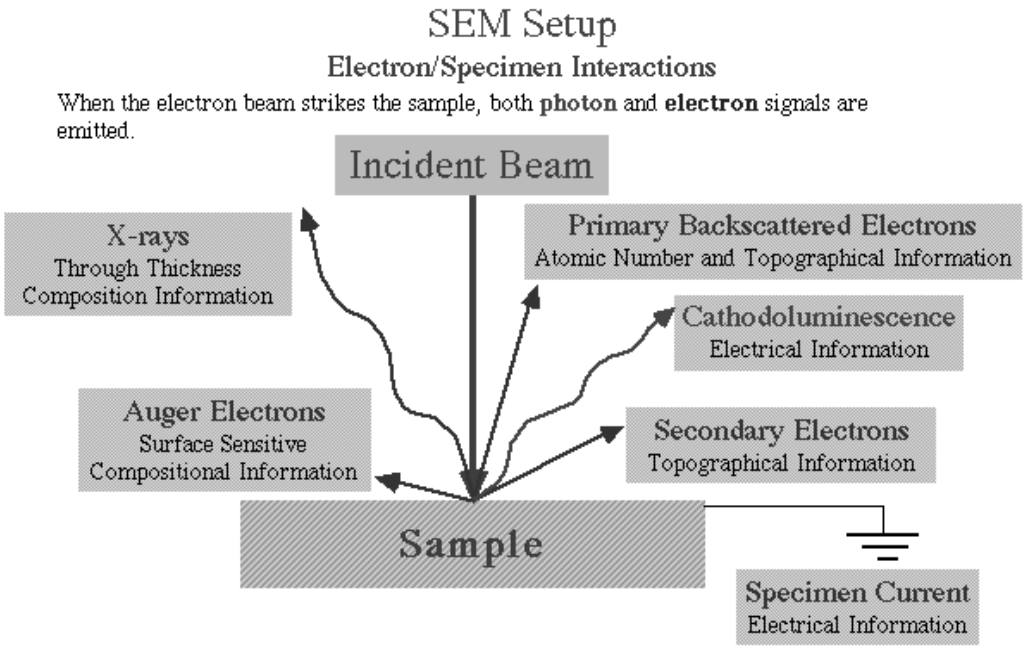

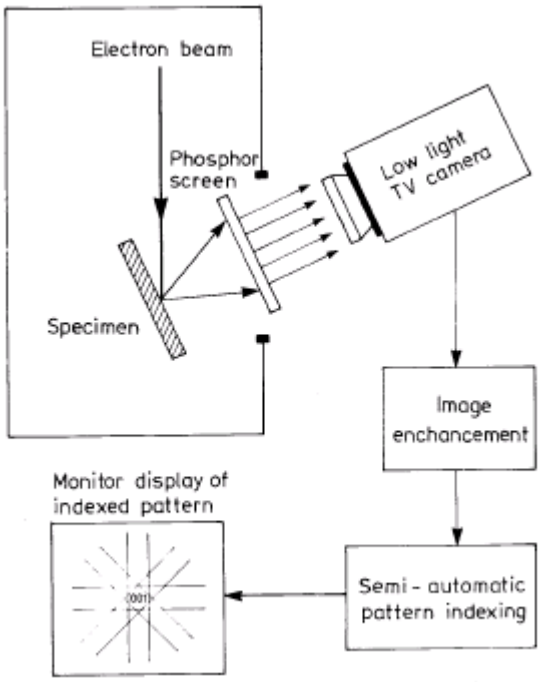

Fig. 3.7: Schematic Diagram of SEM

CHAPTER 4

RESULTS AND DISCUSSIONS

4.1 MICROSTRUCTURAL EXAMINATIONS

Metallographic samples from the 10%, 20%, and 30% v_f Al_2O_3 reinforced Al composites were cut with a low speed diamond-blade wheel. They were wet ground on 320, 400, and 600 grit SiC abrasive paper using water as lubricant, followed by polishing on diamond slurry (1μm) and these samples were cleaned in deionized water. The intrinsic microstructural features (Fig. 4.1- 4.10) showing particle morphology, their size and distribution in the matrix metal were examined using scanning electron microscope (SEM).

Fig. 4.1 - 4.2 shows the microstructure of the 10% v_f Al_20_3 composite, where the uniformly distributed, spherically shaped particles can be clearly seen. As Fig.4.1 shows, no broken Al_2O_3 particles are spotted, but matrix particle decohesion and voids in the matrix were observed. Fig. 4.3 - 4.7 shows the microstructure of 20% v_f Al_20_3 composite. Again, no fractured Al_2O_3 particles can be seen from this figure. However, matrix particle decohesion in addition to voids in the matrix were observed on the polished surfaces, which can be seen in Fig 4.3. In addition, few particle rich (clustering) and particle-deple-

d regions are spotted in Fig. 4.5-4.6. Similar observations can be said for the 30% v_f Al_20_3 composite where no fractured Al_2O_3 particles were seen in Fig 4.8-4.10. There were matrix particle decohesion, voids, and clustering of the particles in the matrix. In Fig 4.10, the Al_20_3 particles clumped together within field of view; a typical clustering site consists of few large Al_2O_3 particles intermingled with smaller, uniform and regular shape particles. The degree of clustering was found to increase in the 6061 Al alloy metal matrix as the volume fraction (v_f) of reinforcement increases (from EDS analysis) It may be concluded that as a result of clustering particles the inter-particle distance hindered matrix infiltration among the particles and as a result, porosity was elevated in these regions.

4.2 TENSILE PROPERTIES

The tensile property measurements were carried out using ASTM standard E 8m [66] procedure. The value of stress corresponding to the yield point is taken as the yield stress of the sample. The elastic modulus of the sample is calculated from the slope of the linear portion of the stress-strain curve. To ensure the accuracy of this measurement, a trend line is drawn using the linear regression fit. The slope of this line is taken as the elastic modulus of the sample. The rate of loading for all the samples was 3 mm/min. The gauge length was 25.4 mm and all the results were average of at least 3 measurements.

Stress-strain curves of all the composites are plotted in Fig. 4.11. As can be seen from this Fig. all the studied composites display different stress-strain behavior. The summary of tensile results for Al reinforced with Al_20_3 PRMMC is reported in Table 4.1. Due to constraints imposed in deformation caused by the presence of the hard and brittle Al_20_3 particles in the soft and ductile 6061 Al alloy matrix, higher applied stress is required to initiate plastic deformation in the matrix. This in turn results in the increase in the elastic

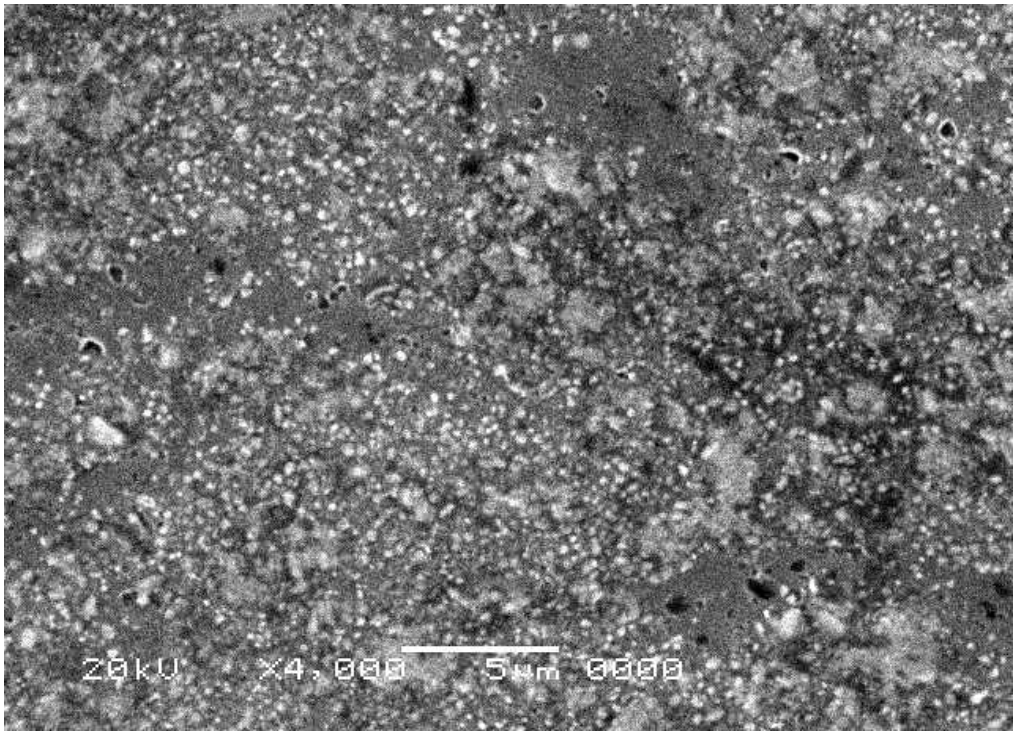

Fig. 4.1 Microstructure of 6061 Aluminum alloy reinforced with 10% Al_2O_3 at magnification 4000X

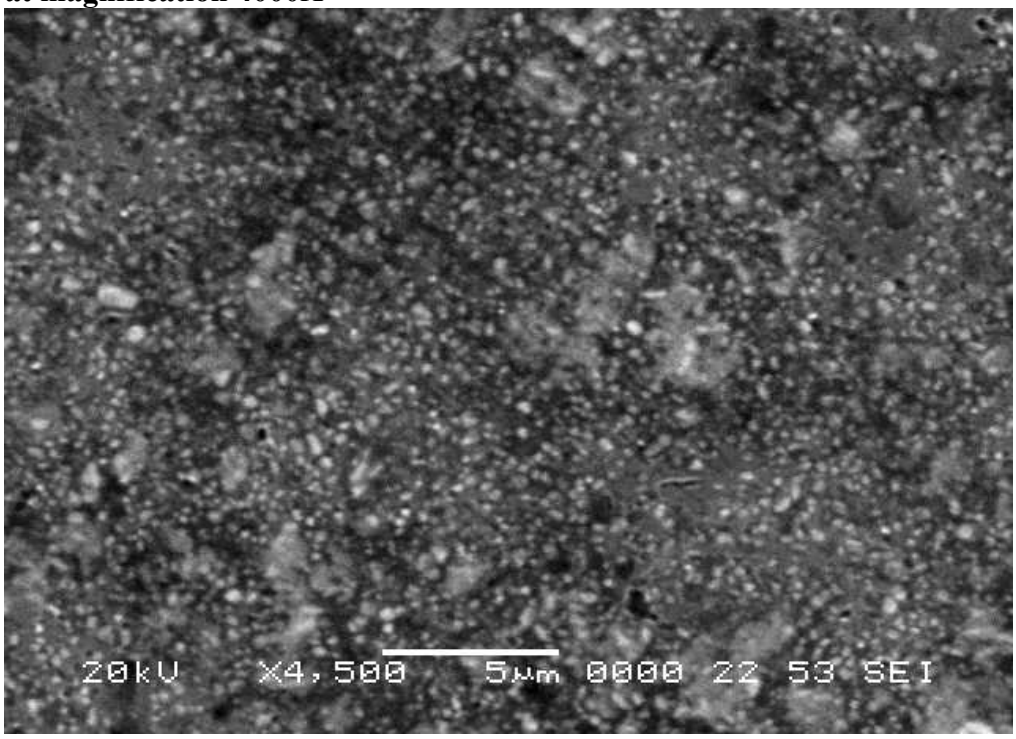

Fig. 4.2 Microstructure of 6061 Aluminum alloy reinforced with 10% Al_2O_3 at magnification 4500X.

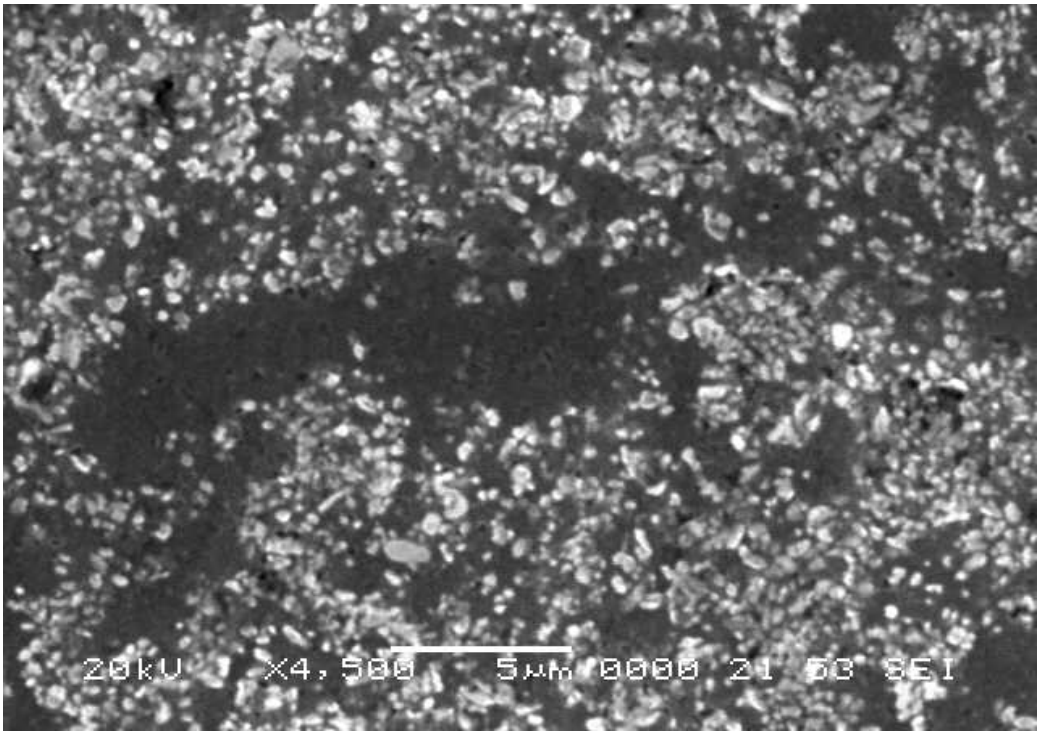

Fig. 4.3 Microstructure of 6061 Aluminum alloy reinforced with 20% Al_2O_3 at magnification 4500X

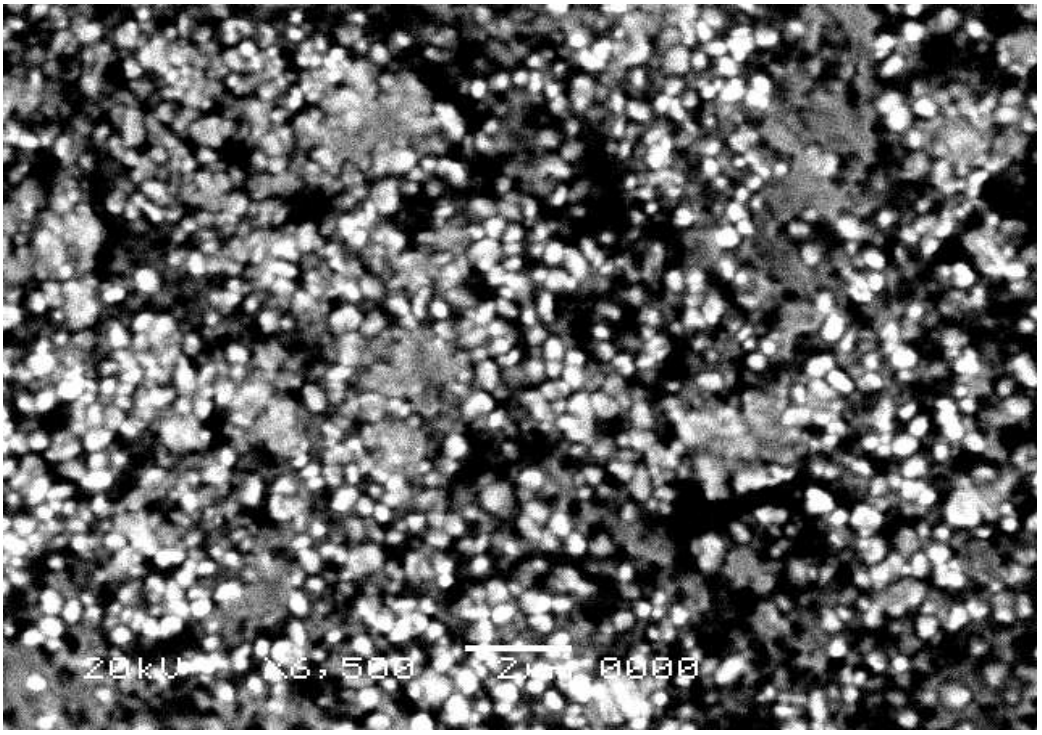

Fig. 4.4 Microstructure of 6061 Aluminum alloy reinforced with 20% Al_2O_3 at magnification 6500X

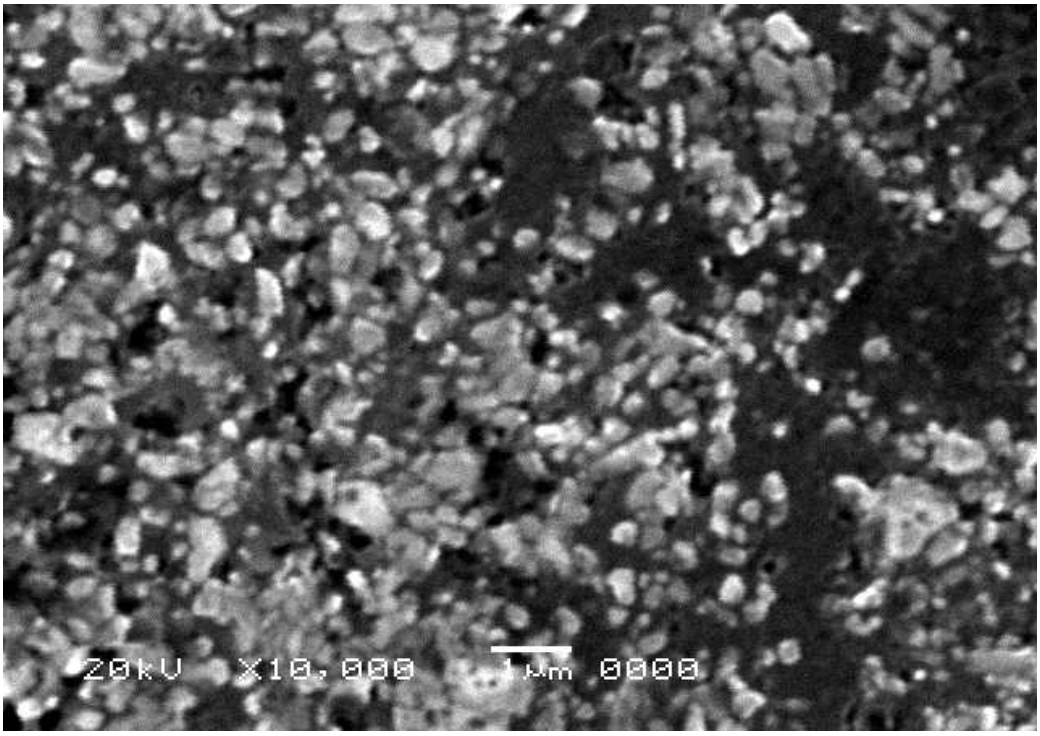

Fig. 4.5 Microstructure of 6061 Aluminum alloy reinforced with 20% Al_2O_3 at magnification 10,000X

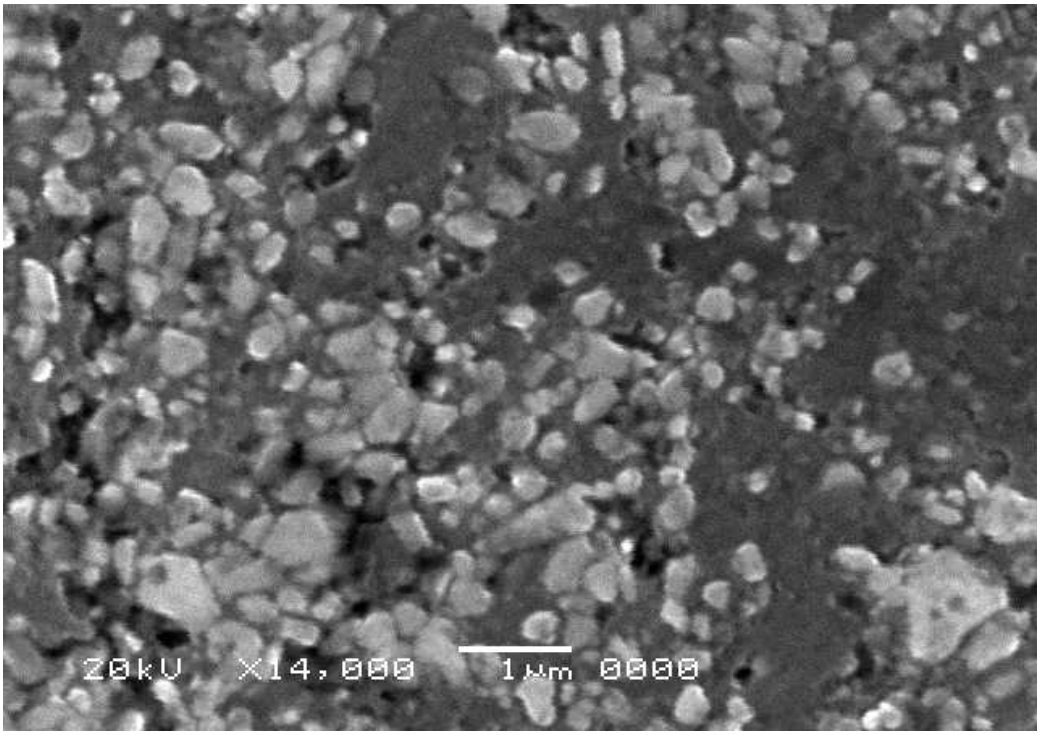

Fig. 4.6 Microstructure of 6061 Aluminum alloy reinforced with 20% Al_2O_3 at magnification 14,000X

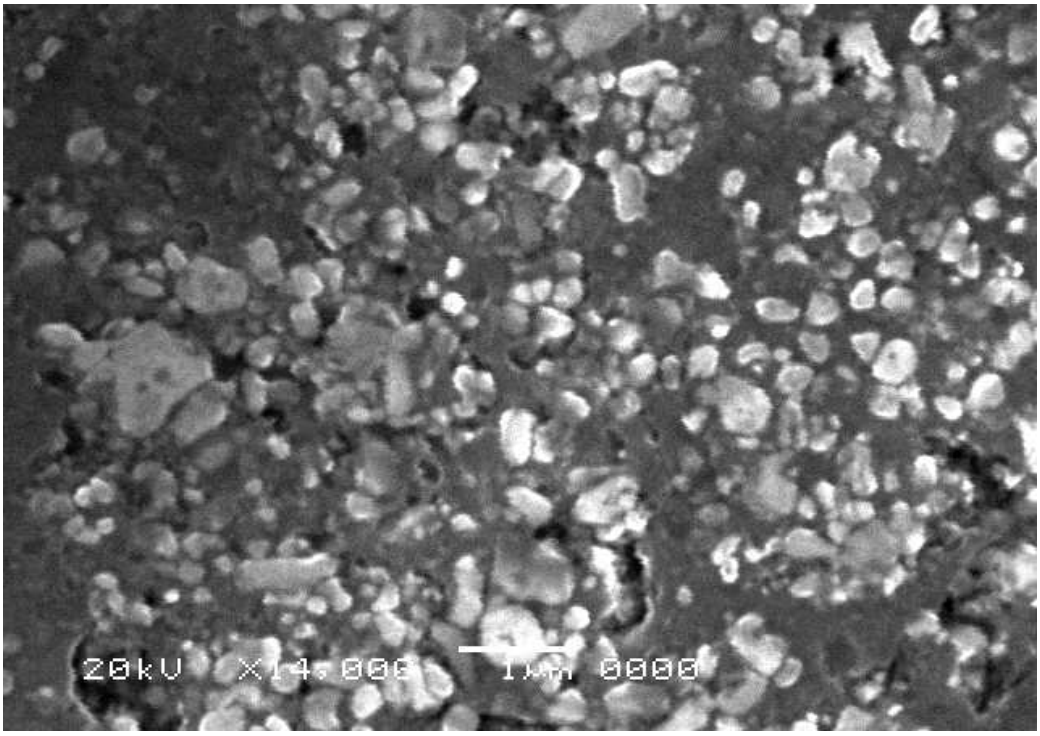

Fig. 4.7 Microstructure of 6061 Aluminum alloy reinforced with 20% Al_2O_3 at magnification 4000X

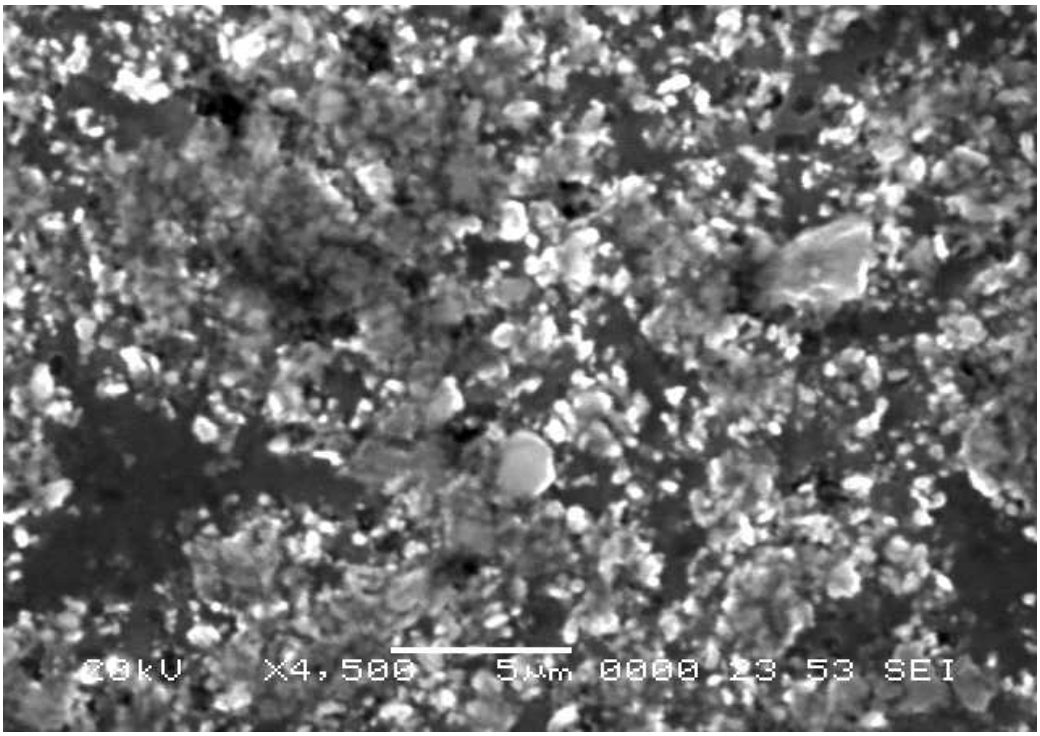

Fig. 4.8 Microstructure of 6061 Aluminum alloy reinforced with 30% Al_2O_3 at magnification 4500X

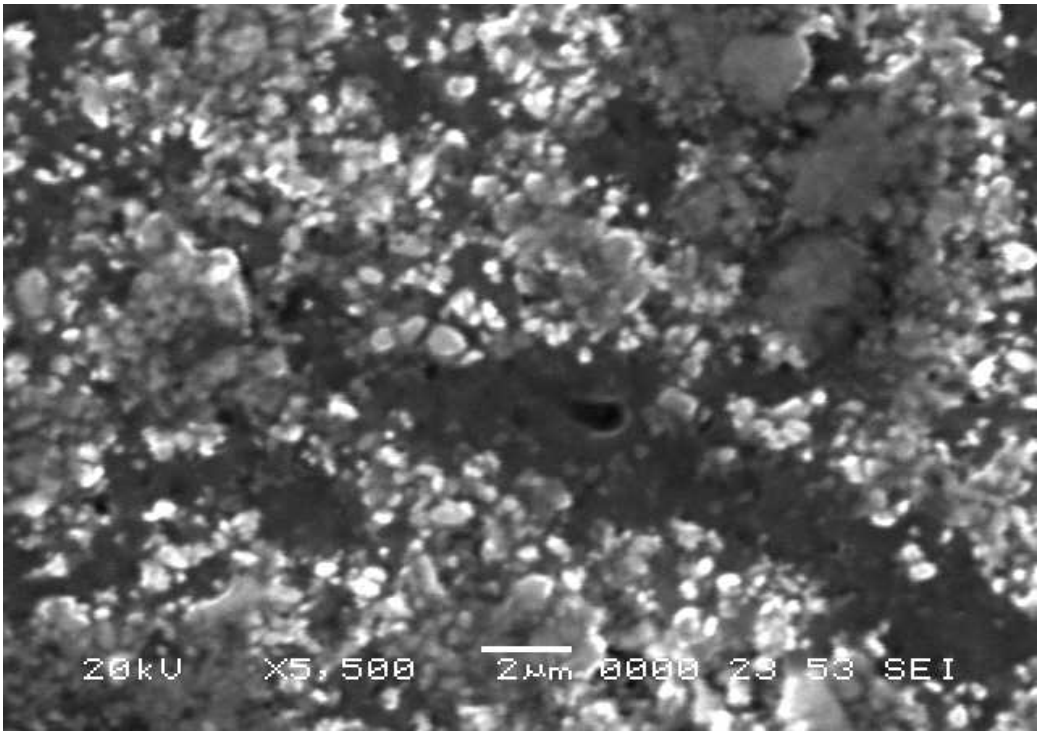

Fig. 4.9 Microstructure of 6061 Aluminum alloy reinforced with 30% Al_2O_3 at magnification 5500X

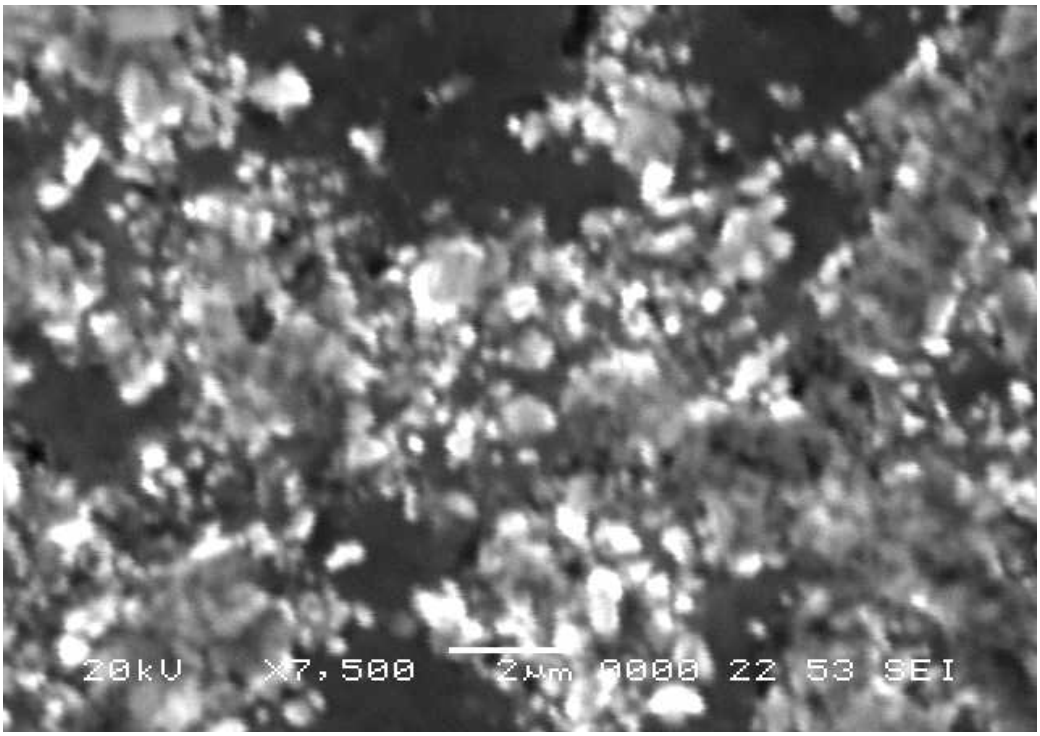

Fig. 4.10 Microstructure of 6061 Aluminum alloy reinforced with 30% Al_2O_3 at magnification 7500X

modulus and strength of the composite.

- **Variation of Elastic modulus**

The elastic modulus of various vol. % reinforcement composites and the unreinforced Al alloy are plotted in Fig. 4.12. Test results show an increase in elastic modulus with an increase in reinforcement (Al_2O_3) content in the 6061 Aluminum alloy metal matrix. The elastic modulus of the 10% v_f Al_2O_3 composite is 86.81 GPa, which is 27.6 % higher than that of the 6061 Al alloy. The elastic modulus of the 20% v_f Al_2O_3 composite is 104.45 GPa, which is 53.53 % higher than that of the 6061 Al alloy. Finally the elastic modulus of the 30% v_f Al_2O_3 composite is 109.9 GPa, which is 61.55 % higher than that of 6061 Al alloy.

- **Variation of Strength**

The σ_{ys} and σ_u values were substantially influenced by the addition of Al_2O_3 particles as shown in Figs. 4.13-4.14. σ_{ys} and σ_u increased with an increase in the reinforcement content in the 6061 Al alloy. The σ_{ys} and σ_u values ranged from 184.33 to 354.67 MPa and from 328.22 to 448.77 MPa for the 10% v_f Al_2O_3 and 30% v_f Al_2O_3 composites, respectively.

- **Variation of Strain to failure**

The variation of strain at failure values with the v_f of reinforcement in the 6061 Al metal matrix is shown in Fig. 4.15. The 6061 Al alloy has the highest strain to failure value, as would be expected; for the composites, this value ranged from 4.72% for the 10% v_f Al_2O_3 composite to 1.42% for the 30% v_f Al_2O_3 composite, compared to a value of 28% for the 6061 Al alloy.

The Al_20_3 particle reinforced metal matrix composites yielded higher stiffness, and strength compared to the unreinforced alloys. The tensile properties of composites are mainly influenced by the amount and distribution of the reinforcing particles. Yield and tensile strengths generally increase with increasing reinforcement content, and a similar increase is obtained for the elastic modulus; however these composites exhibited a much lower tensile elongation.

- ## Tensile fracture behavior

The influence of Al_20_3 particles clustering and the microstructural effects on ductility and fracture properties of the composites were analyzed by examining SEM fracture surfaces of tested samples. Two factors appear to control the tensile fracture of these composites: distribution of the Al_20_3 particles and deformation characteristics of the matrix. In addition, the SEM analysis of fractured surfaces shows no particle fracture which agrees with other studies indicating that large particles are more likely to fail than small ones [28, 35, 69-73].

- **6061 Al alloy**

The 6061 Al alloy contain either inclusions and second phase particles which were added to improve mechanical behavior (or) else not eliminated during processing and remained as impurities. These inclusions act as void nucleation sites during deformation by interfacial decohesion. Material rupture then takes place through a different process, which involves the growth of the voids by plastic straining and their subsequent coalescence by localized necking of the intervoid matrix. The mechanics and mechanisms of failure were the nucleation growth, and coalescence of voids. Necking (diameter contraction) of the sample at the fracture plane can be clearly observed in Fig.

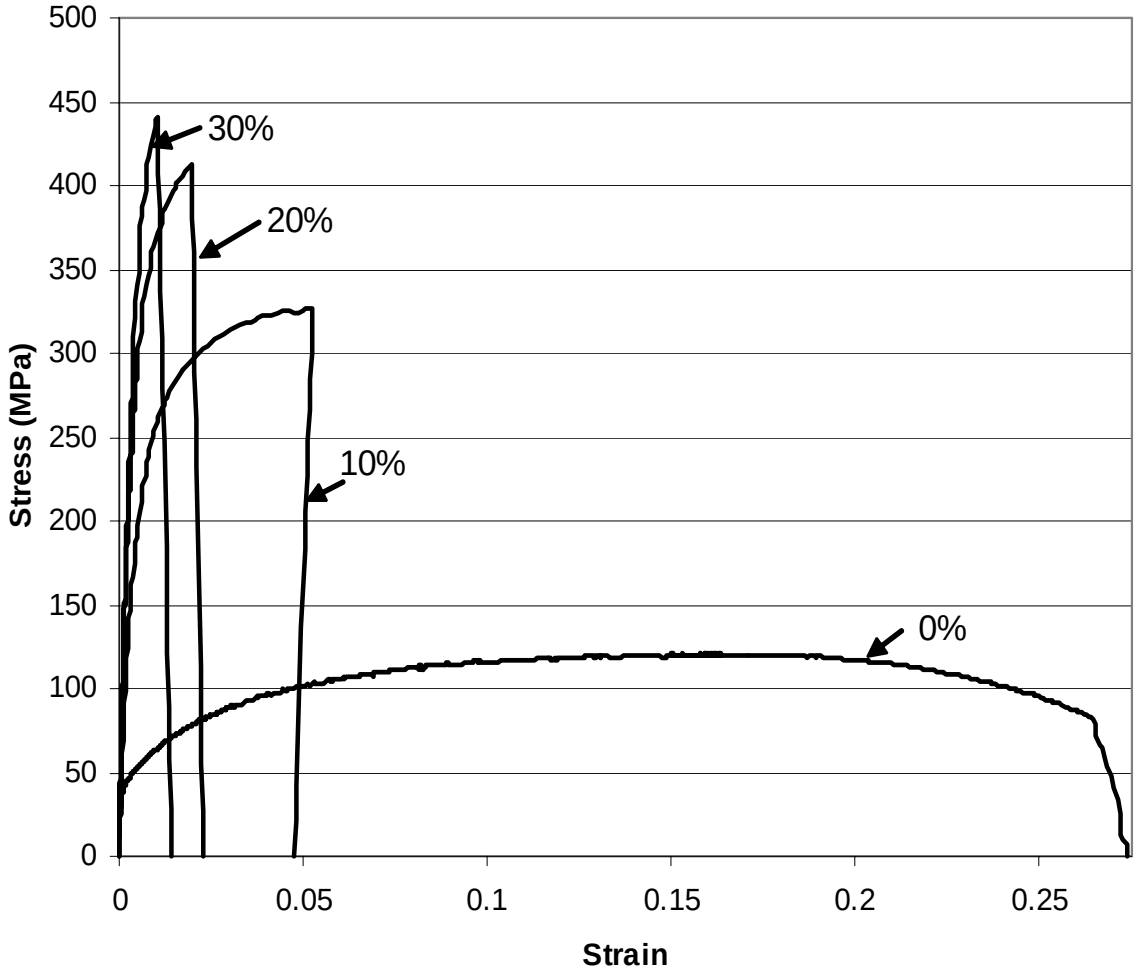

Fig. 4.11: Stress-strain curves for the all Al reinforced with Al_20_3 PRMMC composites.

Table 4.1 Tensile properties of Al reinforced with Al_20_3 PRMMC composites

	SAMPLE	0.2 % Yield strength (MPa)	Ultimate Tensile strength (MPa)	Young's modulus (GPa)	Percent strain to failure (mm/mm)
6061 Al alloy	Sample 1	50	130	70	30
	Sample 2	53	123	65	35
	Sample 3	36.5	112	64.09	23
	Average	68.03	121.53	68.03	29.26
10% v_f Al203 composite	Sample 1	180	326.11	78.48	6.26
	Sample 2	186	329.21	82.33	4.02
	Sample 3	187	329.33	99.62	3.9
	Average	184.33	328.22	86.81	4.72
20% v_f Al_20_3 composite	Sample 1	308	419.87	106.04	2.48
	Sample 2	293.88	392.64	105.91	2.16
	Sample 3	290.8	417.78	101.39	2.25
	Average	297.56	410.1	104.45	2.29
30% v_f Al_20_3 composite	Sample 1	354	452.91	111.06	0.9
	Sample 2	355	451.14	108.05	1.83
	Sample 3	355	442.25	110.59	1.53
	Average	354.67	448.77	109.9	1.42

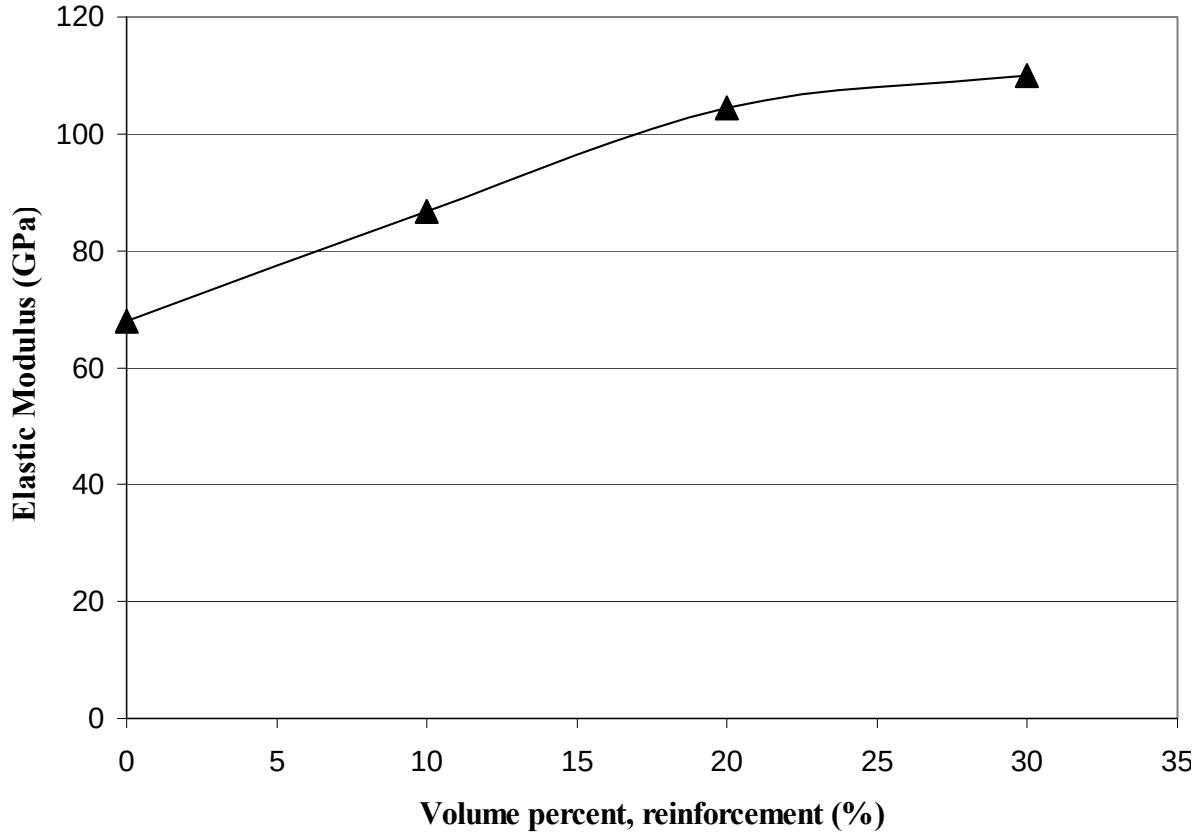

Fig. 4.12: Effect of reinforcement content on elastic modulus of Al reinforced with Al_20_3 PRMMC composites.

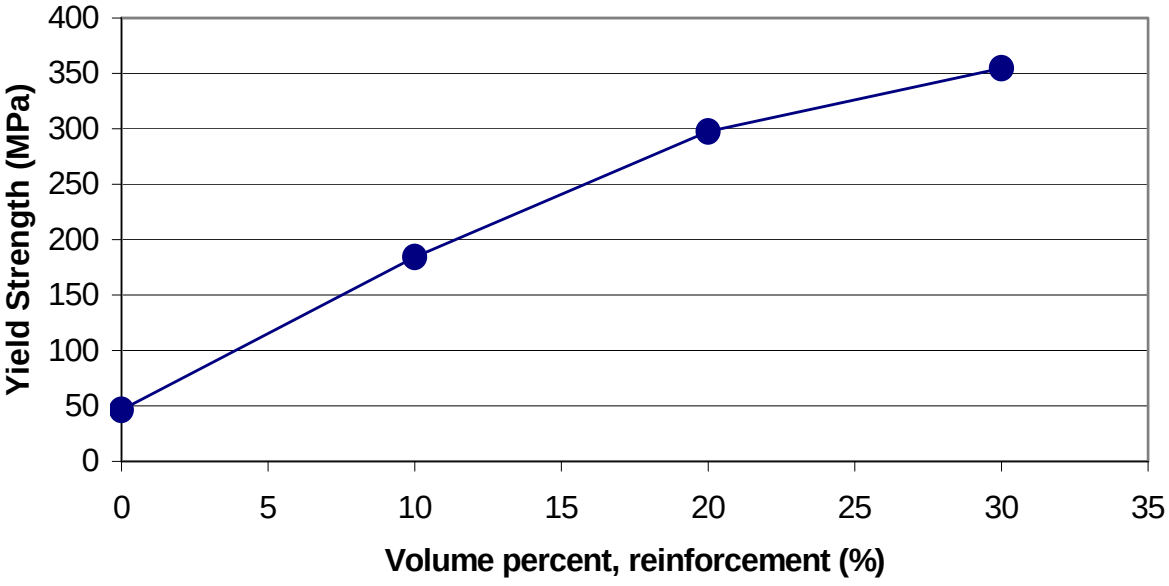

Fig. 4.13: Effect of reinforcement content on yield strength of Al reinforced with Al_20_3 PRMMC composites.

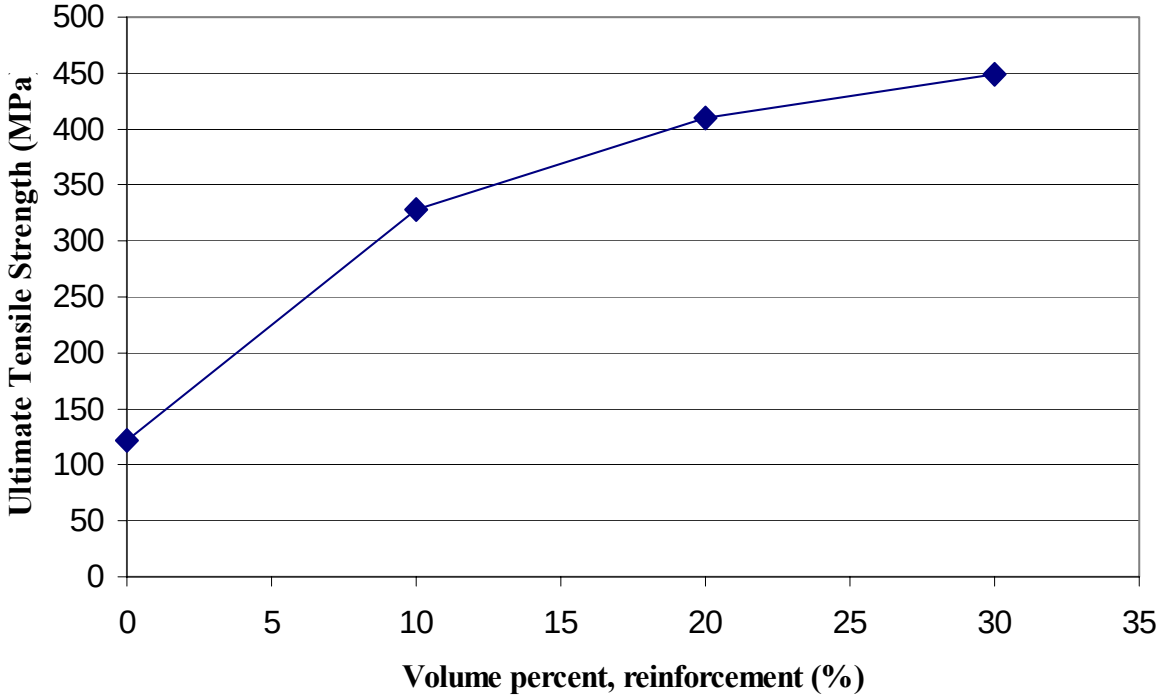

Fig. 4.14: Effect of reinforcement content on ultimate tensile strength of Al reinforced with Al_20_3 PRMMC composites.

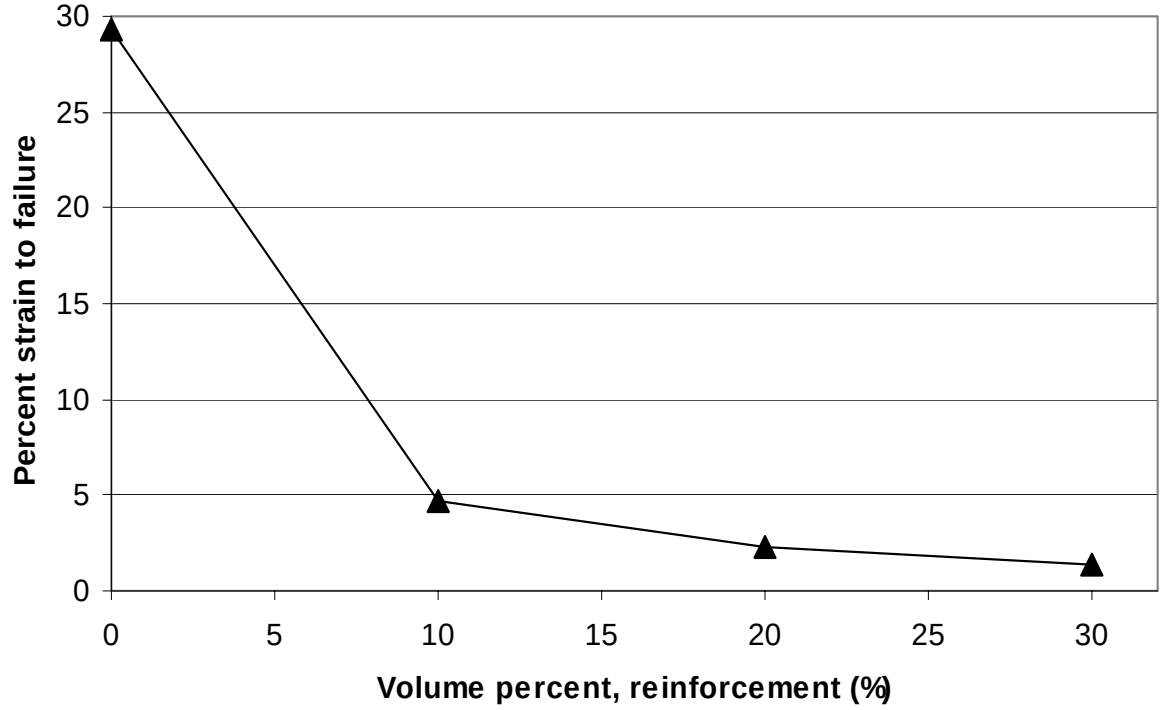

Fig. 4.15: Effect of reinforcement content on percent strain to failure of Al reinforced with Al_20_3 PRMMC composites.

4.16-4.17. The SEM fracture surface (Fig. 4.18-4.19) is dominated by uniform dimples with an average size of 3 to 4 μm, mostly circular shaped. The observed circular- shaped dimples where the necked regions in dimple area usually continuous and close on themselves. On other hand, the tear ridges do not form circular features and are often not continuous. The depth and rounded edges of the dimples indicate that there was considerable plastic deformation involved in the void coalescence process.

- **10% v_f Al_20_3 composite**

Fig. 4.20-4.21 shows the ductile fracture for this composite, with no appreciable necking formed. The fracture surface appearance on a microscopic scale shown in Fig. 4.22. Medium size dimples, with tear ridges, slightly smaller from those in Fig. 4.19 are observed in Fig. 4.22. The existence of the reinforcing Al_20_3 particles caused considerable change in the behavior of the fracture process. Average dimple size and shape are different for this composite from those observed in Fig. 4.19. In Figs. 4.23-4.25 the dimples are neither uniform nor circular in shape. In areas comparatively free of Al_20_3 particles, dimples appeared similar to those observed in the 6061 Al alloy, but their morphology were affected. Most of the particles are firmly embedded in the matrix as can be seen from Fig.4.24-4.25. At higher magnification matrix-particle decohesion was observed (Fig. 4.26). The final fracture was ductile involving the nucleation, growth, and coalescences of voids in the matrix around Al_20_3 particles.

- **20% v_f Al_20_3 Composite**

Fig. 4.27-4.28 reveals a fracture, which is intermediate between the ductile and brittle fracture. The fracture surface at a higher magnification is shown in Fig. 4.29 with extensive microvoids in the matrix. In Fig. 4.30 the dimples are different from those in Fig. 4.19 both in size and shape, but similar to those observed in Fig. 4.23. At a higher

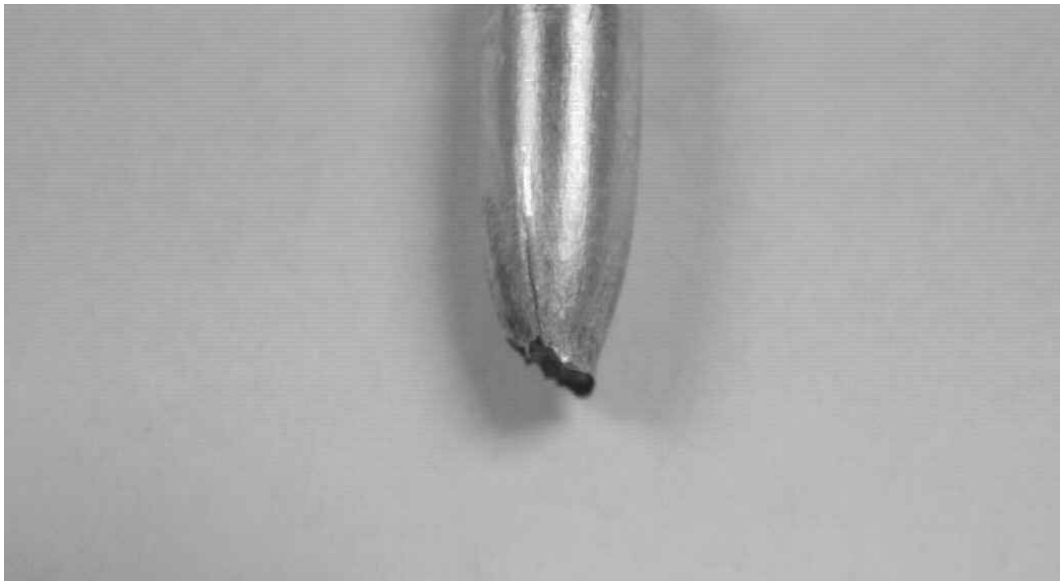

Fig. 4.16: Optical micrograph of 6061 Al alloy showing diameter contraction.

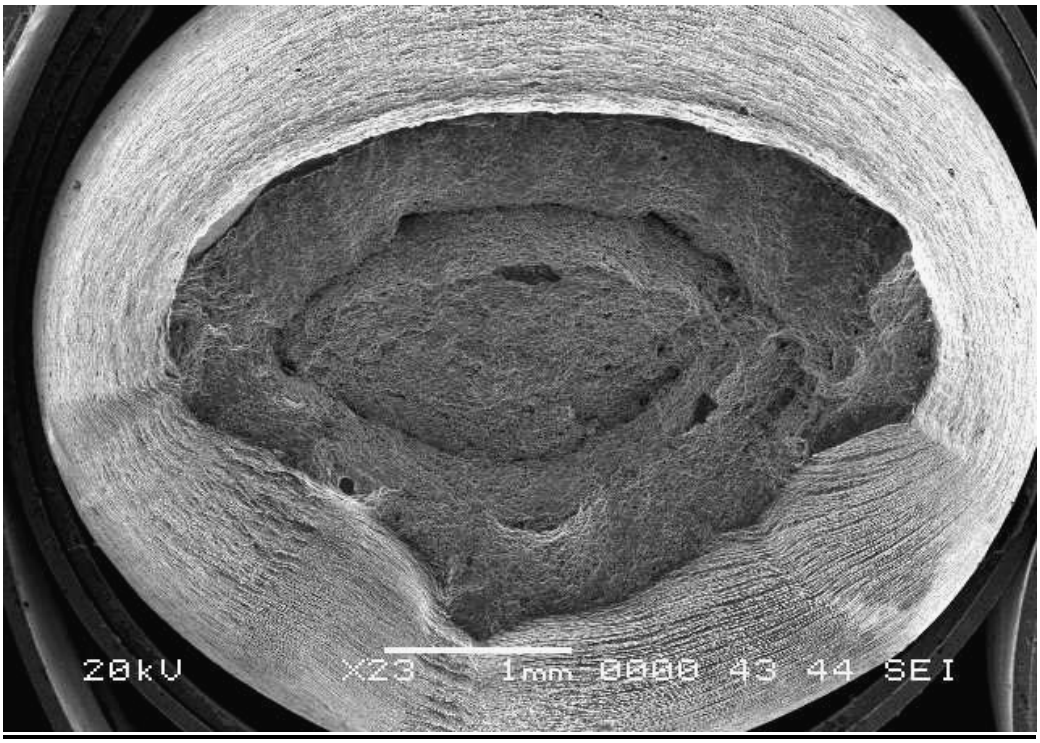

Fig. 4.17: SEM fractograph of 6061 Al alloy showing diameter contraction (cross section) at magnification 23X.

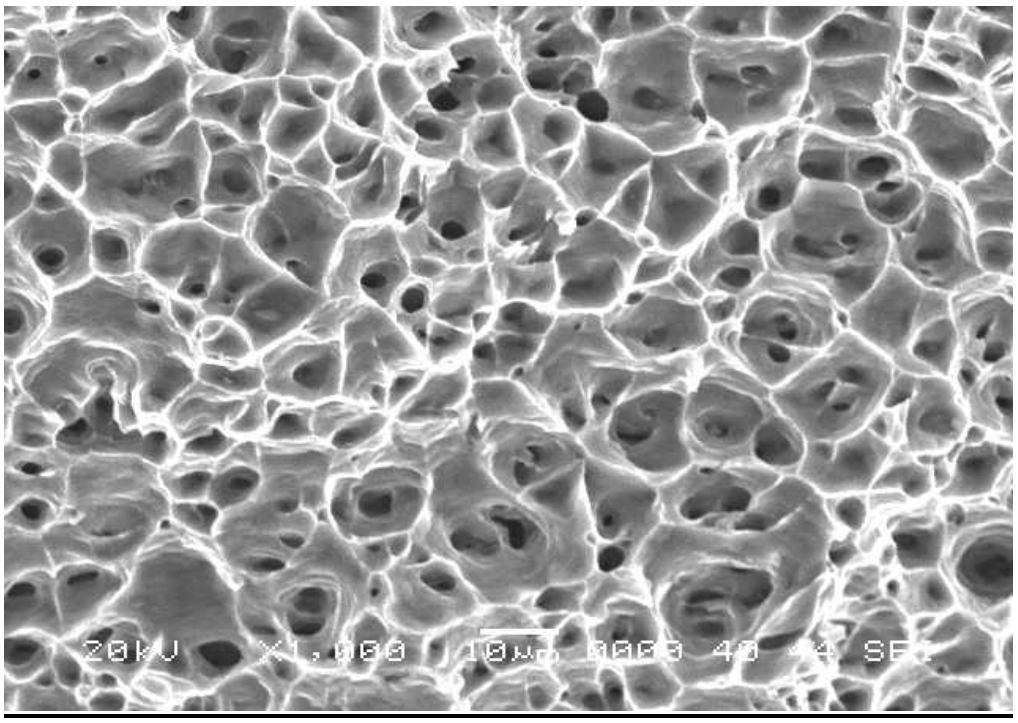

Fig. 4.18: SEM tensile fracture surface of 6061 Al alloy showing dimple structure.

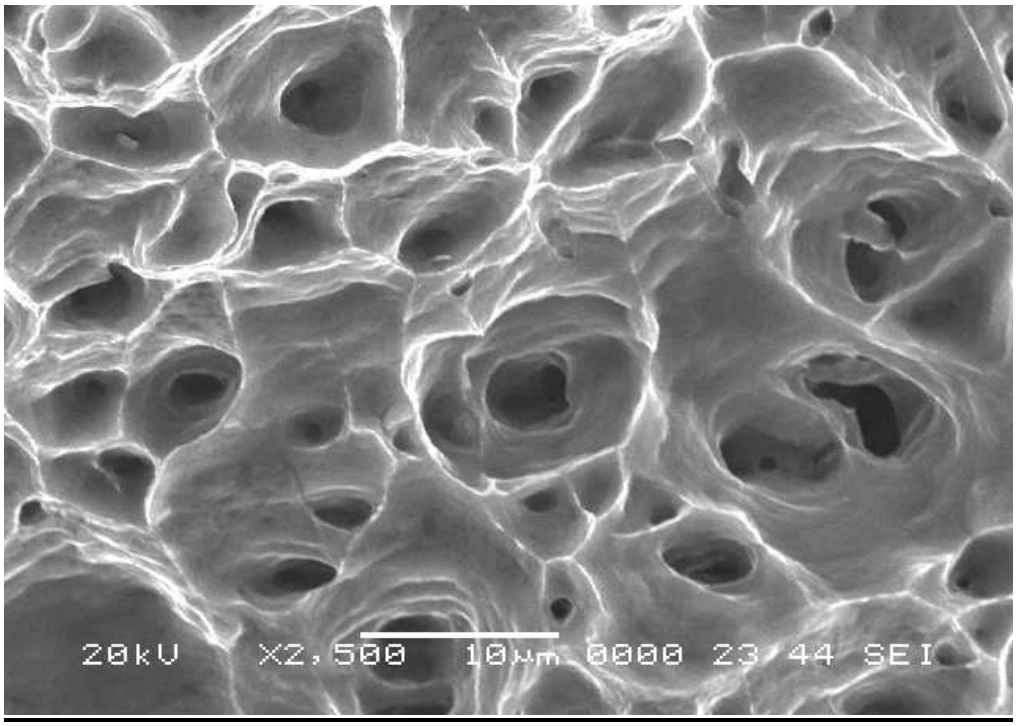

Fig. 4.19: SEM tensile fracture surface of 6061 Al alloy showing dimple structure at magnification of 2500X.

magnification scale matrix-particle decohesion was observed (Fig. 4.31-4.33).

- **30% v_f Al_20_3 Composite**

  Fig. 4.34-4.35 shows the fracture surface of the 30% v_f Al_20_3 composite. The fracture surface appears to be flat and normal to stress axis. At higher magnification (Fig. 4.36), the fracture surface appears to contain many microvoids in the matrix, with dimples that are much different from those observed in Fig. 4.23, both in size and shape. When compared with the fracture surface of the 10% v_f Al_20_3 composite (Fig. 4.23) and the 20% v_f Al_20_3 composite (Fig. 4.30) the number of dimples (density) in Fig. 4.37 are fewer, even though they are similar both in size and shape. Matrix-particle decohesion was also observed for this composite, but more extensively than those observed for the 10%, 20% v_f composites (Fig. 4.38-4.39).

Sudden failure of the sample indicates that void growth and coalescence occurred rapidly. When one decohesion occurred the stresses released cannot be taken up by the matrix and are transferred to neighboring particles, initiating a chain reaction. The final fracture mechanism in tensile test was the growth and coalescence of voids in the matrix. Voids were nucleated and contributed to final coalescence. Also Fig. 4.40 shows extensive decohesion at matrix-particle interface.

Smaller interparticle distance hindered matrix infiltration among the particles, and as a result, the interfacial bonding was poor and the porosity elevated in these regions. The fewer number of dimples in the matrix as a dominant fracture mode is primarily due to the constraints on plastic flow caused by the Al_20_3 particles, (i.e.) the deformation incompatibility between the plastically deforming 6061 Al metal matrix and the elastically deforming Al_20_3 particles.

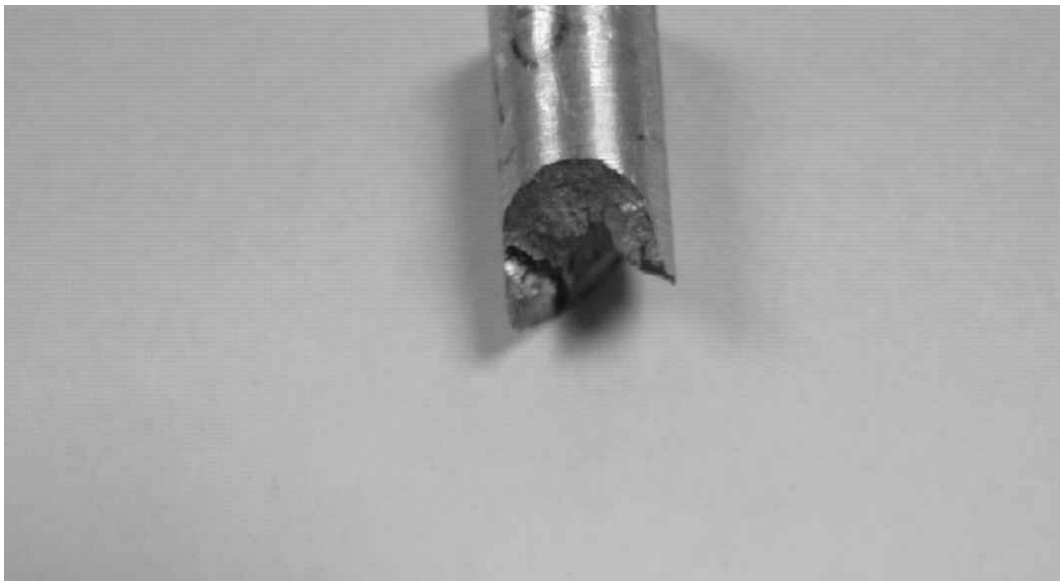

Fig. 4.20: Optical micrograph of 10% v_f Al_2O_3 composite showing no necking.

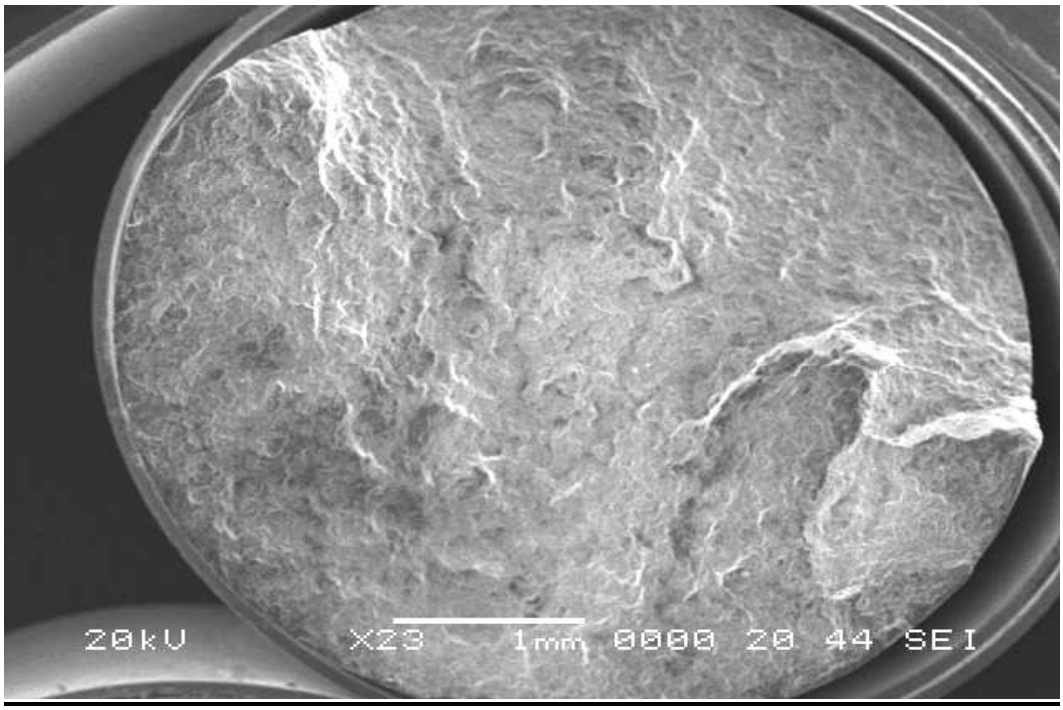

Fig. 4.21: SEM tensile fracture surface of 10% v_f Al_2O_3 composite showing no necking (cross section) at magnification of 23X.

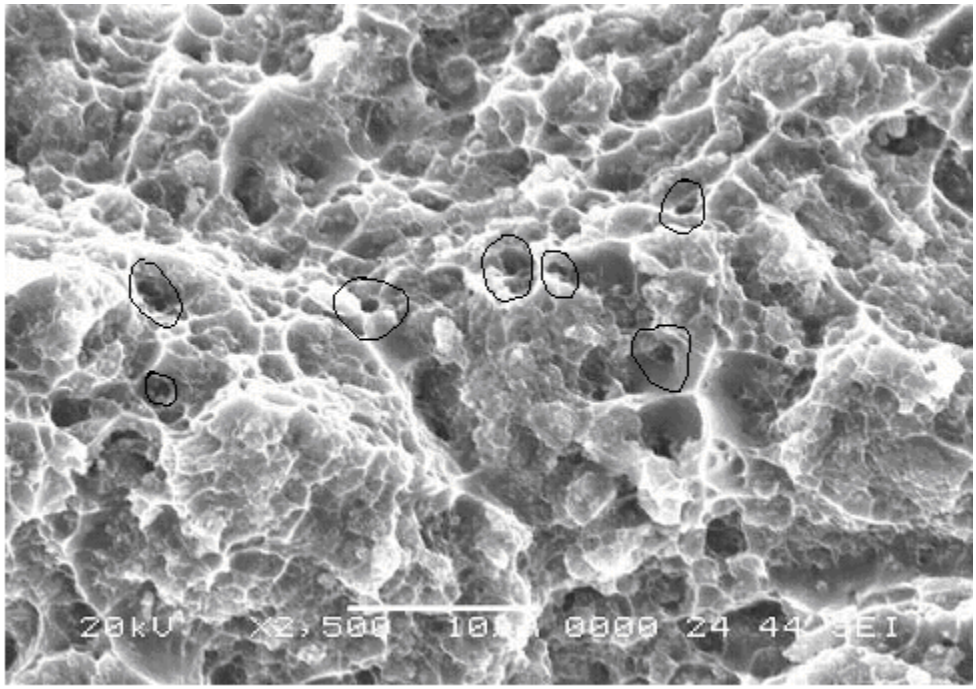

Fig. 4.22: SEM tensile fracture surface of 10% v_f Al_2O_3 composite at magnification of 2500X. Circled regions show voids.

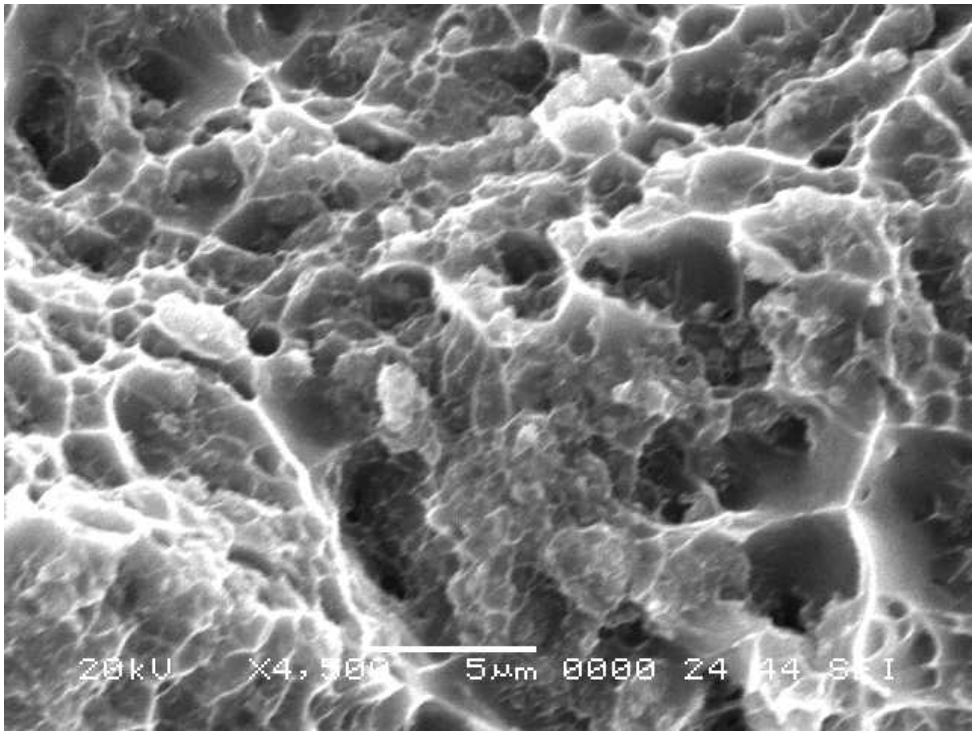

Fig. 4.23: SEM tensile fracture surface of 10% v_f Al_2O_3 composite showing dimples at magnification 4500X.

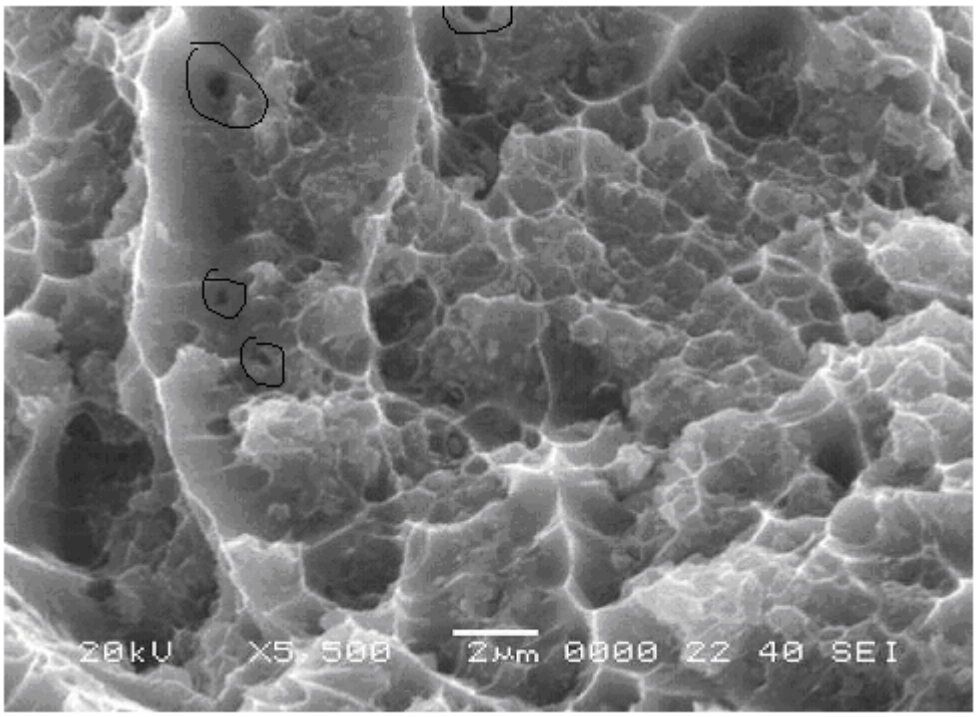

Fig. 4.24: SEM tensile fracture surface of 10% v_f Al_2O_3 composite showing dimples at magnification of 5500X. Circled regions show voids.

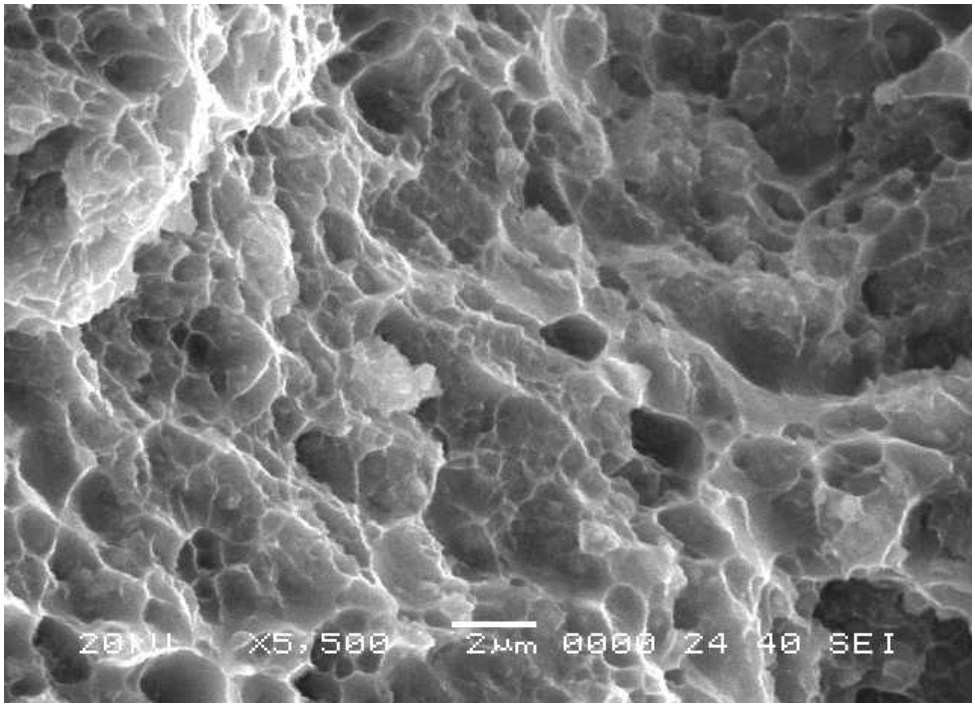

Fig. 4.25: SEM tensile fracture surface of 10% v_f Al_2O_3 composite showing dimples at different location (at magnification 5500X).

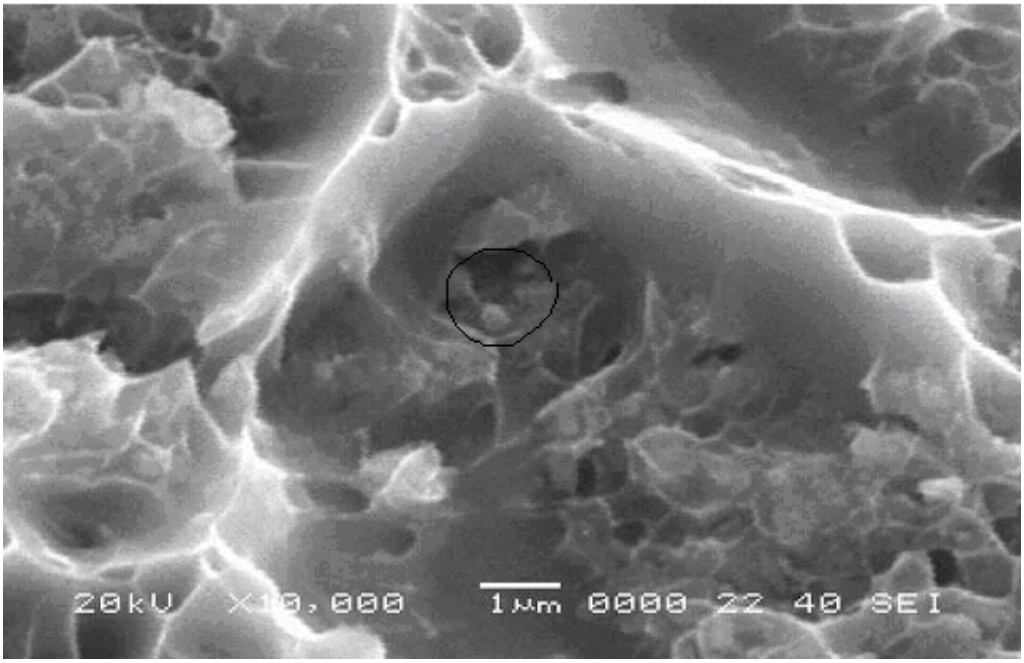

Fig. 4.26: SEM tensile fracture surface of 10% v_f Al_2O_3 composite showing matrix particle decohesion (circled region) at magnification of 10,000X.

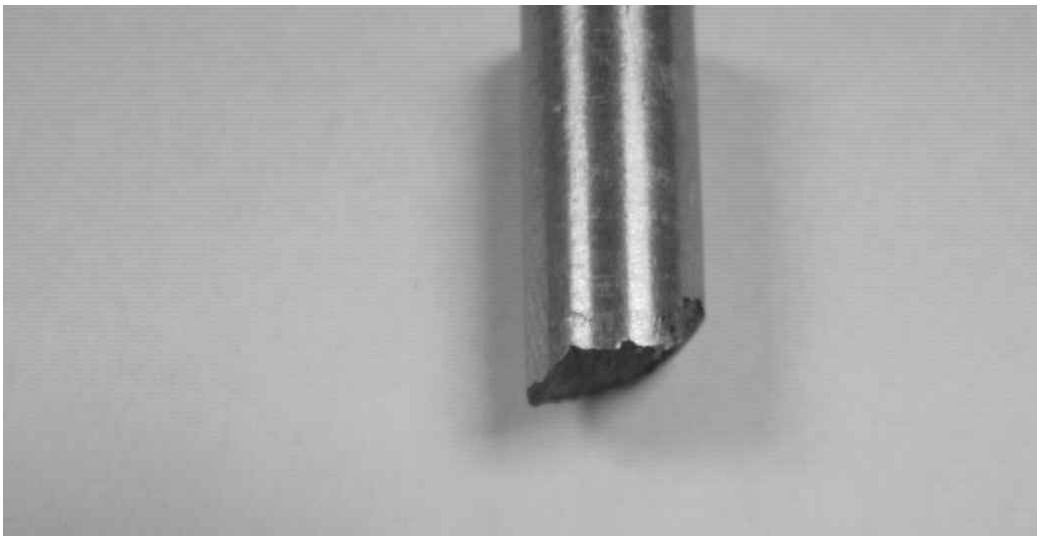

Fig. 4.27: Optical micrograph showing tensile fracture of 20% v_f Al_2O_3 composite.

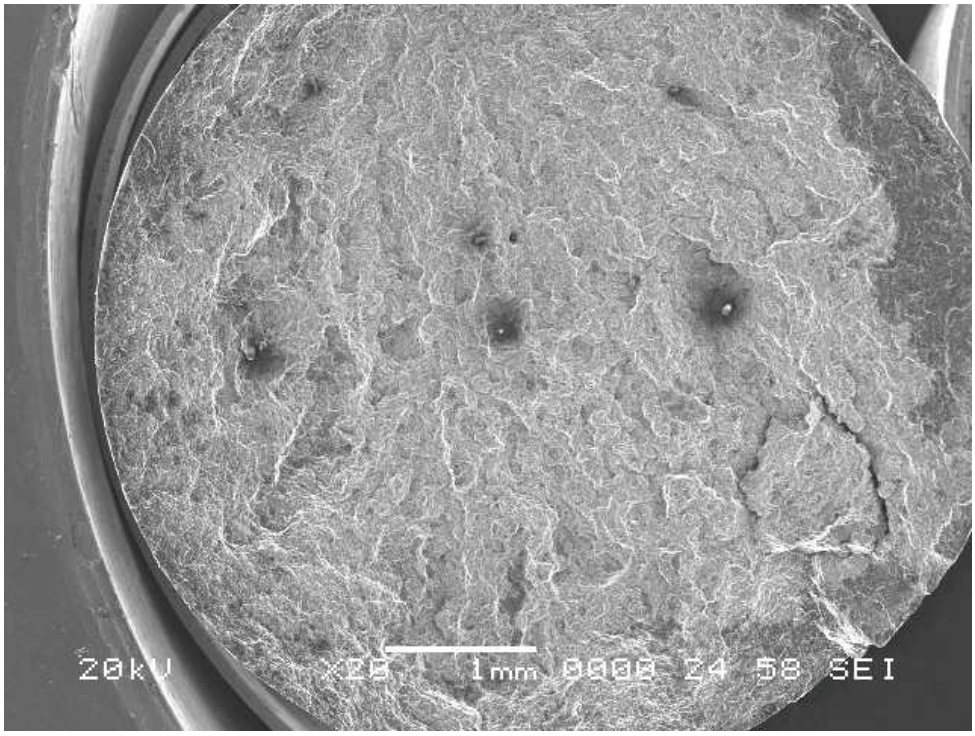

Fig. 4.28: SEM tensile fracture surface of 20% v_f Al_2O_3 composite at magnification of 20X.

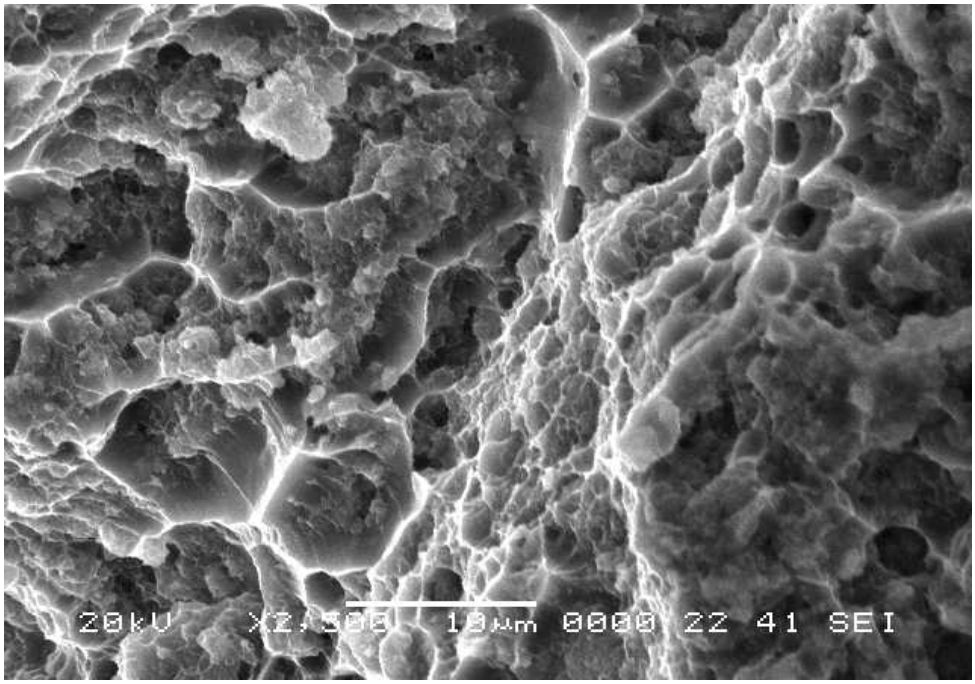

Fig. 4.29: SEM tensile fracture surface of 20% v_f Al_2O_3 composite at magnification of 2500X.

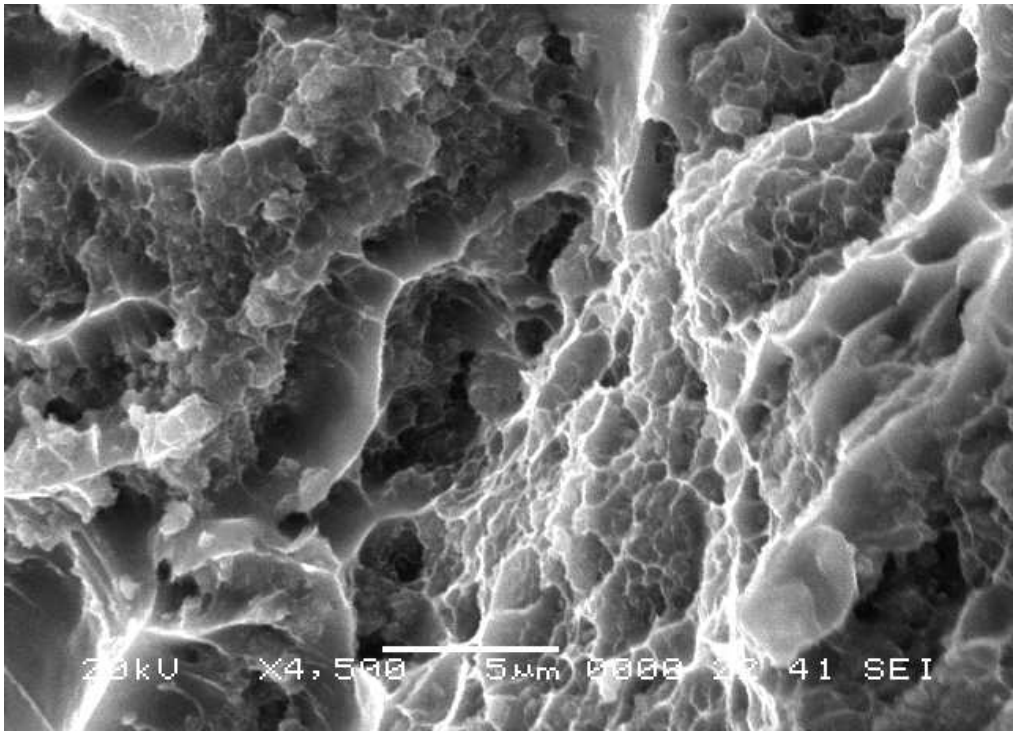

Fig. 4.30: SEM tensile fracture surface of 20% v_f Al_2O_3 composite showing dimples at magnification of 4500X.

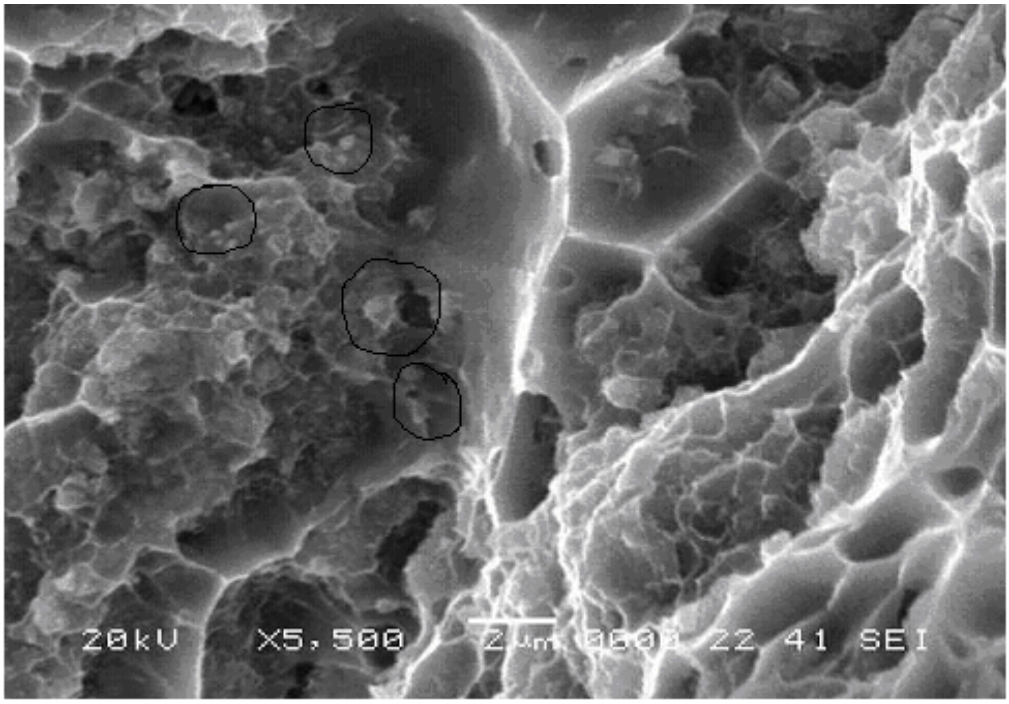

Fig. 4.31: SEM tensile fracture surface of 20% v_f Al_2O_3 composite showing matrix-particle decohesion (circled regions) at magnification of 5500X.

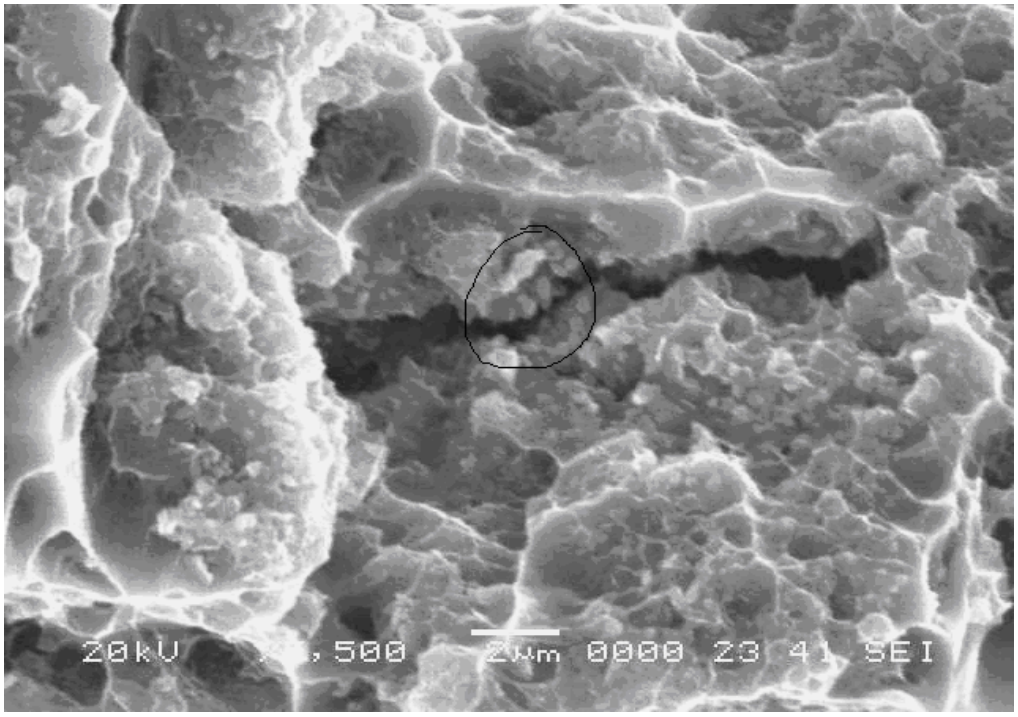

Fig.4.32: SEM tensile fracture surface of 20% v_f Al_2O_3 composite showing matrix-particle decohesion at cracking (magnification of 5500X).

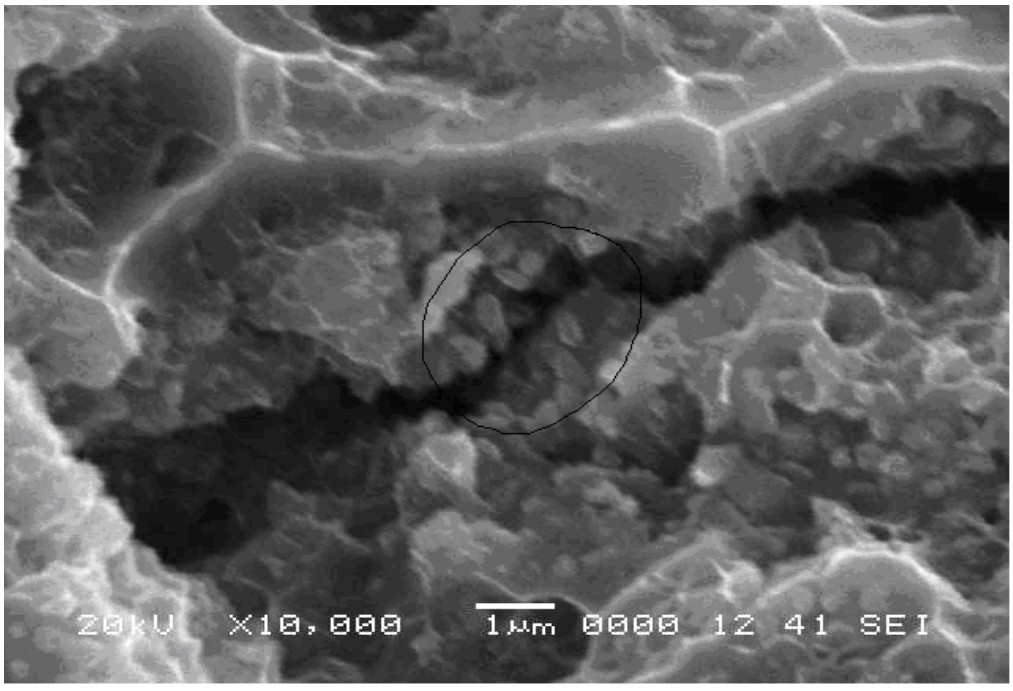

Fig. 4.33: SEM tensile fracture surface of 20% v_f Al_2O_3 composite showing matrix-particle decohesion (at cracking) at magnification of 10,000X.

Fig. 4.34: Optical micrograph showing tensile fracture surface of 30% v_f $Al_2 0_3$ composite, which is flat and normal to stress axis.

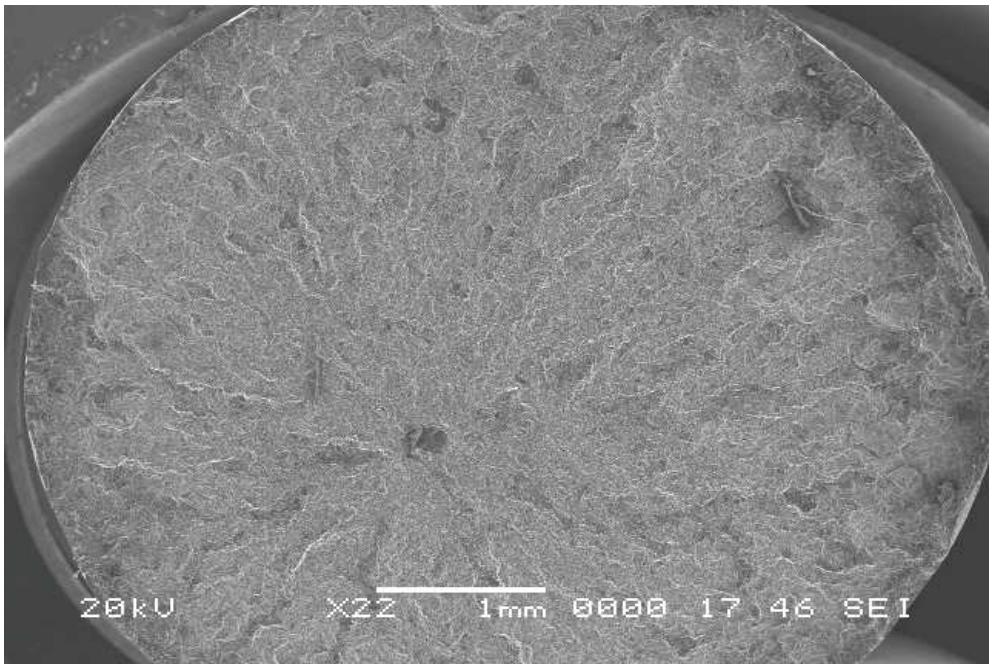

Fig. 4.35: SEM tensile fracture surface of 30% v_f $Al_2 0_3$ composite, which is flat and normal to stress axis (cross section) at magnification of 22X.

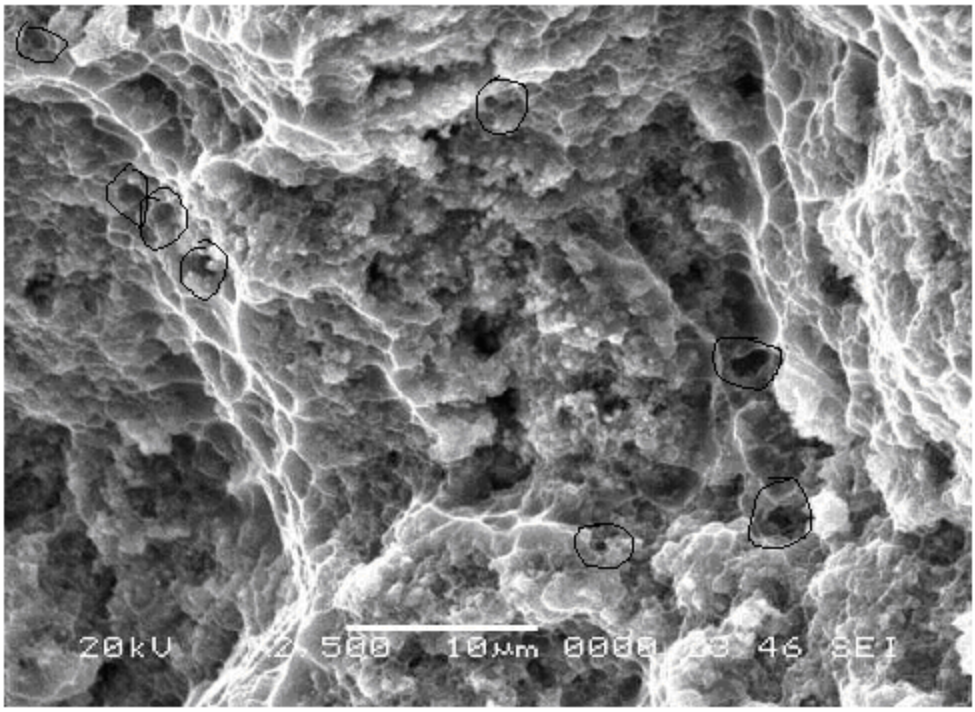

Fig. 4.36: SEM tensile fracture surface of 30% $v_f Al_2 0_3$ composite at magnification of 2500X.

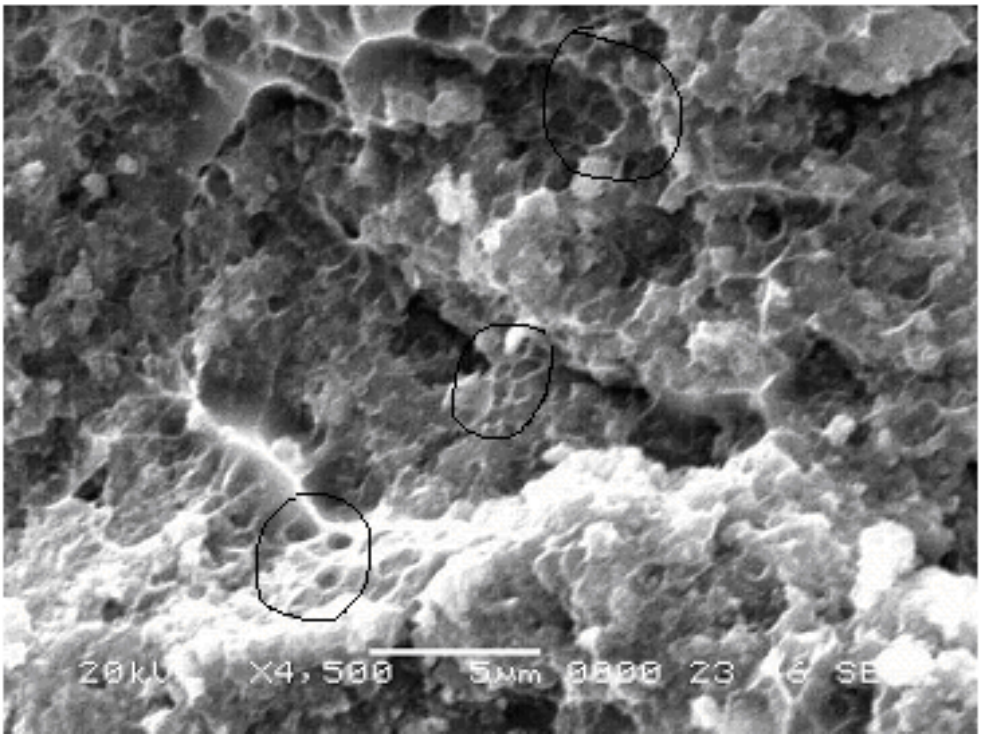

Fig. 4.37: SEM tensile fracture surface of 30% $v_f Al_2 0_3$ composite showing dimples (circled regions).

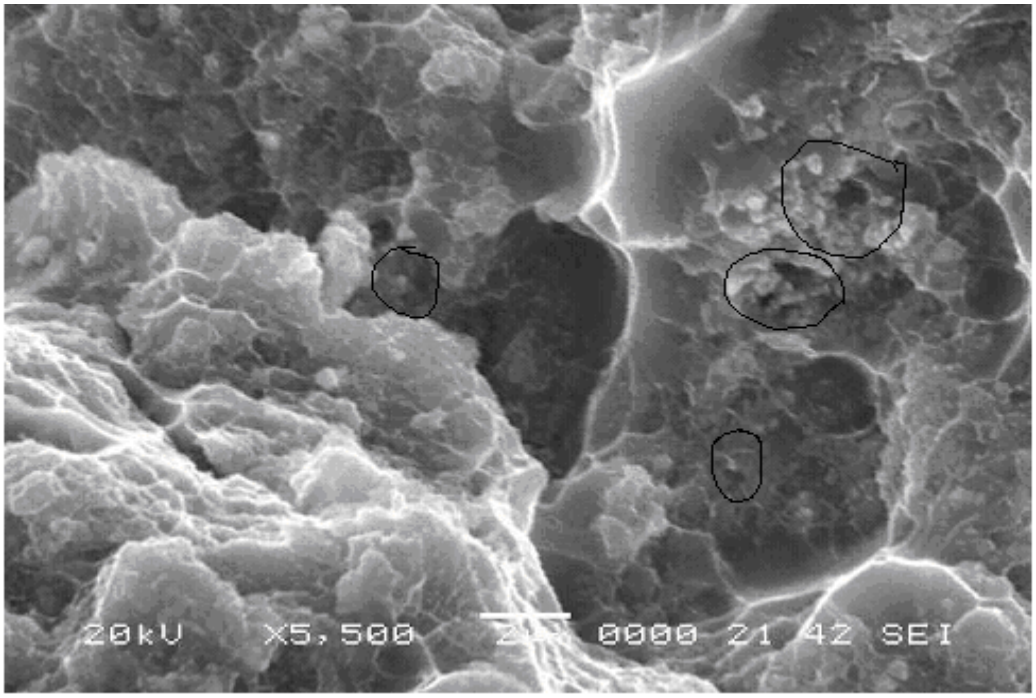

Fig. 4.38: SEM tensile fracture surface of 30% $v_f Al_2 0_3$ composite showing matrix-particle decohesion (circled regions) at magnification of 5500X.

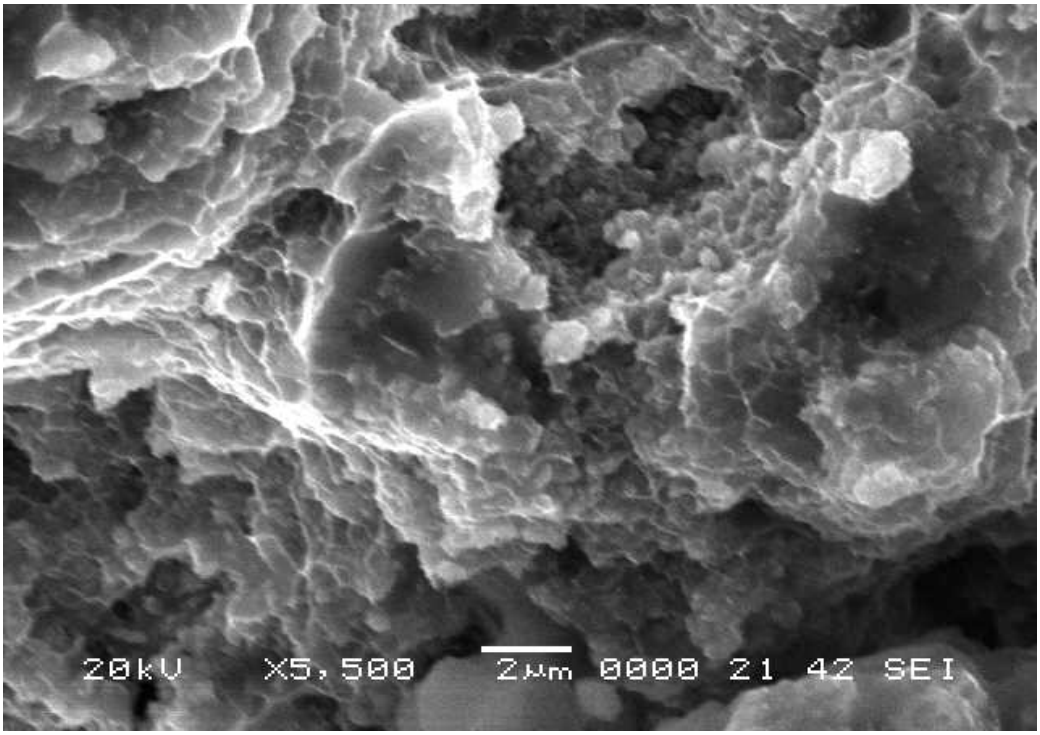

Fig. 4.39: SEM tensile fracture surface of 30% $v_f Al_2 0_3$ composite showing dimples at magnification of 5500X.

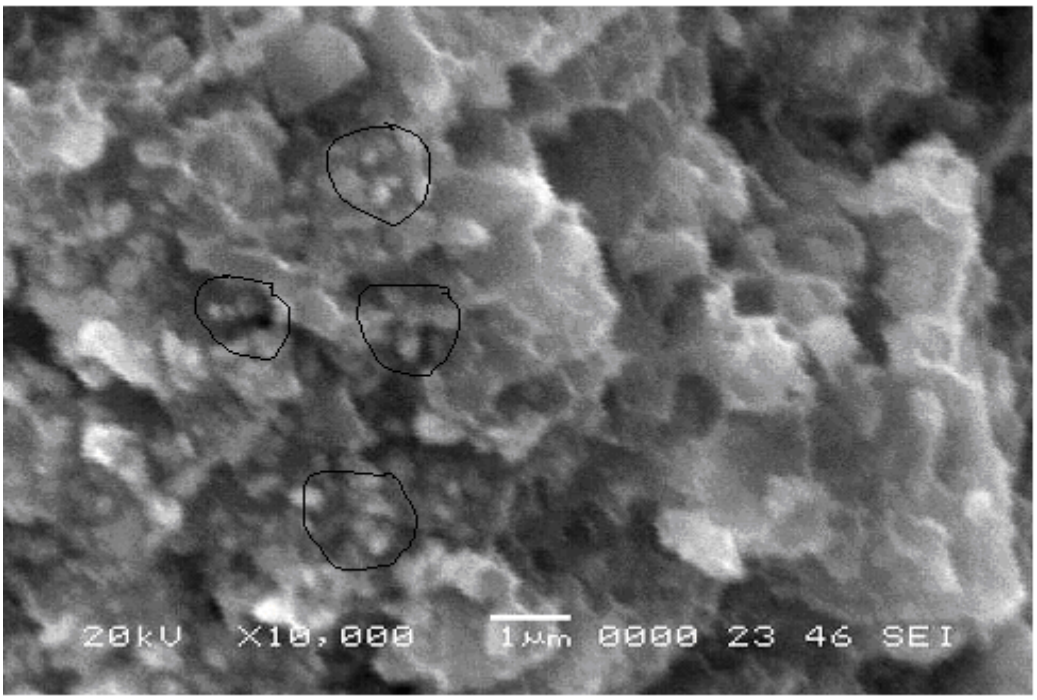

Fig. 4.40: SEM tensile fracture surface of 30% $v_f Al_2 0_3$ composite showing matrix-particle decohesion (circled regions) at magnification of 10,000X.

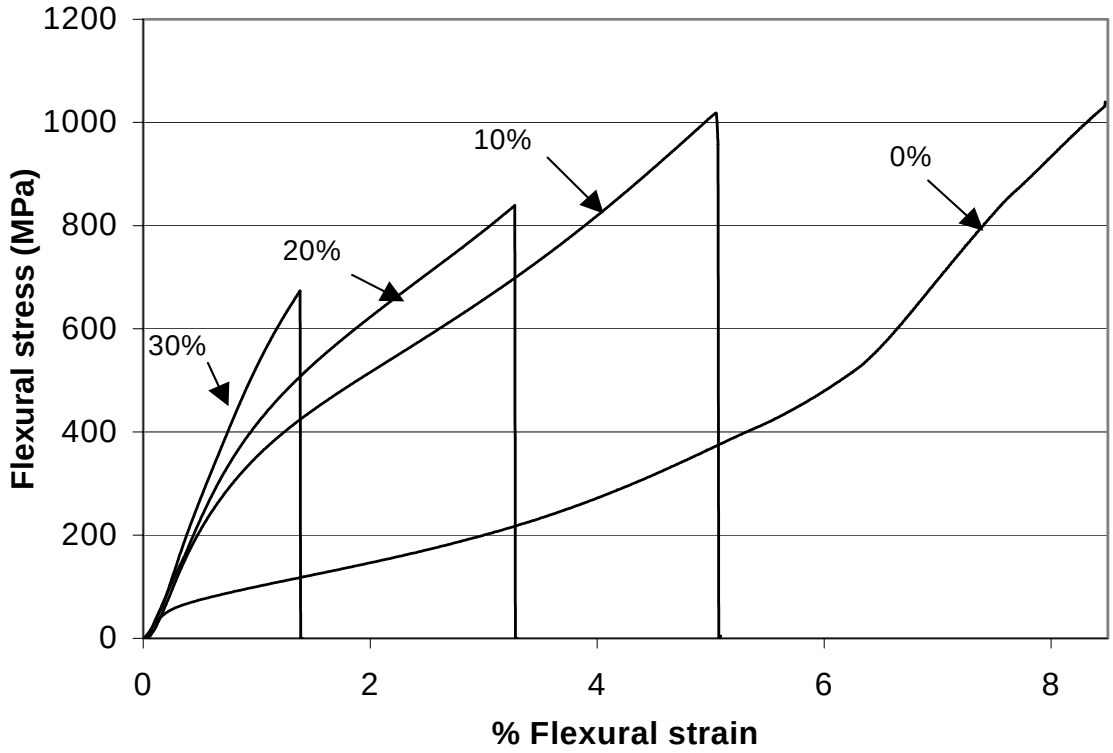

Fig. 4.41: Flexural stress-flexural strain curves for Al alloy reinforced with $Al_2 0_3$ PRMMC composites.

4.3 FLEXURAL STRENGTH

Rectangular composite samples of 8 x 6 mm cross-section and 40 mm span were placed inside a four-point support fixture, such that polished surfaces (l μm finish) of the inner span were loaded in tension. The load was applied at the crosshead speed of 0.254 mm/min until the sample was fractured, using an Instron 5569 testing machine. Inspection of fractured pieces recovered after each test revealed that fractures occurred somewhere within the inner span of tested samples. The fracture load (P) for each test was recorded, and the bending strength of the composite (σ_b) was calculated according to:

$$\sigma_b = \frac{3PL}{4bd^2}$$

Flexural stress- strain curves of all composites are plotted in the Fig. 4.41. The summary of flexural test results for Al alloy reinforced with Al_2O_3 PRMMC composites is listed in Table 4.2. The values of flexural stress are 1025.22, 829.34 and 708.51 MPa for the 10%, 20% and 30% v_f Al_2O_3 composites, respectively. The same difference, which is observed in tensile properties, that is the constraint imposed on the matrix is also observed in the flexural strength data. The aluminum alloy is able to flow plastically and blunt fracture-initiating flaws. Therefore the unreinforced 6061 alloy is much stronger in flexural loading than composites. Similarly is the case with the lower vol. % reinforced composites. The higher 30% v_f Al_2O_3 reinforced composite contained high pore density and voids; these pores and voids serve as large flaw sites, which enhance an advancing crack by creating stress concentrations.

The behavior of all the composites under flexural loading is shown in Fig. 4.41. The 30% v_f Al_20_3 composite absorbed less energy in fracture compared with the other composites, as demonstrated by the reduced area under stress-strain curve (Fig. 4.41).

- **Flexure fracture behavior**

- **10% v_f Al_20_3 Composite**

This composite exhibited a ductile fracture. A cross section of the fracture surface is shown in the Fig. 4.42. In Fig. 4.43-4.44 many dimples with tear ridges can be observed. The existence of the reinforcing Al_20_3 particles caused considerable change in the behavior of the fracture process. As can be seen in the fracture surface (Fig. 4.43-4.44) the dimples are neither uniform nor circular in shape. In areas comparatively free of Al_20_3 particles, dimples appeared to be uniform. Most of the particles are firmly embedded in the matrix (Fig. 4.45). One can see the existence of small microcracks (Fig. 4.46). At a higher magnification matrix-particle decohesion was also observed (Fig. 4.47).

The large number of dimples in Figs. 4.43-4.46 shows that great amount of plastic deformation occurred prior to crack initiation. This is related with good amount of ductility which can also be evidenced from the Fig 4.41, showing more area under stress-strain curve for the 10% v_f Al_20_3 composite. The final fracture was ductile involving the nucleation, growth, and coalescences of voids in the matrix around Al_20_3 particles.

- **20% v_f Al_20_3 Composite**

The fracture surface of the 20% v_f Al_20_3 composite is shown in the Figs. 4.48-4.51. Fig. 4.48 and 4.49 shows many micro cracks and microvoids in the matrix. At a

Table 4.2 Flexural properties of Al reinforced with Al_20_3 PRMMC composites

	Sample	Maximum Flexure load (KN)	Flexural strength (MPa)	Flexural modulus (MPa)
6061 Al alloy	sample 1	10.0543	1047.32	23969.63
	sample 2	9.83641	1024.63	23464.77
	sample 3	9.89771	1031.01	20644.19
	Average	9.92947	1034.32	22692.86
10% v_f Al_20_3 composite	sample 1	9.77553	1018.28	41141.83
	sample 2	9.57841	997.75	39331.08
	sample 3	10.17236	1059.62	38840.31
	Average	9.8421	1025.22	39771.07
20% v_f Al_20_3 composite	sample 1	6.41951	668.7	58533.64
	sample 2	8.05362	838.92	48701.48
	sample 3	9.41176	980.39	53794.72
	Average	7.96163	829.34	53676.61
30% v_f Al_20_3 composite	sample 1	6.3539	661.86	69298.68
	sample 2	7.58731	790.35	60618.94
	sample 3	6.46378	673.31	60603.31
	Average	6.80166	708.51	63506.98

higher magnification matrix-particle decohesion was observed (Fig. 4.50-4.51). In Fig. 4.50 it is obvious that the crack deviated by the presence of the particles. The fracture behavior of this composite is one, which is intermediate between the ductile and brittle fracture. This fact is also clear from the stress–strain curve (Fig. 4.41) where area under stress-strain curve for this composite is intermediate between those for the 10 and the 30% v_f Al_2O_3 composites, respectively.

- **30% v_f Al_2O_3 Composite**

Cross sections of fracture surface for the 30% v_f Al_2O_3 composite are shown in the Figs. 4.52-4.55. Fig. 4.52 shows many microvoids and minute cracks in the matrix. Fig. 4.53-4.54, which is a higher magnification show several matrix-particle decohesion and cracks. Fig. 4.54 shows extensive decohesion at matrix-particle interface. The higher magnification of Fig. 4.54, which is shown in Fig. 4.55, clearly shows the deviation of cracks at the particles. The sharp load drop showed in Fig. 4.41 for the 30% v_f Al_2O_3 composite can be attributed to the formation of macroscopic cracks in the composite; this is also evidenced from Figs. 4.52, 4.54 and 4.55 by the increase in the number of cracks.

Fig.4.55 also shows other particle profile irregularities at the matrix-particle interfaces, with sharp corners of the particles that tend to increase the constraint to plastic flow and increase the local triaxial stresses. The high triaxial stresses and plastic strains increase the chances of damage initiation by void formation and debonding. Therefore matrix-particle interface are often the probable site for the initiation of damage. This 30% v_f Al_2O_3 composite has many pores and voids, which serve as large flaws. The presence of voids, triaxial stresses and less ductile aluminum alloy to provide for blunting of the cracks makes fracture path easier, resulting in a brittle like fracture

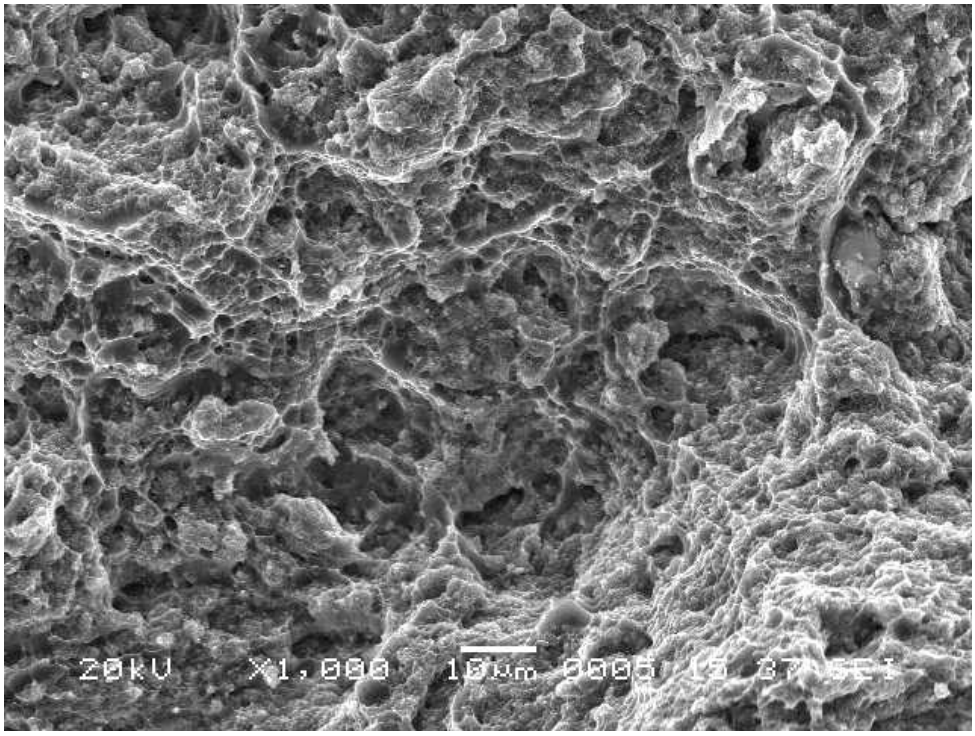

Fig. 4.42: SEM flexural fracture surface of 10% v_f Al_2O_3 composite at magnification of 1000X.

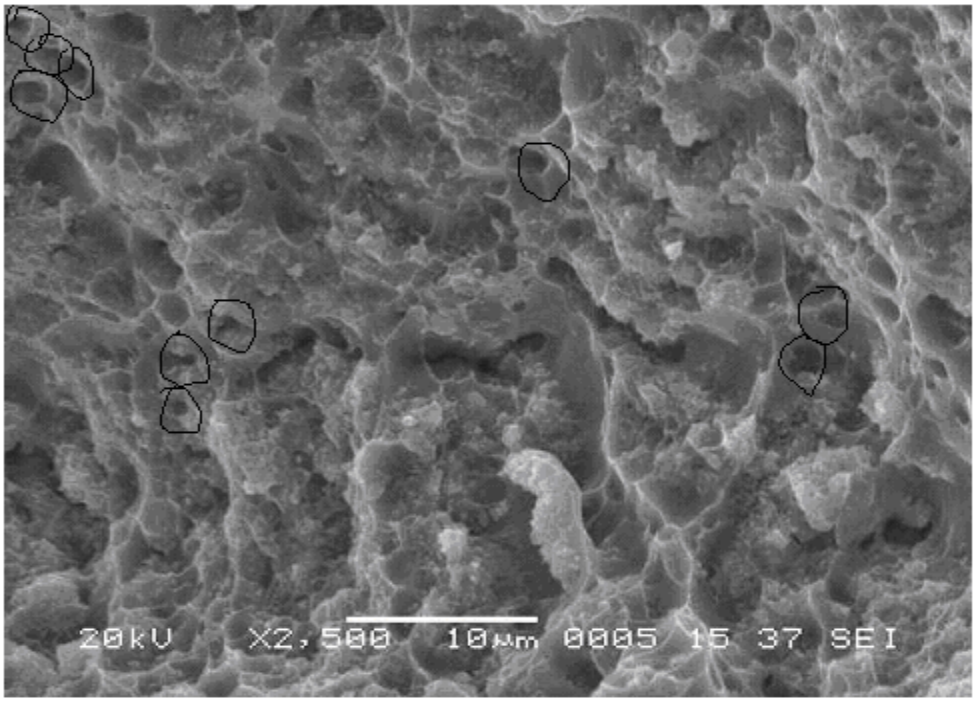

Fig. 4.43: SEM flexural fracture surface of 10% v_f Al_2O_3 composite at magnification of 2500X showing dimples, circled regions show voids.

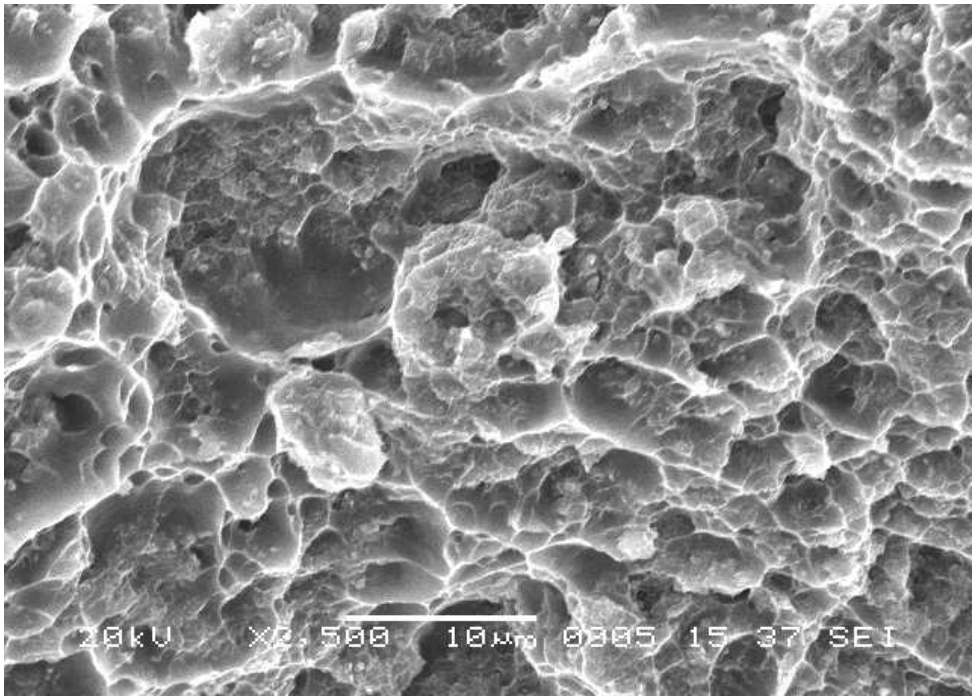

Fig. 4.44: SEM flexural fracture surface of 10% v_f Al_2O_3 composite at magnification of 2500X showing dimples with tear ridges.

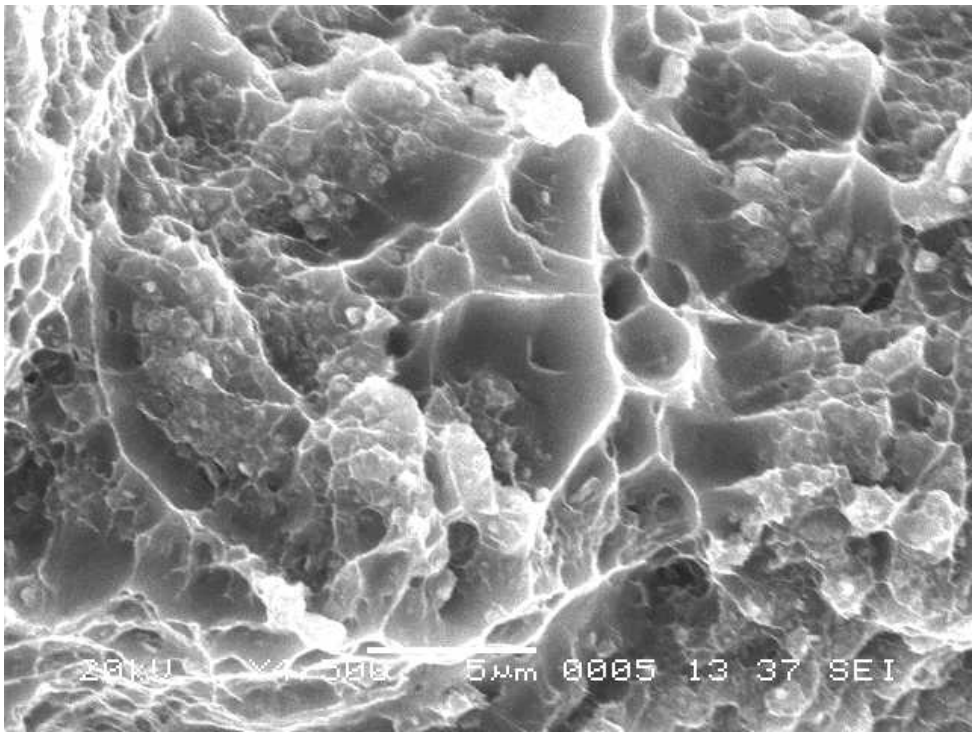

Fig. 4.45: SEM flexural fracture surface of 10% v_f Al_2O_3 composite showing dimples with embedded particles at magnification of 4500X.

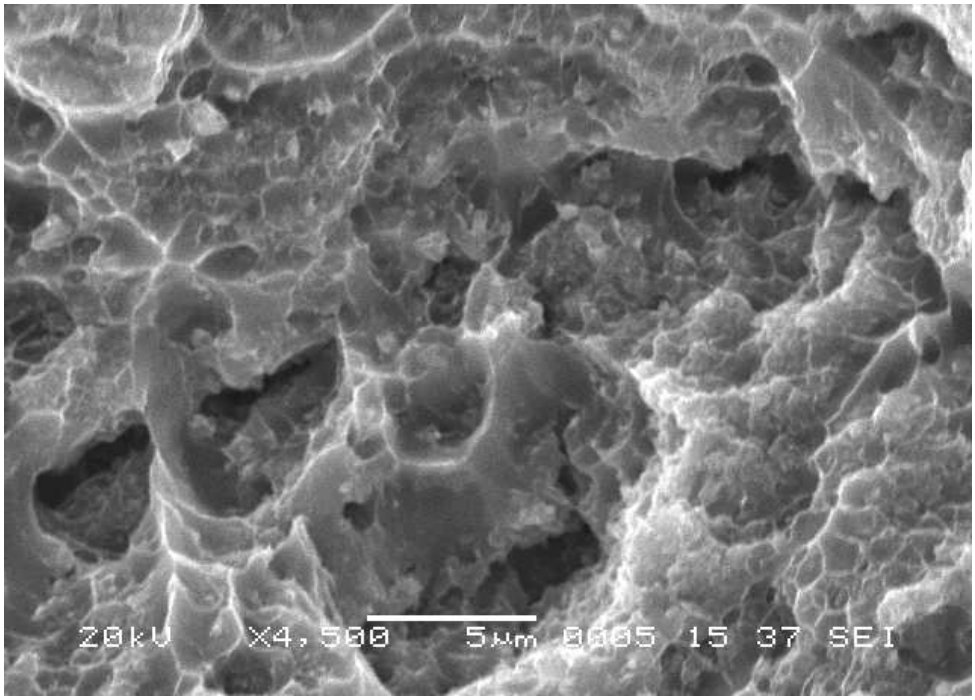

Fig. 4.46: SEM flexural fracture surface of 10% $v_f Al_2 0_3$ composite showing cracks at magnification of 4500X.

Fig. 4.47: SEM flexural surface of 10% $v_f Al_2 0_3$ composite showing matrix particle decohesion (circled regions) at magnification of 10,000X.

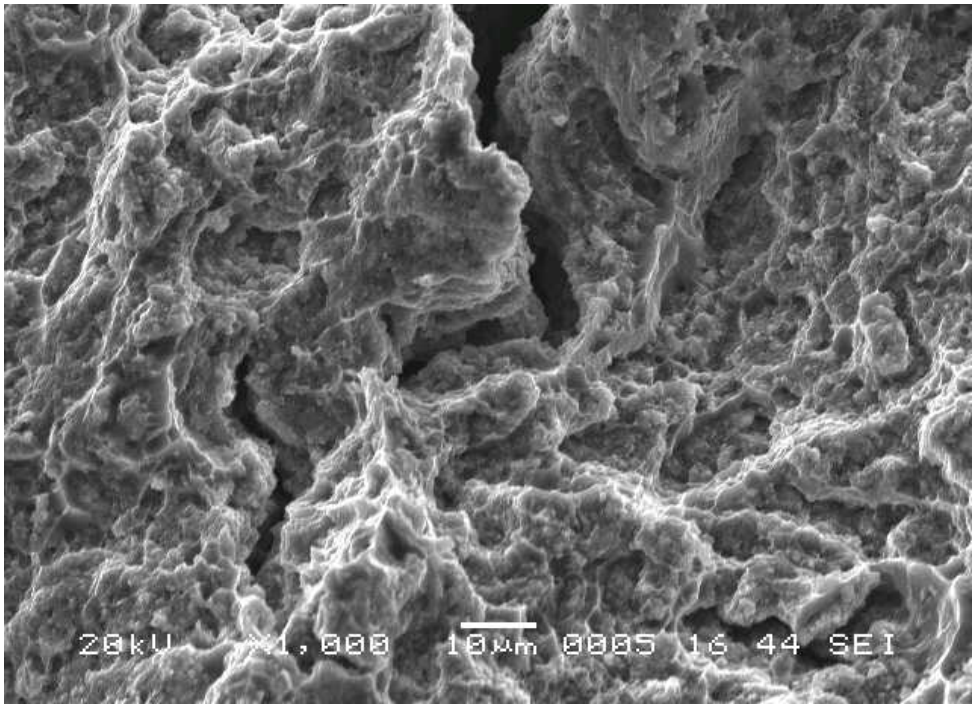

Fig. 4.48: SEM flexural fracture surface of 20% v_f Al_2O_3 composite at magnification of 1000X.

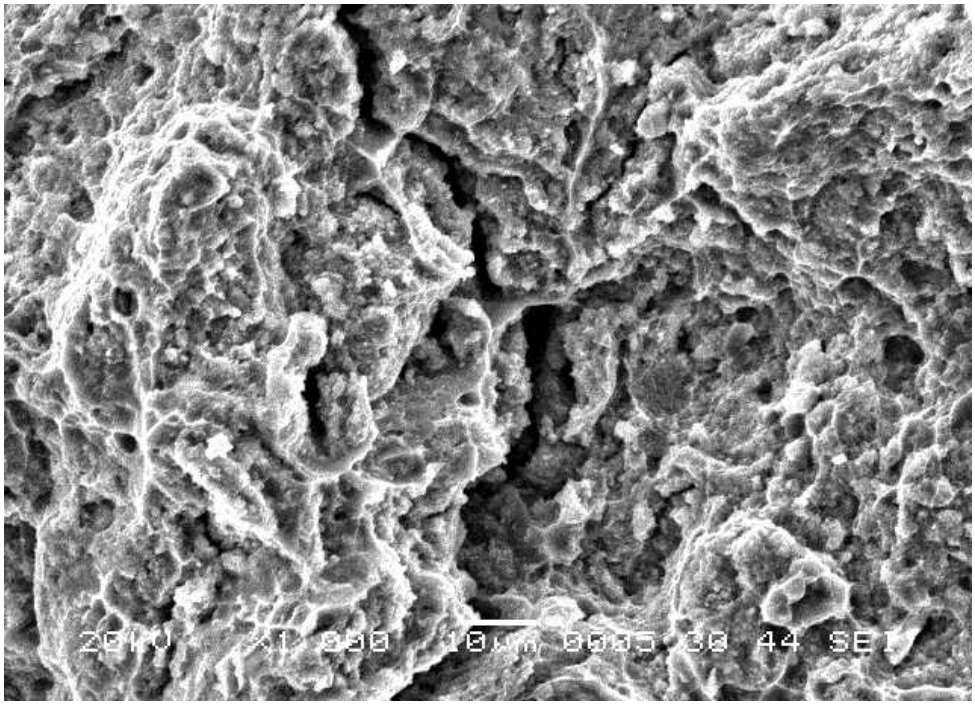

Fig. 4.49: SEM flexural fracture surface of 20% v_f Al_2O_3 composite showing extensive cracking at magnification of 1000X.

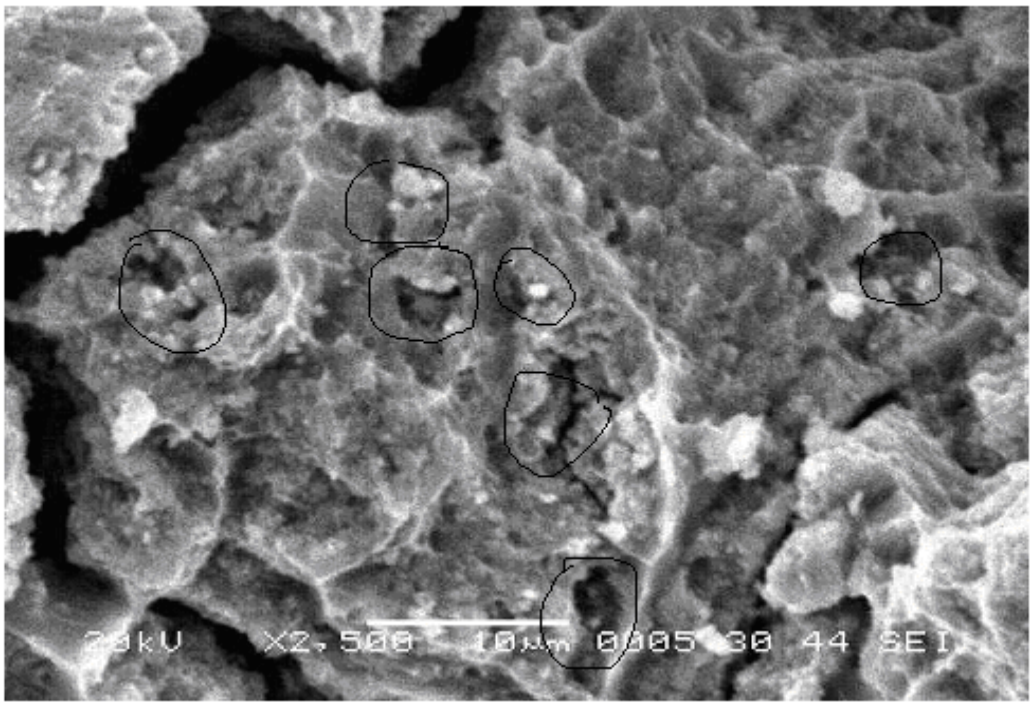

Fig. 4.50: SEM flexural fracture surface of 20% v_f Al_2O_3 composite showing cracks and decohesion (circled regions) at magnification of 2500X.

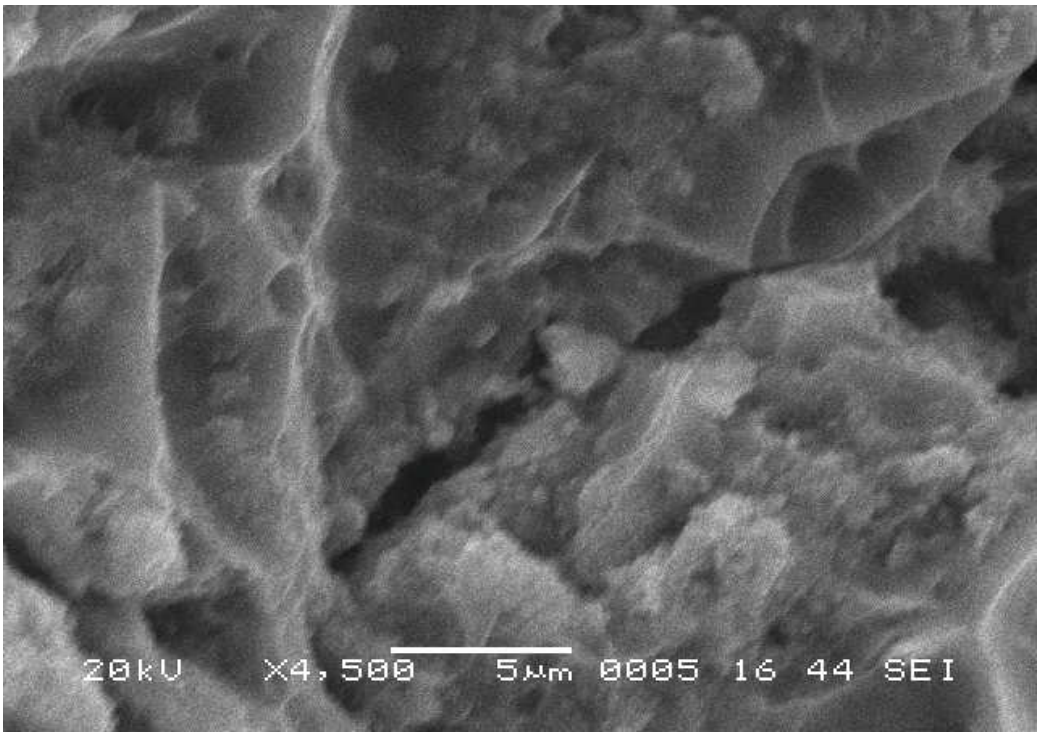

Fig. 4.51: SEM flexural fracture surface of 20% v_f Al_2O_3 composite showing matrix particle decohesion (at crack) at magnification of 4500X.

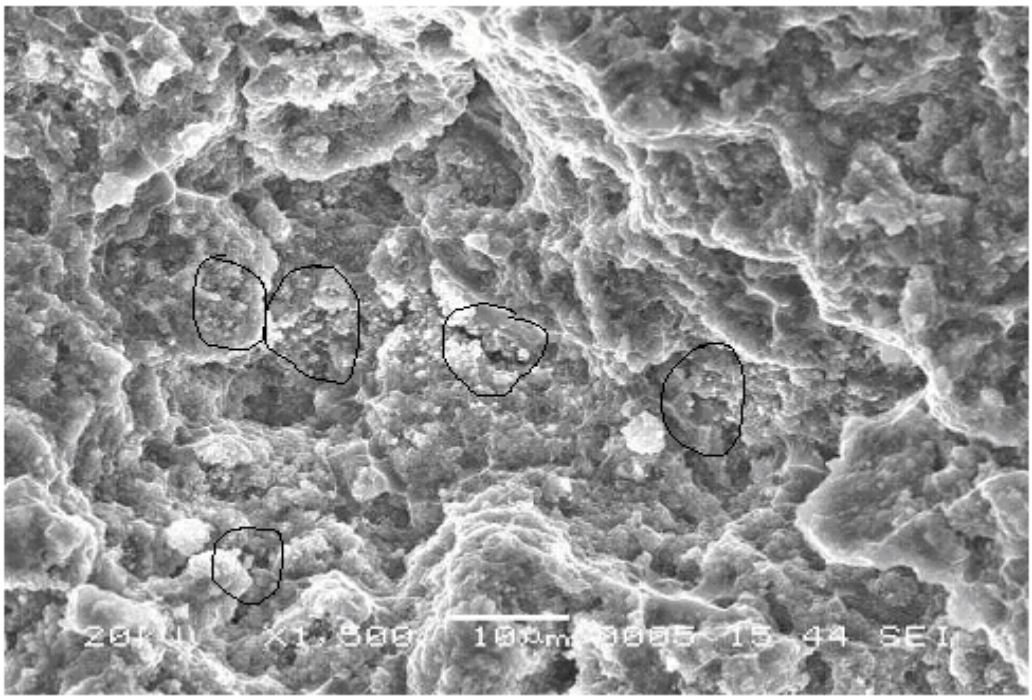

Fig. 4.52: SEM flexural fracture surface of 30% $v_f Al_2 0_3$ composite showing cracks and decohesion (circled regions) at magnification of 1500X.

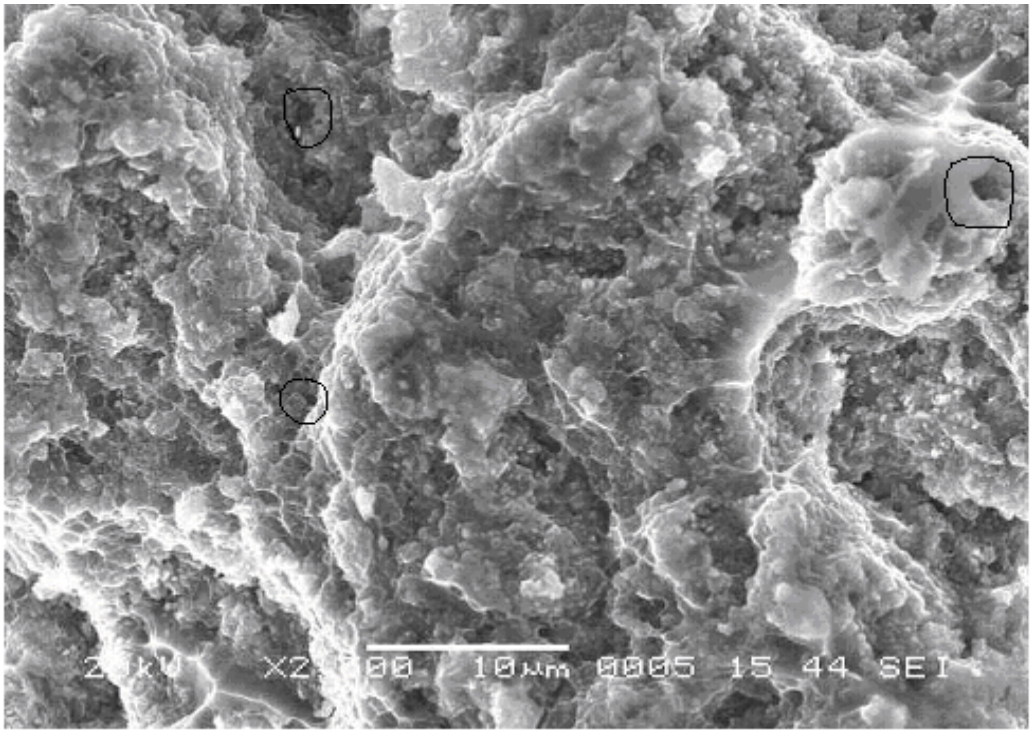

Fig. 4.53: SEM flexural fracture surface of 30% $v_f Al_2 0_3$ composite showing cracks at magnification of 2500X. Circled regions show voids.

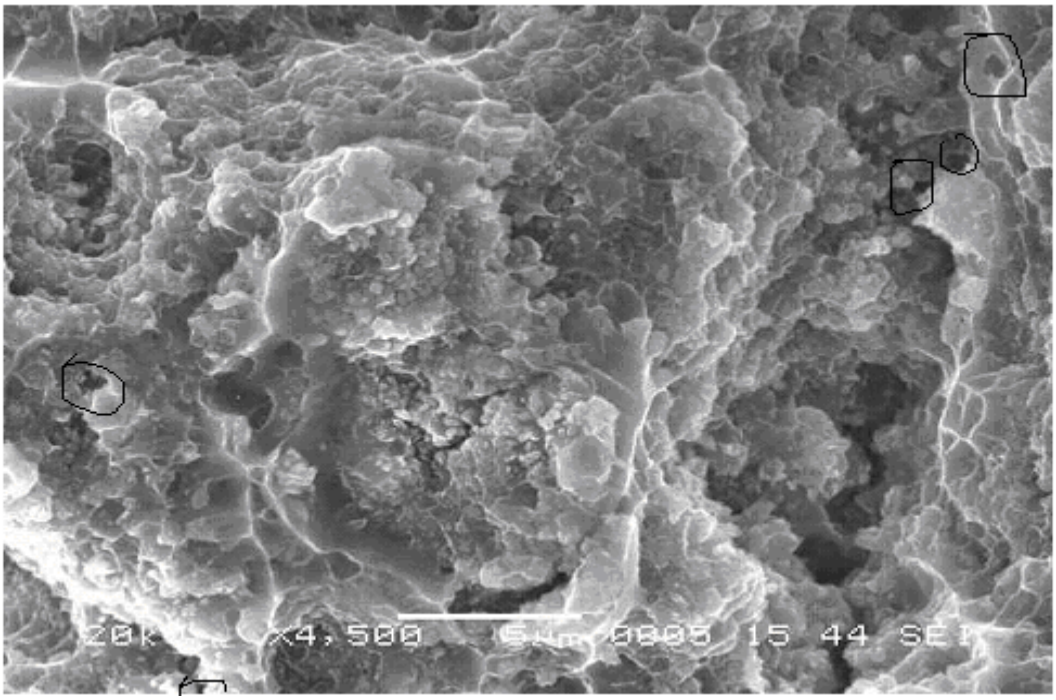

Fig. 4.54: SEM flexural fracture surface of 30% v_f Al_2O_3 composite showing dimples and cracks at magnification of 4500X.

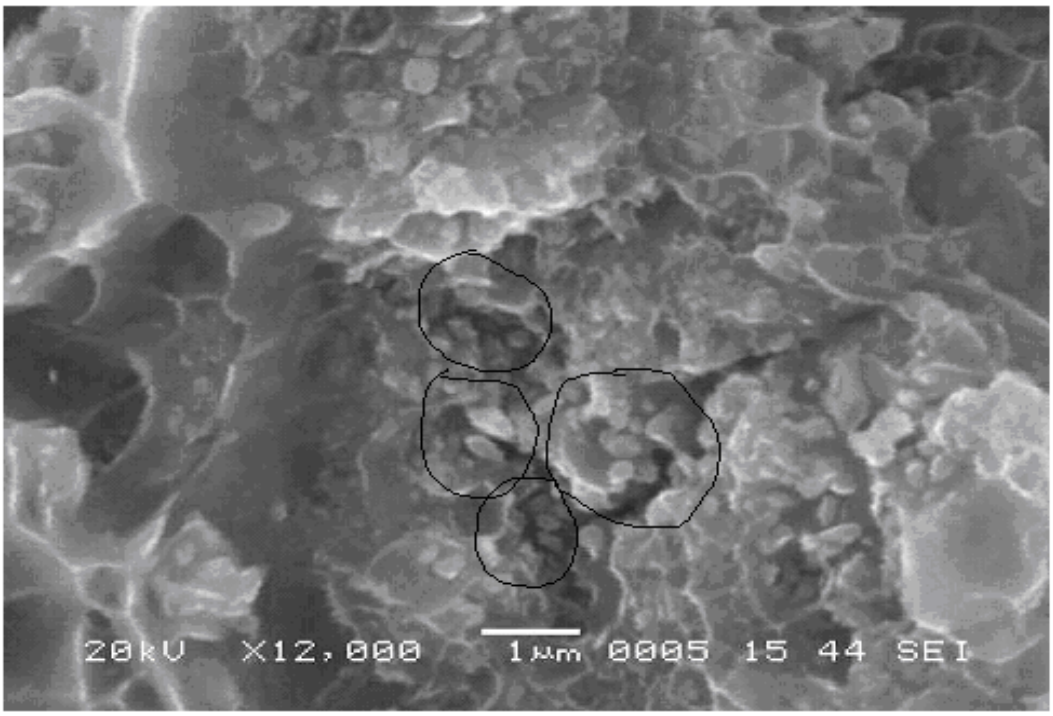

Fig. 4.55: SEM flexural fracture surface of 30% v_f Al_2O_3 composite showing matrix particle decohesion (circled regions) and dimples at magnification of 12000X.

4.4 FRACTURE TOUGHNESS

Three indentations of proper size were introduced and aligned 5mm apart on the tensile (polished) surfaces of the inner span of four-point bend rectangular samples (of similar dimensions as those used for bending strength tests), using Vickers diamond indentor at the indentation load of 10 kg for the samples. The samples were indented such that the crack arms emanating from the indentation corners were perpendicular and parallel to the sample length. Indented samples were placed inside a four-point fixture, with the three indentations positioned on the middle of the tensile surface of the inner span, the load was applied under the same test conditions as those used for bending strength measurement (see Section 3.3.2), until the sample fractured. Surface inspections under an optical microscope confirmed that fractures initiated from one of the three indentations. The crack lengths emanating from the two remaining indentations, perpendicular to the tensile direction, were then measured and averaged to give the critical crack length (c_m).

Based on the above experimental results, the fracture toughness (K_{Ic}) was calculated using a relationship between the maximum stress at failure (σ_m) and critical crack length (c_m), according to.

$$K_{Ic} = 2.02\ \sigma_m \sqrt{c_m} - 0.68\ \text{MPa}\ \sqrt{\text{m}}$$

K_{Ic} values for the Al alloy reinforced with Al_2O_3 PRMMC composites are listed in Table 4.3.Two factors appear to control the fracture toughness of the composites studied here; distribution of the particles and deformation characteristics of the matrix. The variation of fracture toughness values with reinforcement volume fraction (Al_2O_3) is depicted in Fig. 4.56. Fig. 4.56 shows that an increase in vol. % reinforcement of Al_2O_3

particles in the 6061 Al metal matrix causes a decrease in fracture toughness. The 6061 alloy has the highest fracture toughness value. This value decreased from 31.74 MPa√m for the 10% v_f Al_2O_3 composite to 17.61 MPa√m for the 30% v_f Al_2O_3 composite, which corresponds to a decrease of 25.6% to 58.72% compared to the unreinforced alloy. Increasing the volume fraction of Al_2O_3 particles considerably weakens the crack arresting capability of the matrix alloy via its plastic deformation. However the value of the fracture toughness is 9 times higher for the 10% v_f Al_2O_3 composite, 6.5 times higher for the 20% v_f Al_2O_3 composite and 5 times higher for 30% v_f Al_2O_3 composite than the Al_2O_3 ceramic, indicating that the presence of the particle matrix interface and the metal matrix between the particles considerably raises the energy dissipation during crack propagation, leading to a significant improvement in fracture toughness of the ceramic material.

To some extent fracture toughness mirrors the tensile elongation; it decreases with increase in Al_2O_3 particle reinforcement. The decrease is most significant for composites with v_f from 0 to 20% Al_2O_3 and only a slight decrease for the higher reinforced v_f Al_2O_3 composites. The addition of Al_2O_3 reinforced particles to aluminum matrix significantly improves the strength, but decreases ductility. The same trend is followed for fracture toughness.

- **Fracture behavior**

Fracture consisting of void formation and coalescence was observed as the main fracture mechanism for all the composites. Fracture will occur when the strain at the particle-matrix interface is sufficient to start voids, this strain is found to depend on the

volume fraction of the reinforcement. Particles contribute to the fracture process by imposing strong constraints on the matrix, increasing the matrix deformation around particles, raising the stress in the matrix to a level considerably greater than that normally associated with the matrix failure. Fracture morphology is produced similar to that of the bending (flexural) fracture surfaces.

- **10% v_f $Al_2 0_3$ Composite**

Fig. 4.57 show fracture surface halves of the sample placed side by side. The zig zag path of the fracture indicates that the crack deviated much while traversing. Therefore, crack blunting, due to plastic deformation of metal is followed by crack propagation, and by breakage of the metallic phase around the ceramic particles. The metal matrix absorbs most of the energy by deforming plastically around the indentation.

Fig. 4.58-4.59 show many dimples with tear ridges with dimples, neither uniform nor circular in shape; these dimples appear to be similar to the dimples shown in Figs. 4.43-4.44. In areas comparatively free of $Al_2 0_3$ particles, dimples appeared to be uniform. Most of the particles are firmly embedded in the matrix (Fig. 4.60). In Fig. 4.61 matrix-particle decohesion was observed. There were no broken particles observed in the fractured surface. Therefore from the above observation it is clear that the final fracture mechanism is ductile.

- **20% v_f $Al_2 0_3$ Composite**

Fig. 4.62 shows fracture surface halves of the sample placed side by side. The fracture path for the 20% v_f $Al_2 0_3$ composite shows less deviation while traversing when compared to fracture path of the 10% v_f $Al_2 0_3$ composite. Fig. 4.63 clearly shows the

deviation of fracture path. Fig. 4.64 shows the deviation of the crack path at the particles. Fig. 4.65 shows the fracture surface of a particle-free region at which many dimples are observed. A higher magnification matrix-particle decohesion can be clearly observed in Fig. 4.66. The fracture behavior of this composite is one, which is intermediate between the ductile and brittle fracture.

- **30% v_f Al_2O_3 Composite**

Fig. 4.67 shows the fracture surface halves of this composite placed side by side. It is obvious that the fracture appears to be perpendicular to the loading axis, with minor deviation of the crack path when compared to fracture path for the 10% v_f Al_2O_3 (Fig.4.57) and 20% v_f Al_2O_3 composites (Fig.4.61). Fig. 4.68 clearly shows many microvoids and minute cracks in the matrix. At higher magnification minute crack and decohesion can be seen in Fig. 4.69-4.70. Dimpled structures at particle free regions. and matrix-particle decohesion can also be observed from Fig 4.71-4.72. Fig. 4.73 shows extensive decohesion at matrix-particle interface. The restricted local matrix plasticity is not adequate to overcome the embrittling effect of 30% v_f Al_2O_3 particles. Hence the 30% v_f Al_2O_3 composite undergoes brittle fracture.

4.5 LOW-VELOCITY IMPACT TEST REULTS

Low-velocity impact tests were conducted using an instrumented drop weight impact testing machine (DYNATUP 9250G) to evaluate the impact strength of tested composites. The impactor, which was used to strike the samples, is a cylindrical indenter (tup) with a 10mm diameter spherical head. Force/absorbed energy-time plots were generated for each impact test. With the height and weight known, impact energy can be

Table 4.3 Fracture toughness of Al reinforced with Al_20_3 PRMMC composites

	Sample	c_{m1}(µm)	c_{m2}(µm)	c_m(µm)	σ_m (MPa)	K_{Ic} (MPa √m)
6061 Al alloy	sample 1	440.01	435.15	437.58	1021.69	42.49
	sample 2	433.59	431.53	432.56	1028.45	42.53
	sample 3	443.01	433.3	438.16	1032.09	42.96
	Average	438.87	433.33	436.10	1027.41	42.66
10% v_f Al_20_3 composite	sample 1	252.62	251.03	251.83	989.56	31.04
	sample 2	251.08	257.34	254.21	1018.06	32.11
	sample 3	262.75	254.18	258.47	1008.51	32.07
	Average	255.48	254.18	254.83	1005.38	31.74
20% v_f Al_20_3 composite	sample 1	224.3	211.5	217.9	725.98	20.97
	sample 2	218.43	213.17	215.8	815.55	23.52
	sample 3	215.8	224.17	219.98	781.59	22.74
	Average	219.51	216.28	217.89	774.37	22.41
30% v_f Al_20_3 composite	sample 1	177.91	184.18	181.04	680.21	17.81
	sample 2	185.32	179.11	182.21	649.6	17.03
	sample 3	177.33	185.24	181.29	687	18
	Average	180.18	182.84	181.51	672.27	17.61

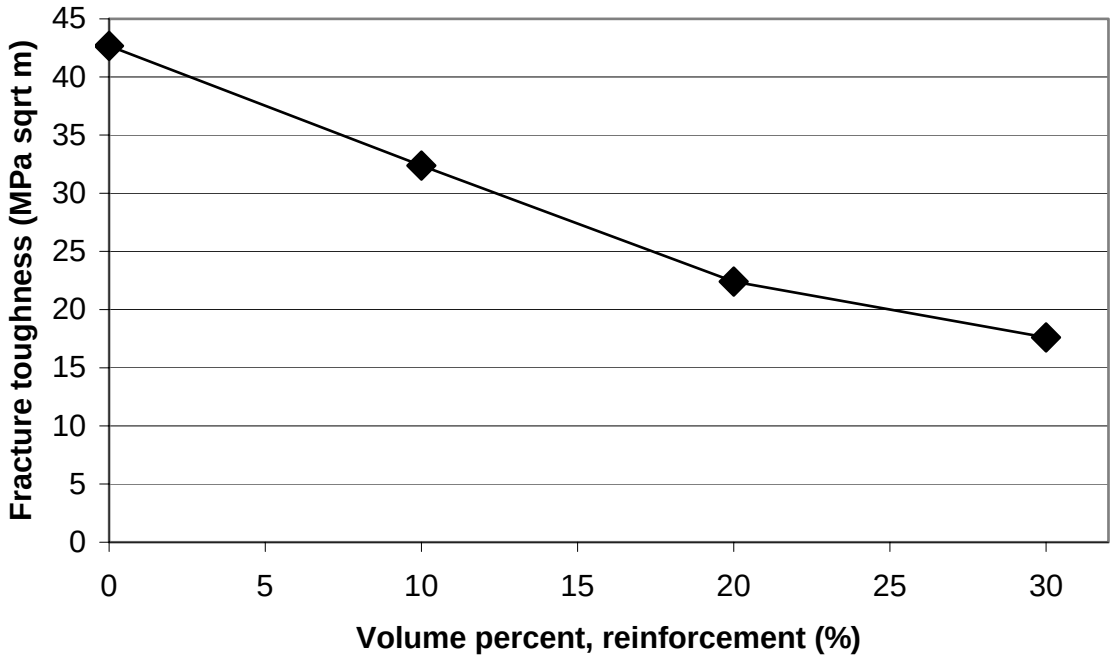

Fig. 4.56: Effect of reinforcement content on Fracture toughness of 6061 Aluminum alloy reinforced with Al_2O_3 particles.

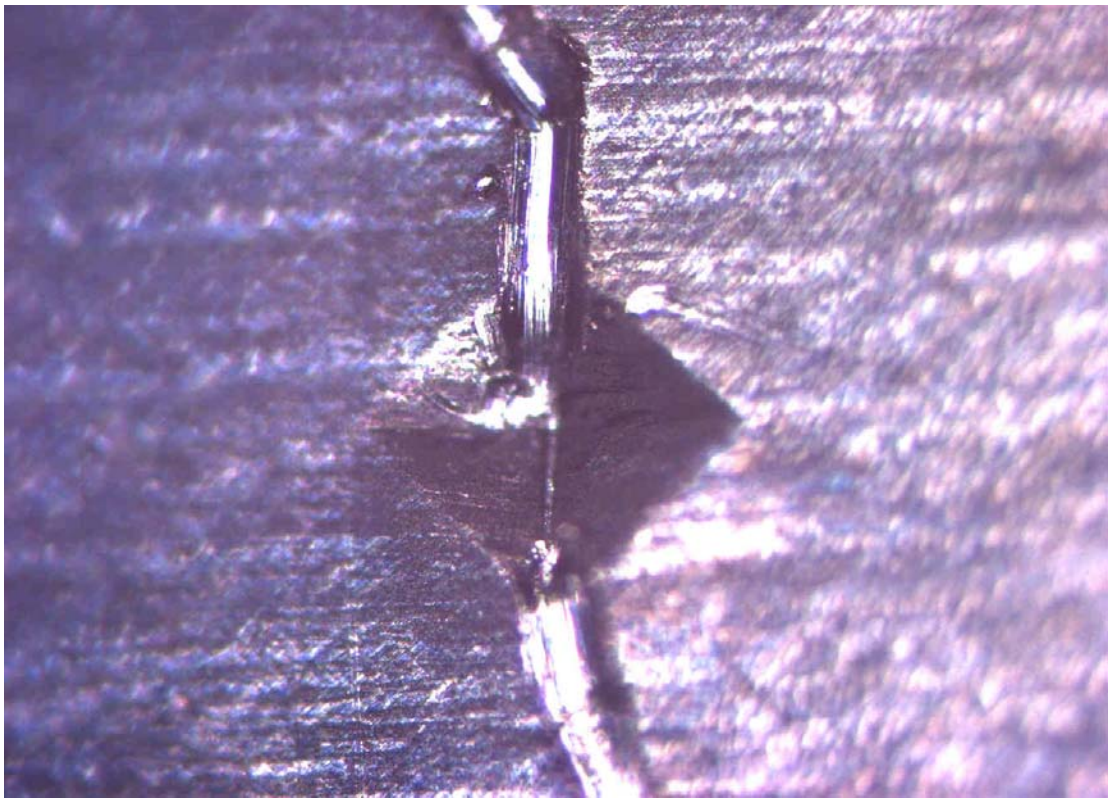

Fig. 4.57: The fracture halves of the 10% v_f Al_20_3 composite placed together.

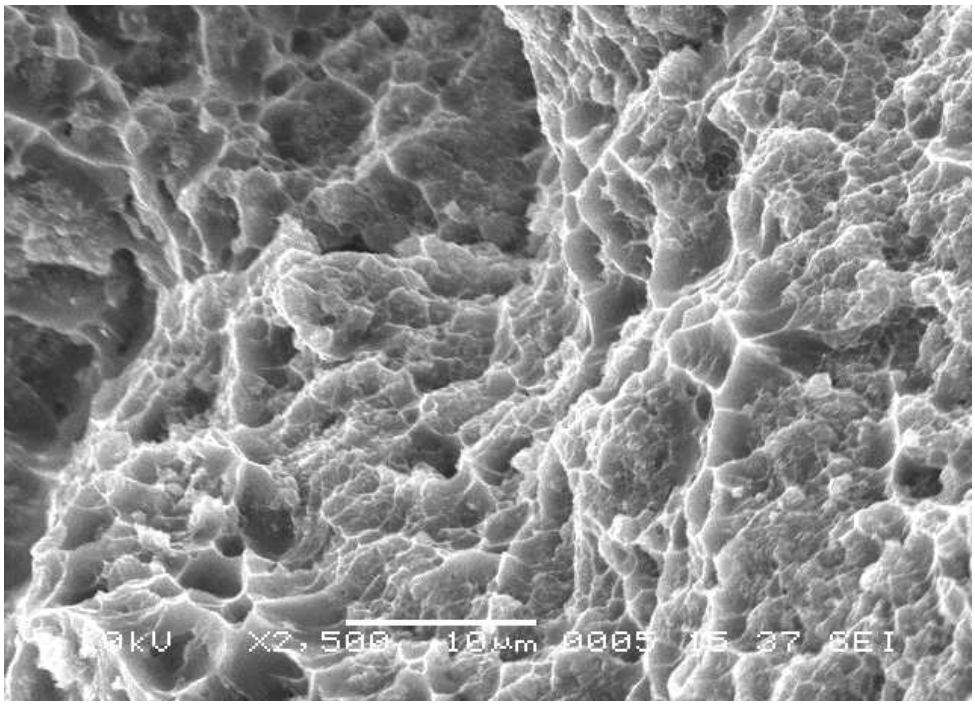

Fig. 4.58: SEM fracture surface of 10% $v_f Al_2 0_3$ composite at magnification of 2500X showing dimples with tear ridges.

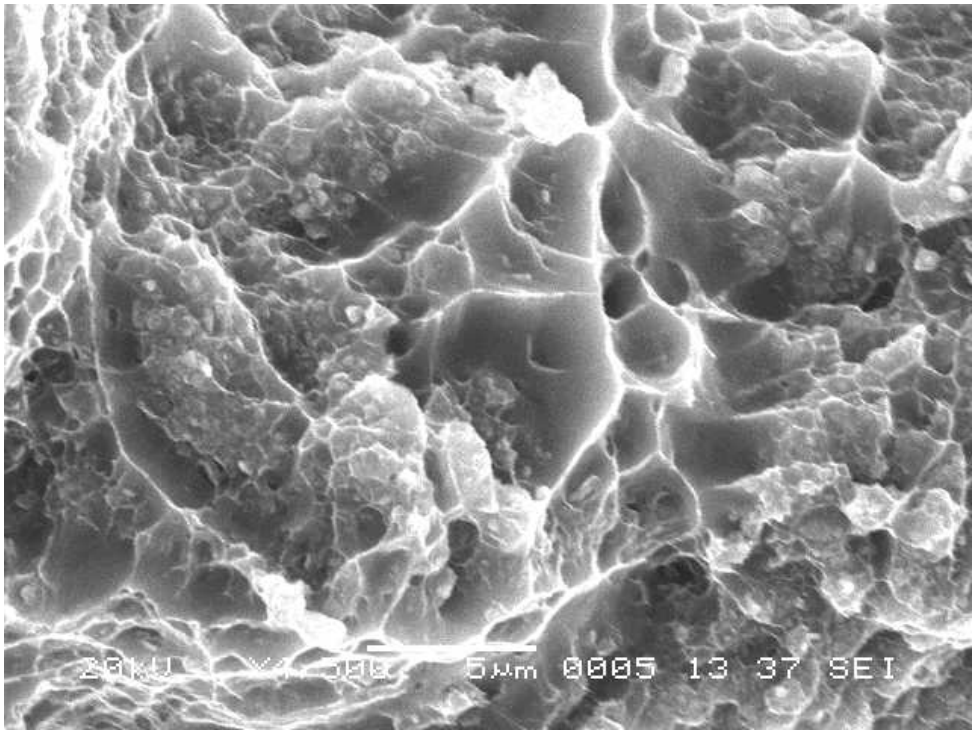

Fig. 4.59: SEM fracture surface of 10% $v_f Al_2 0_3$ composite at magnification of 4500X showing dimples with tear ridges.

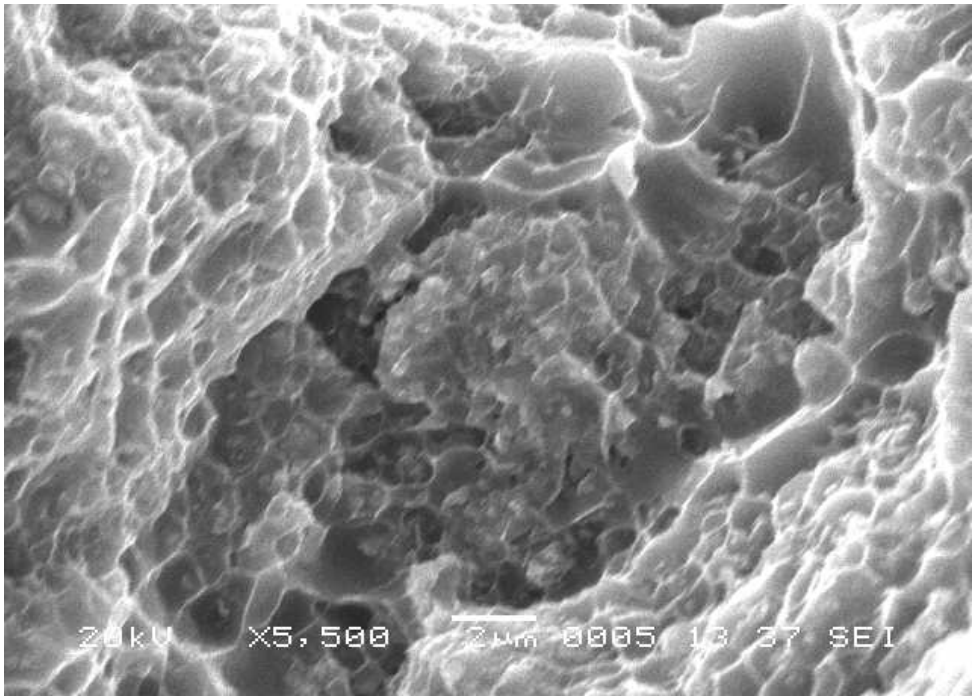

Fig. 4.60: SEM fracture surface of 10% $v_f Al_2 0_3$ composite showing cracks with embedded particles at magnification of 5500X.

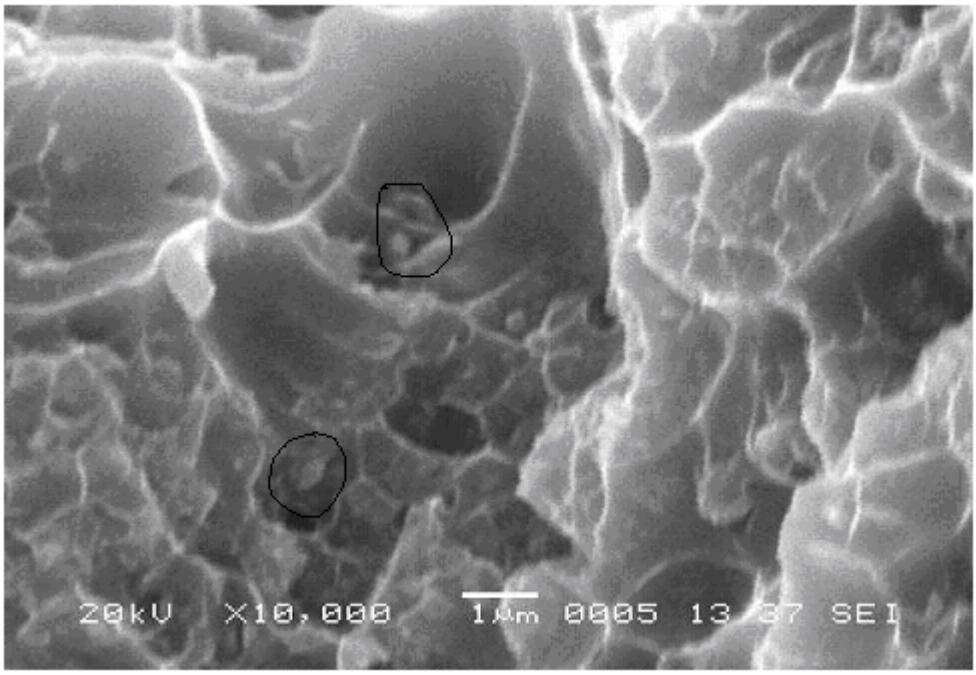

Fig. 4.61: SEM surface of 10% $v_f Al_2 0_3$ composite showing matrix-particle decohesion (circled regions) at magnification of 10,000X.

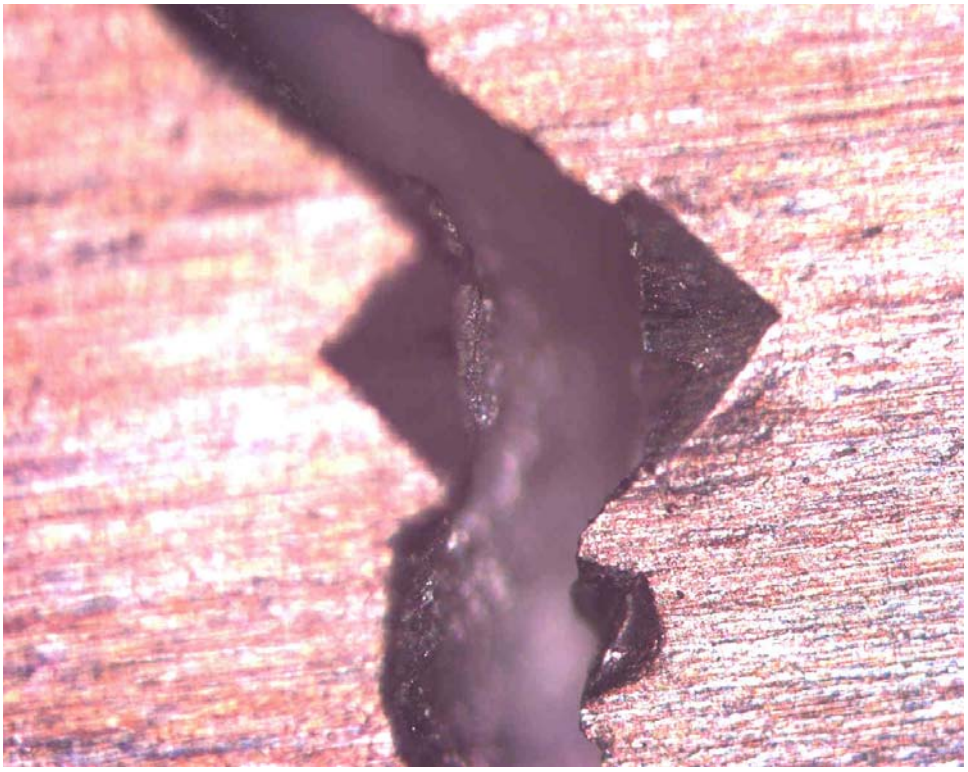

Fig. 4.62: The fracture halves of the 20% v_f Al_2O_3 composite placed together.

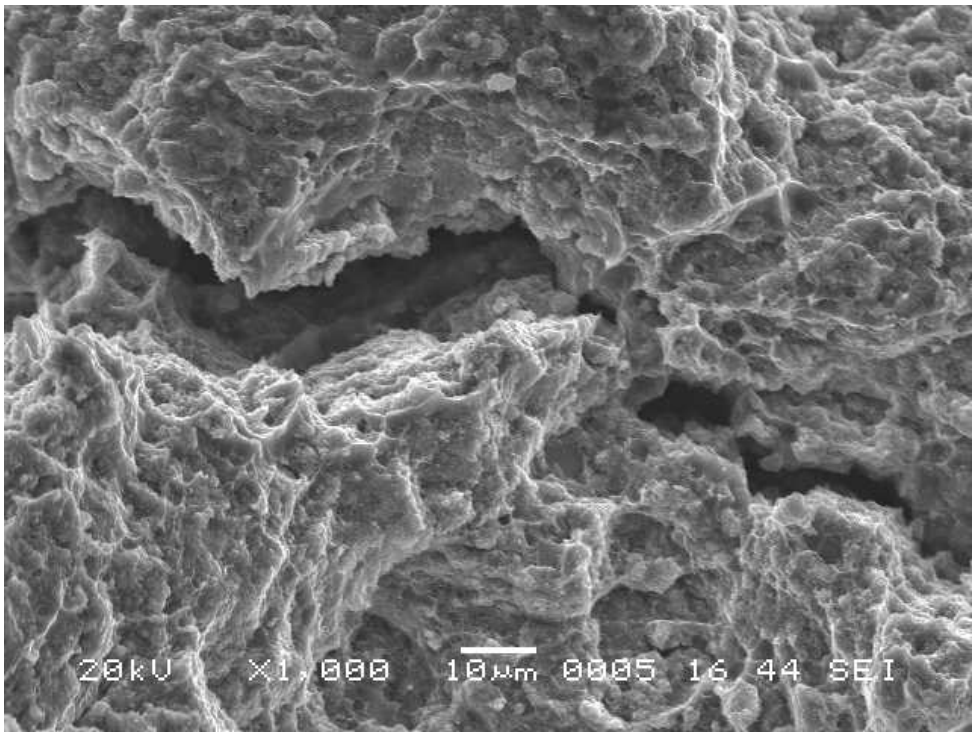

Fig. 4.63: SEM fracture surface of 20% v_f Al_2O_3 composite showing crack at magnification of 1000X.

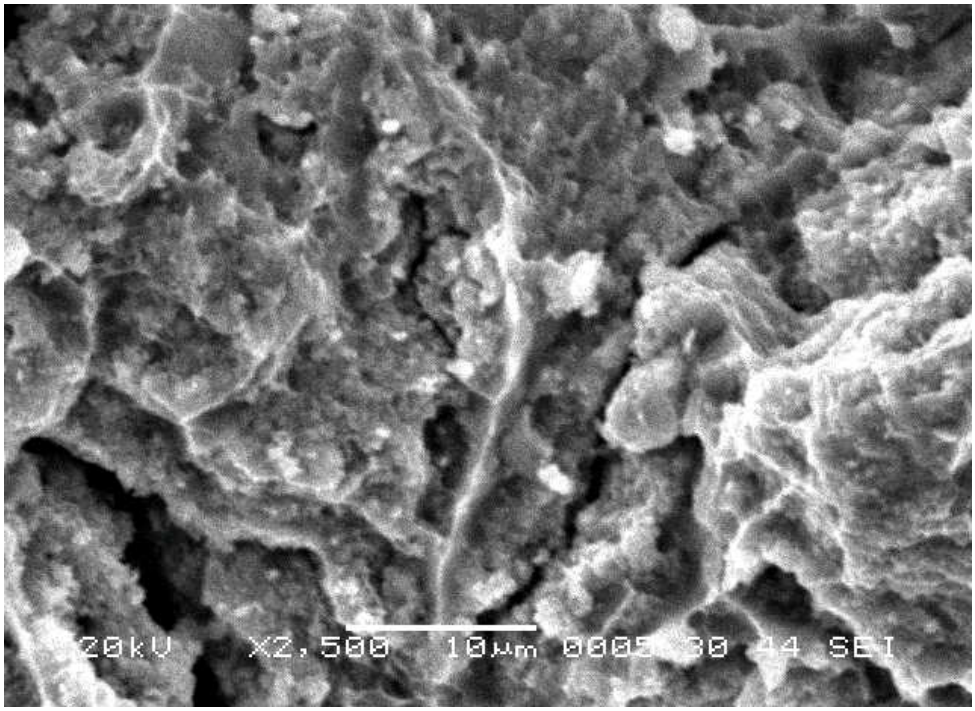

Fig. 4.64: SEM fracture surface of 20% $v_f Al_2 0_3$ composite showing minute crack at magnification of 2500X.

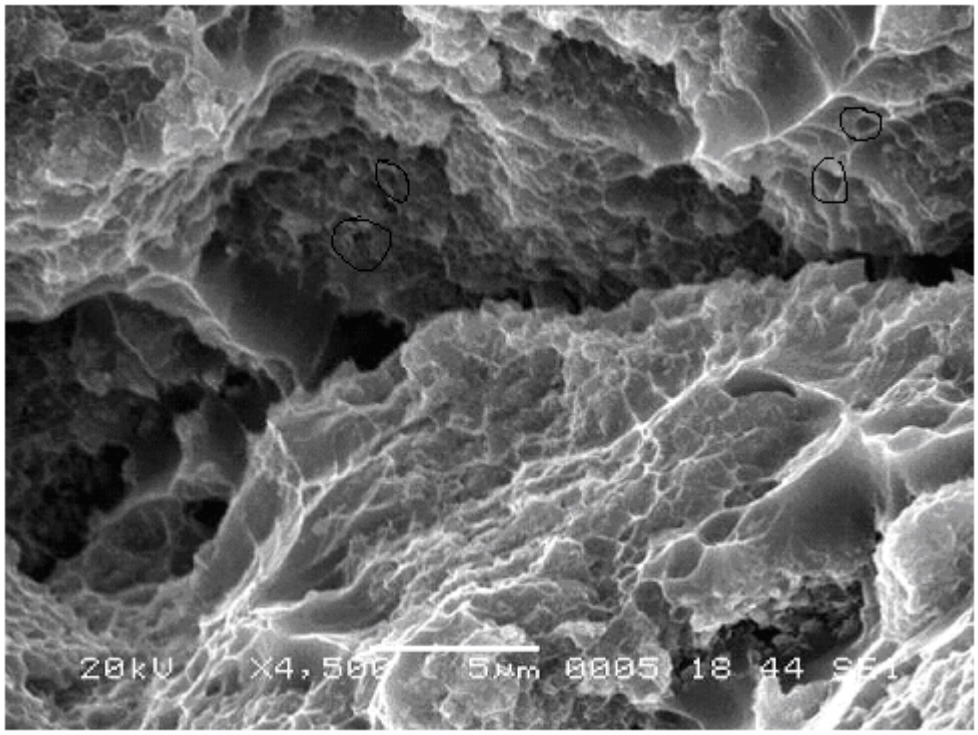

Fig. 4.65: SEM fracture surface of 20% $v_f Al_2 0_3$ composite showing dimples and crack at magnification of 4500X. Circled regions show voids.

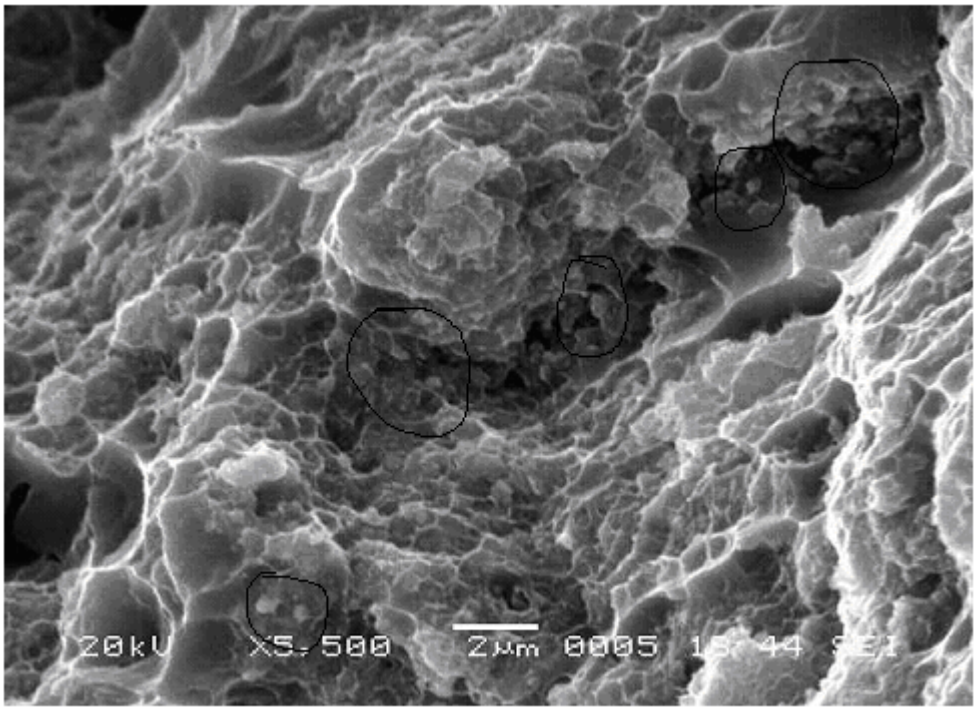

Fig. 4.66: SEM fracture surface of 20% $v_f Al_2 0_3$ composite showing matrix particle decohesion (circled regions) at magnification of 5500X.

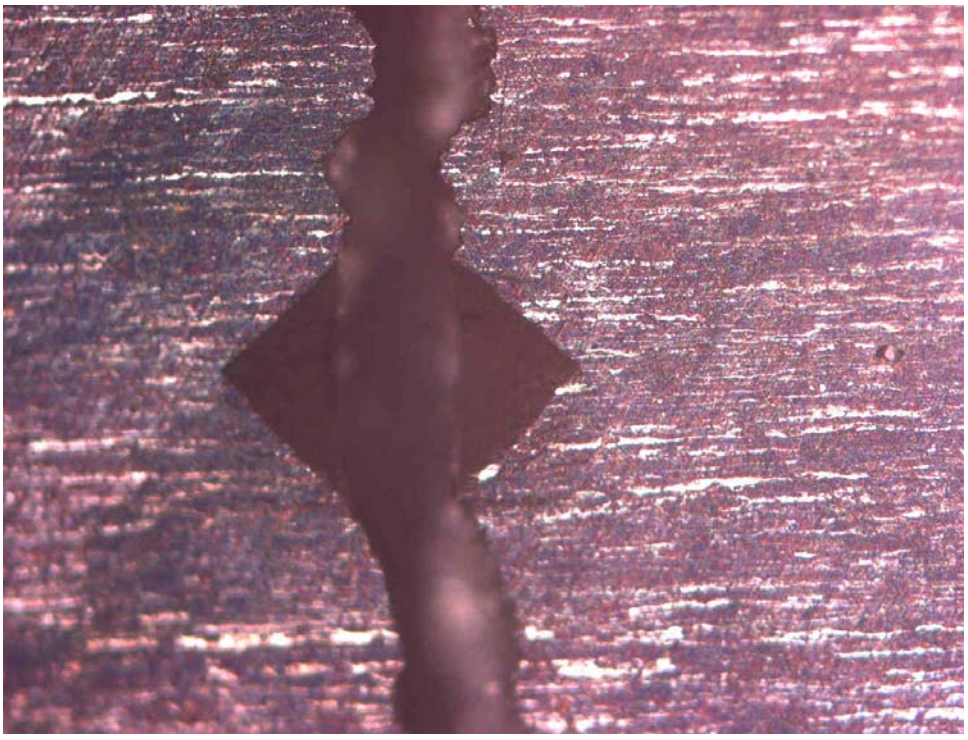

Fig. 4.67: The fracture halves of the 30% $v_f Al_2 0_3$ composite placed together.

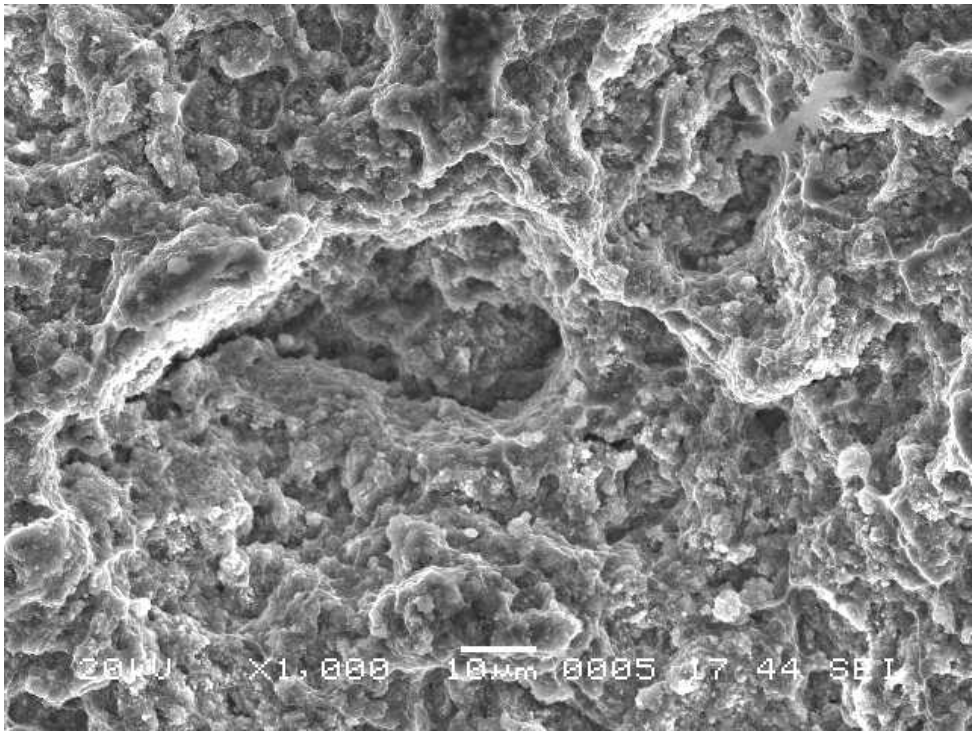

Fig. 4.68: SEM fracture surface of 30% $v_f Al_2 0_3$ composite showing crack at magnification of 1000X.

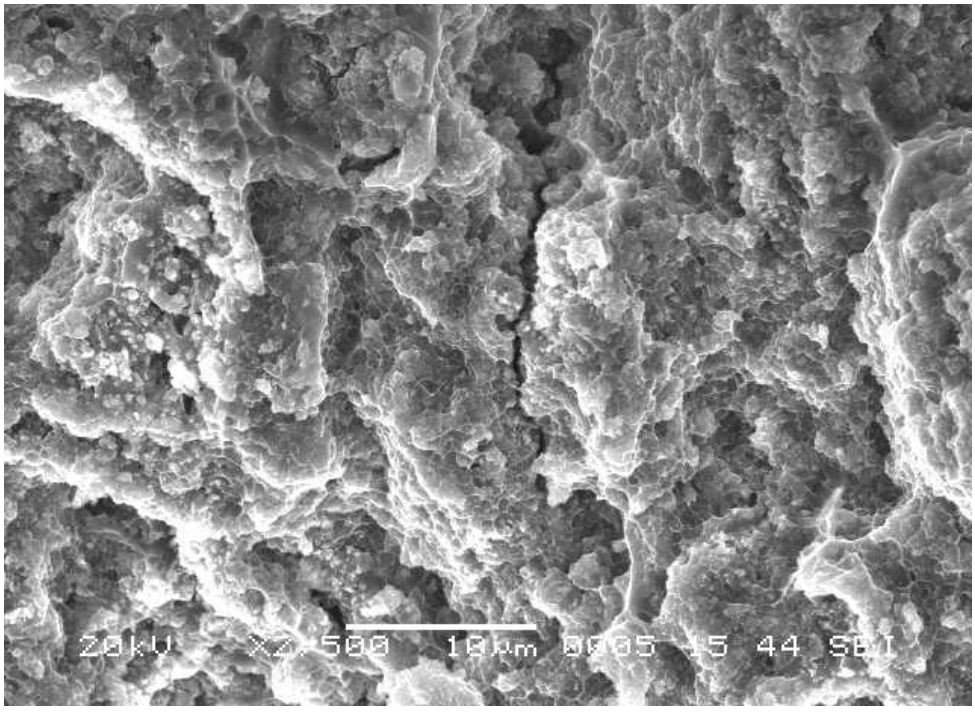

Fig. 4.69: SEM fracture surface of 30% $v_f Al_2 0_3$ composite showing minute cracks at magnification of 2500X.

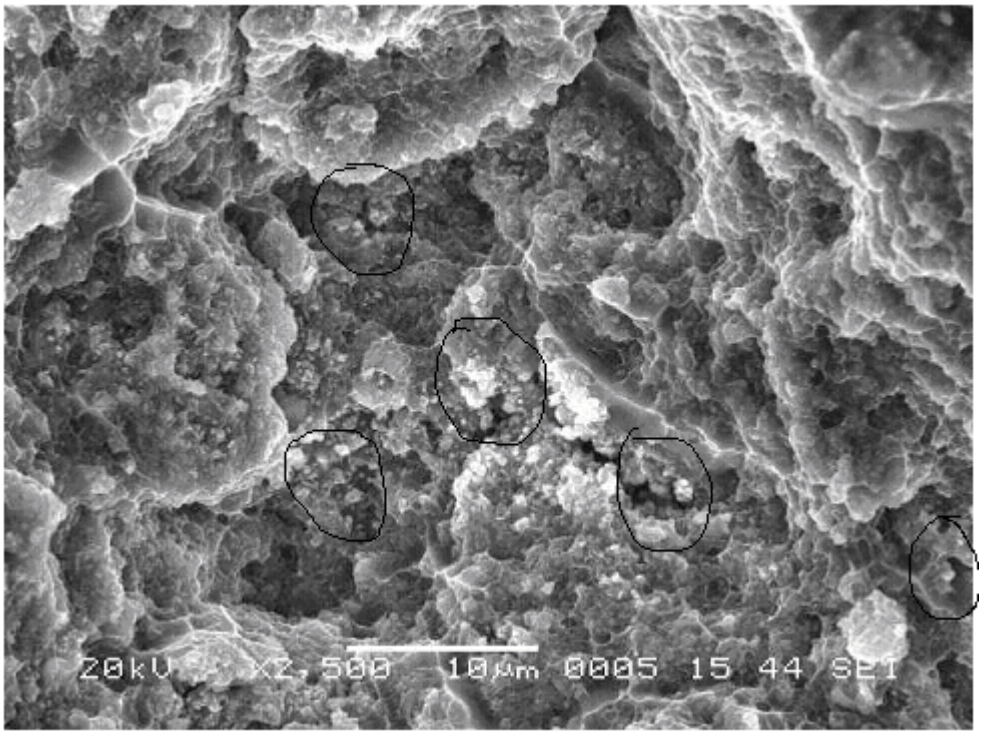

Fig. 4.70: SEM fracture surface of 30% $v_f Al_2 0_3$ composite showing minute crack and decohesion (circled regions) at magnification of 2500X.

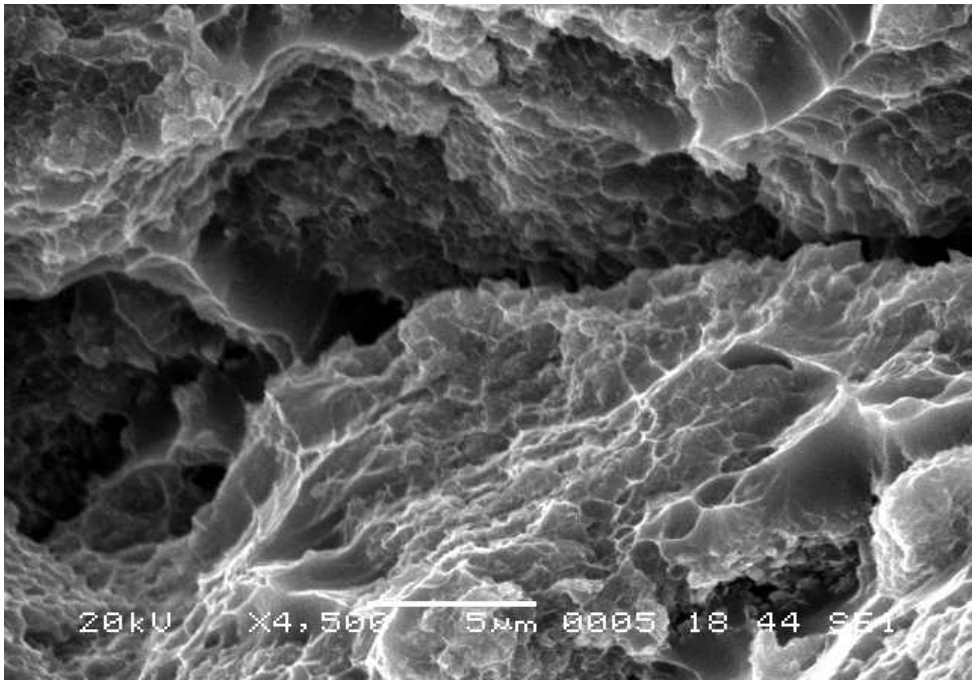

Fig. 4.71: SEM fracture surface of 30% $v_f Al_2 0_3$ composite showing dimples and crack at magnification of 4500X.

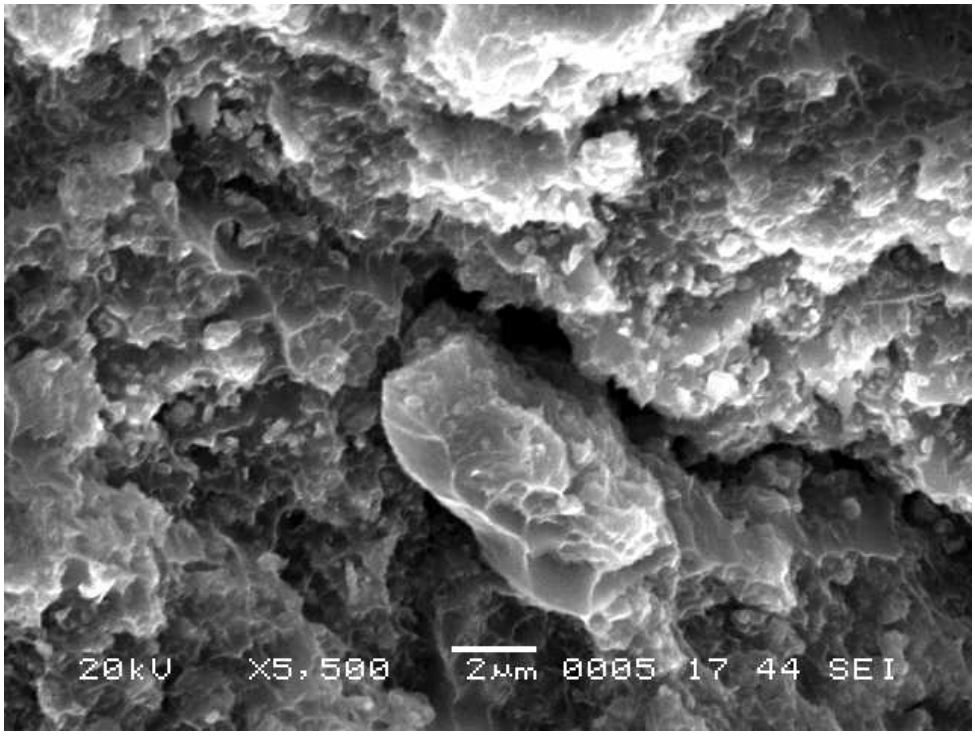

Fig. 4.72: SEM fracture surface of 30% $v_f Al_2 0_3$ composite showing crack at magnification of 5500X.

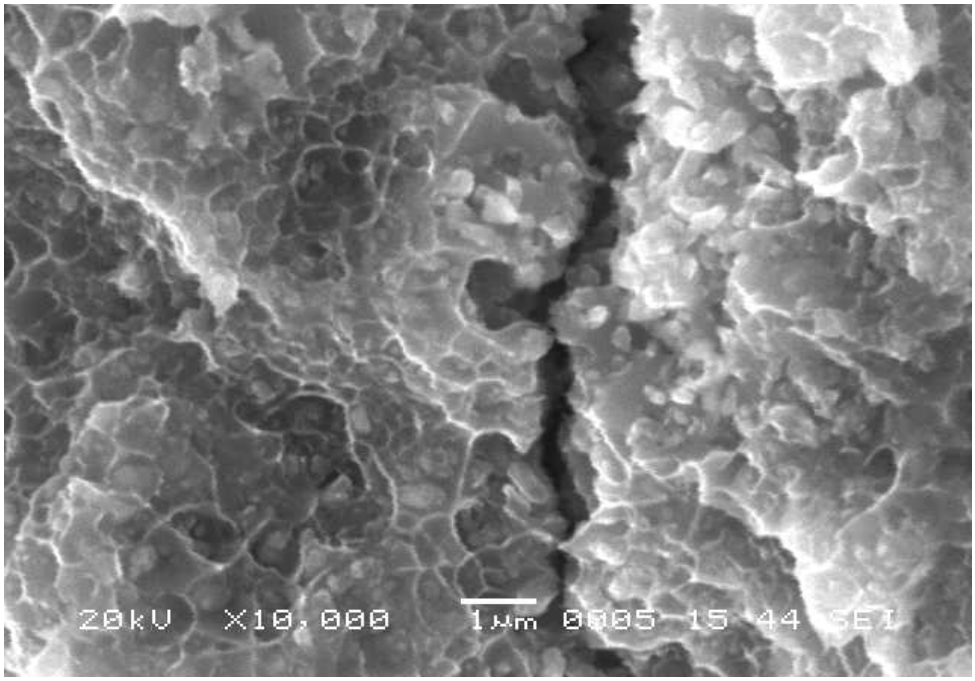

Fig. 4.73: SEM fracture surface of 30% $v_f Al_2 0_3$ composite showing matrix particle decohesion (at crack) at magnification of 10000X.

calculated. Rectangular composite samples of 40 mm span were placed inside a charpy fixture. The mass of drop weight was maintained constant at 8.2 kg and height of the drop weight was varied. Inspection of fractured pieces was done after each test. The above procedure, maintaining mass constant and changing the height, was carried out till we found out the height required to just initiate the fracture in the samples. With the height and weight known, maximum (peak) load, energy to maximum load, impact energy, deflection to maximum load, and impact velocity were calculated for Al alloy reinforced with Al_20_3 PRMMC composites are listed in table 4.4

The force vs time curves for all composites are plotted in Fig. 4.74. The curve can be characterized by the peak force, the energy to peak force, total energy, and displacement to maximum load. The peak (maximum) load is the peak in force vs time curve and it is a point, which the sample can increasingly resist the progress of impactor and it is taken as the impact strength. The maximum force is a measure of ease with which cracks begin to propagate on a large scale, and this is much greater for the 30% v_f Al_20_3 composite as shown in the Fig. 4.75 than for other studied composites. The energy observed up to the maximum force is greatest for 30% v_f Al_20_3 composite and least for 6061 aluminum alloy. A 6061-aluminum alloy composite absorbs more energy, which largely results from a more ductile matrix (Fig. 4.75). The unloading part of the curves and total energies absorbed is greatest for the 6061 aluminum alloy followed by 10% v_f Al_20_3, 20% v_f Al_20_3 and 30% v_f Al_20_3 composites (Fig. 4.74).

The addition of 10, 20, and 30% Al_20_3 particles to a 6061 Al alloy metal matrix causes decrease in the impact energy from 19.62 to 2.28 J as listed in table 4.4. This drop

Table 4.4 Impact properties of Al reinforced with Al_20_3 PRMMC composites

	Sample	Peak(Maximum) Load (kN)	Deflection at Peak Load (mm)	Energy to peak load (J)	Height to failure (mm)	Total energy (J)
6061 Al alloy	sample 1	0.99	8.86	7.13	247.9	19.83
	sample 2	0.95	8.82	6.86	232.7	18.62
	sample 3	1.03	9.8	8.24	255	20.4
	Average	0.99	9.16	7.41	245.2	19.62
10% v_f Al_20_3 composite	sample 1	2.89	3.13	7.13	116.5	9.32
	sample 2	2.83	3.61	6.75	98.7	7.9
	sample 3	2.91	3.53	7.64	116	9.28
	Average	2.88	3.42	7.17	110.4	8.83
20% v_f Al_20_3 composite	sample 1	3.4	1.84	4.14	59.8	4.78
	sample 2	3.44	1.54	3.55	52.7	4.22
	sample 3	3.42	1.62	3.39	50.6	4.05
	Average	3.42	1.67	3.69	54.37	4.35
30% v_f Al_20_3 composite	sample 1	3.4	1	1.58	27.2	2.17
	sample 2	3.56	0.89	1.76	29.5	2.36
	sample 3	3.42	0.92	1.73	29	2.32
	Average	3.46	0.94	1.69	28.57	2.28

is accompanied by an increase in the maximum load from 0.99 to 3.46 KN and a reduction in total deflection from 9.16 to 0.94 mm.

The presence of Al_20_3 particles in an Al matrix produces reduction in energy absorbing capacities under impact conditions as demonstrated by the impact test results (Figs. 4.74-4.76). The 30% v_f Al_20_3 composite has a low energy for initiation and propagation of fracture compared to the unreinforced 6061 alloy. Low fracture initiation energy results from the low failure strain and high elastic modulus.

Two factors may contribute to this decrease in properties. The Al_20_3 particles can act as void nucleation sites by their presence at the center of the dimples on the fracture surface. Secondly a high state of restraint exists in the Al matrix situated between Al_20_3 particles, which can lead to rapid void nucleation, growth and coalescence.

- **Impact fracture behavior**

The fracture mechanism was discussed and fracture surfaces of impact tests were examined under SEM. At high strain rate testing, the impact wave will enlarge the void and produce the plastic deformation in the matrix. All composites of impact fracture exhibited enlarged interfacial voids, which was not the case for the static tested composites.

- **10% v_f Al_20_3 composite**

The cross section of the fracture surface for 10% v_f Al_20_3 composite tested under impact is shown in Fig. 4.78. Fig. 4.78 clearly shows the fissure with no particles in it and also there was embedded particles in the matrix around the crack. Fig. 4.79 shows many dimples with tear ridges, which indicates there is considerable change in the behavior of

impact fracture process due to the existence of the reinforcing Al_20_3 particles. In areas comparatively free of Al_20_3 particles, dimples appeared to be uniform. Fig. 4.80 shows the separation of matrix where particles are present only on one side of the separated matrix. At higher magnification matrix-particle decohesion was observed (Fig. 4.81). There were no broken particles observed in the fractured surface.

The unloading part of the curves (Fig.4.74) and total energies absorbed are a measure of the work necessary to cause large scale cracking in the samples, this is greatest for the 10% v_f Al_20_3 composite when compared with other two composites (Fig. 4.74).

- **20% v_f Al_20_3 composite**

Fig. 4.82 show cross-sections of impact fracture of the 20% v_f Al_20_3 composite. In Fig. 4.82 many micro cracks, microvoids and embedded particles in the matrix can be seen. Unlike the 10% v_f Al_20_3 composite, which contain dimples for the 20% v_f Al_20_3 composite, dimples in Fig. 4.83-4.84 are present around the particles in particle-free regions.

- **30% v_f Al_20_3 composite**

The impact fracture surface cross section of 30% v_f Al_20_3 composite tested under impact is shown in the Fig. 4.85. As Fig. 4.85 shows many microvoids in the matrix can be seen. The number of dimples present at particle free region are fewer than for the 10%, 20% v_f composites (Fig. 4.86). At higher magnification matrix-particle decohesion and cracks can be observed in Fig. 4.87, with extensive decohesion at matrix-particle interface (Fig. 4.88). Other shape particles are also present (Fig. 4.86).

4.6 COMPARISON OF STATIC AND IMPACT STRENGTHS

- **Comparison of tensile (static) and impact strengths**

A comparison of tensile (static) and low–velocity impact (dynamic) strengths for Al-based Al_2O_3 PRMMC composites is shown in Fig. 4.89. The impact strength of the 10% v_f Al_2O_3 composite is 190.34 % higher than that of the 6061 alloy, that of the 20% v_f Al_2O_3 composite is 18.68 % higher than that of the 10% v_f Al_2O_3 composite, and that of the 30% v_f Al_2O_3 composite is 1.3% higher than that of 20% v_f Al_2O_3 composite. On the other hand, the tensile strength of the 10% v_f Al_2O_3 composite is 170.07 % higher than that of the 6061 alloy, that of the 20% v_f Al_2O_3 composite is 24.95 % higher than that of the 10% v_f Al_2O_3 composite, and that of the 30% v_f Al_2O_3 composite is 9.43 % higher than that of 20% v_f Al_2O_3 composite.

- **Comparison of flexural (static) and impact strengths**

A comparison of flexural and low–velocity impact strengths for Al-based Al_2O_3 PRMMC composites is shown in Fig. 4.90. The variation of impact strength with volume fraction (v_f) was described above. The flexural strength of the 10% v_f Al_2O_3 composite is 0.88 % lower than that of the 6061 alloy, that of the 20% v_f Al_2O_3 composite is 19.11 % lower than that of the 10% v_f Al_2O_3 composite, and that of the 30% v_f Al_2O_3 composite is 14.57 % lower than that of 20% v_f Al_2O_3 composite.

The maximum impact strength is a measure of ease with which cracks begin to propagate on a large scale. As the force increases cracks are initiated, these cracks lead to plastic deformation. Due to the constraints imposed in deformation caused by the

presence of the hard and brittle Al_20_3 particles in the soft and ductile 6061 alloy matrix a higher applied stress is required to initiate plastic deformation in the matrix. This in turn results in the increase in the impact strength of the composites with increasing volume fraction of the particle reinforcement. On the other hand reinforced Al_20_3 particles act as surface flaws, which create large stress concentrations and weakens the material strength under flexural loadings [74]. In addition, the ductile aluminum alloy is able to flow plastically and blunt fracture-initiating flaws. The unreinforced 6061 alloy contains less surface flaws, and therefore less susceptible to flexural loading than composites. As the volume percent of reinforced composites increases the flexural strength decreases. The 30% v_f Al_20_3 composite contained more pores and voids than the other composites with lower volume fraction (v_f); these flaws creates local stress concentrations which results in easy fracture path.

The impact energies absorbed are a measure of the work necessary to cause large scale cracking. The 6061 alloy composite absorbed more impact energy than the reinforced composites; this impact energy decreases with increasing volume fraction of the particle reinforcement.

4.7 COMPARISON OF STATIC AND DYNAMIC FRACTURE MECHANISMS

- **6061 alloy**

The fracture surfaces under static and dynamic tests for the 6061 alloy were compared under same magnification (Fig.4.18 & Fig.4.77). This comparison, as shown by Figs.4.18 & 4.77 revealed minor difference in the fracture mechanisms under both

static and impact testing. The effect of rate of loading on fracture mechanisms of 6061 alloy is very small.

- **10% v_f Al_2O_3 composite**

The fracture surfaces under static (tensile and flexural) (Fig. 4.22 & Fig. 4.43) and dynamic (impact) tests (Fig.4.79-4.81) for the 10% v_f Al_2O_3 composite were compared under same magnification. Fig. 4.79–4.80 show enlarged voids for the 10% v_f Al_2O_3 composite, which are different from those observed in Fig. 4.22 for the tensile fracture and Fig. 4.43 for the flexural fracture.

- **20% v_f Al_2O_3 composite**

Fig. 4.82-4.84 show cross-sections of impact fracture surfaces of the 20% v_f Al_2O_3 composite. A comparison of fracture surfaces under static (tensile and flexural) (Fig. 4.31 & Fig.4.65) and dynamic (impact) tests (Fig. 4.84) may be attempted. Fig. 4.84 shows enlarged voids for the 20% v_f Al_2O_3 composite, which are different from those observed in Fig. 4.31 for the tensile fracture and Fig. 4.65 for the flexural fracture..

- **30% v_f Al_2O_3 composite**

The fracture surfaces under static (tensile and flexural) (Fig.4.36 & Fig. 4.53) and dynamic (impact) tests (Fig.4.85-4.86) for the 30% v_f Al_2O_3 composite were compared under same magnification. This 30% v_f Al_2O_3 composite contained large pores and voids. Fig. 4.85 shows quite large number of enlarged voids for the 30% v_f Al_2O_3 composite, which are quite different from those observed in Fig. 4.36 for the tensile fracture and Fig. 4.53 for the flexural fracture.

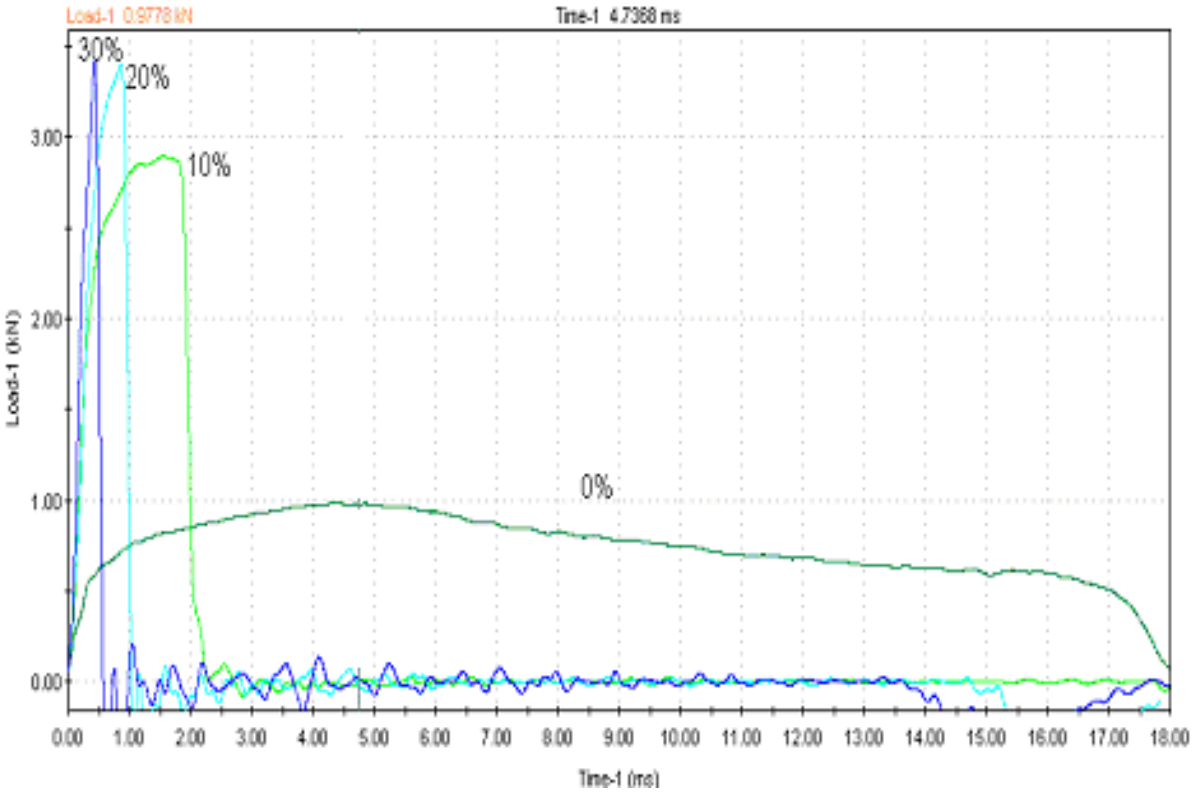

Fig. 4.74: Force – time curves of Al reinforced with Al_20_3 PRMMC composites.

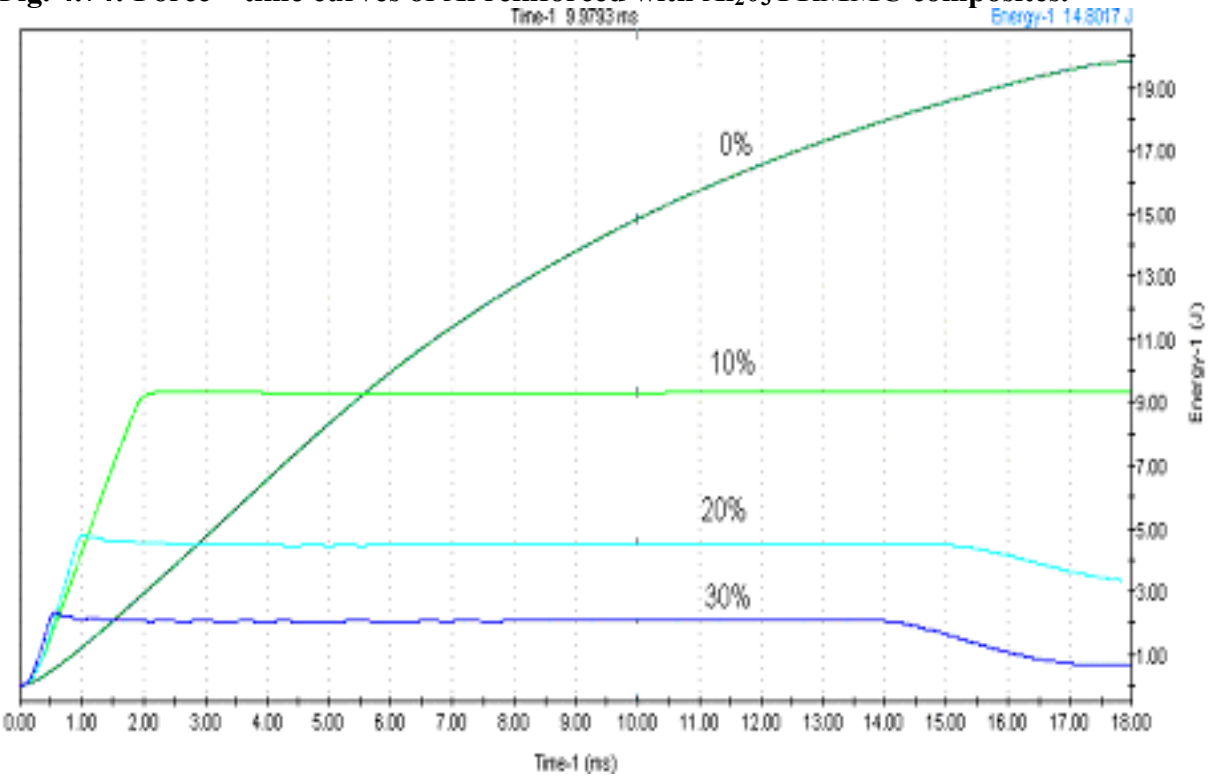

Fig. 4.75: Energy – time curves of Al reinforced with Al_20_3 PRMMC composites.

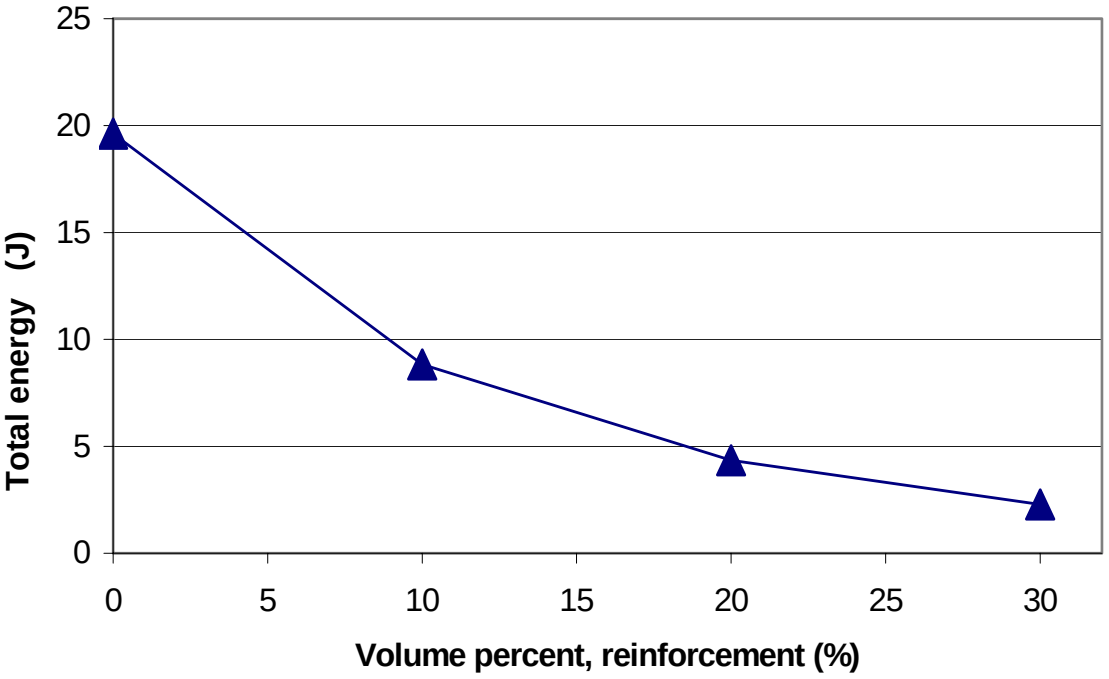

Fig: 4.76: Effect of reinforcement content on Fracture toughness of Al reinforced with Al_20_3 PRMMC composites.

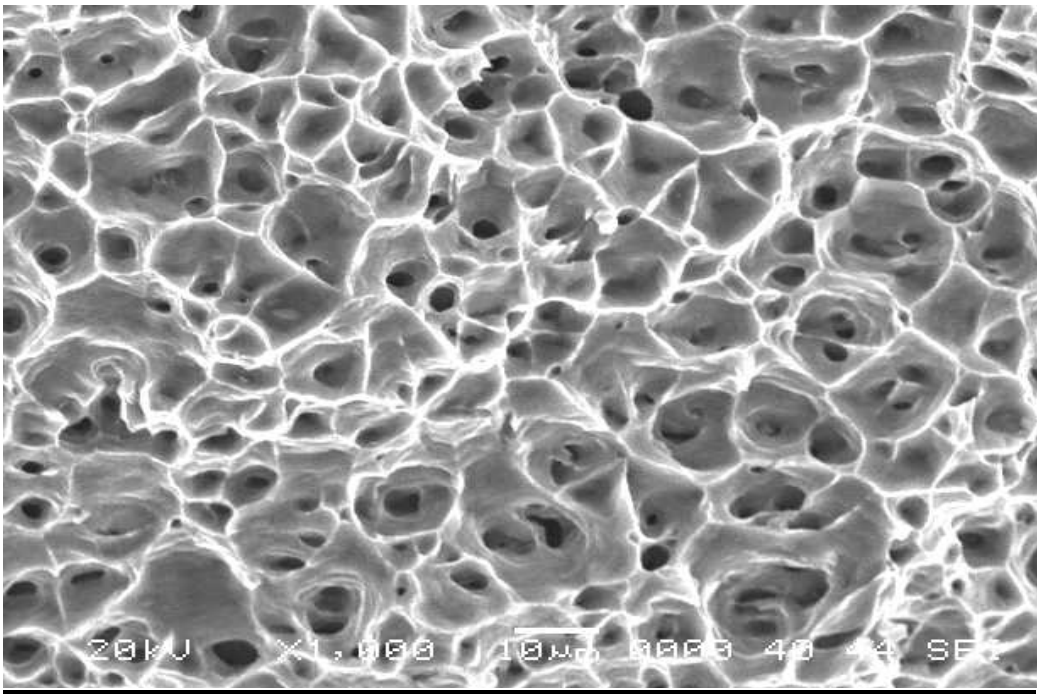

Fig. 4.77: SEM impact fracture surface of 6061 Al alloy at magnification of 1000X.

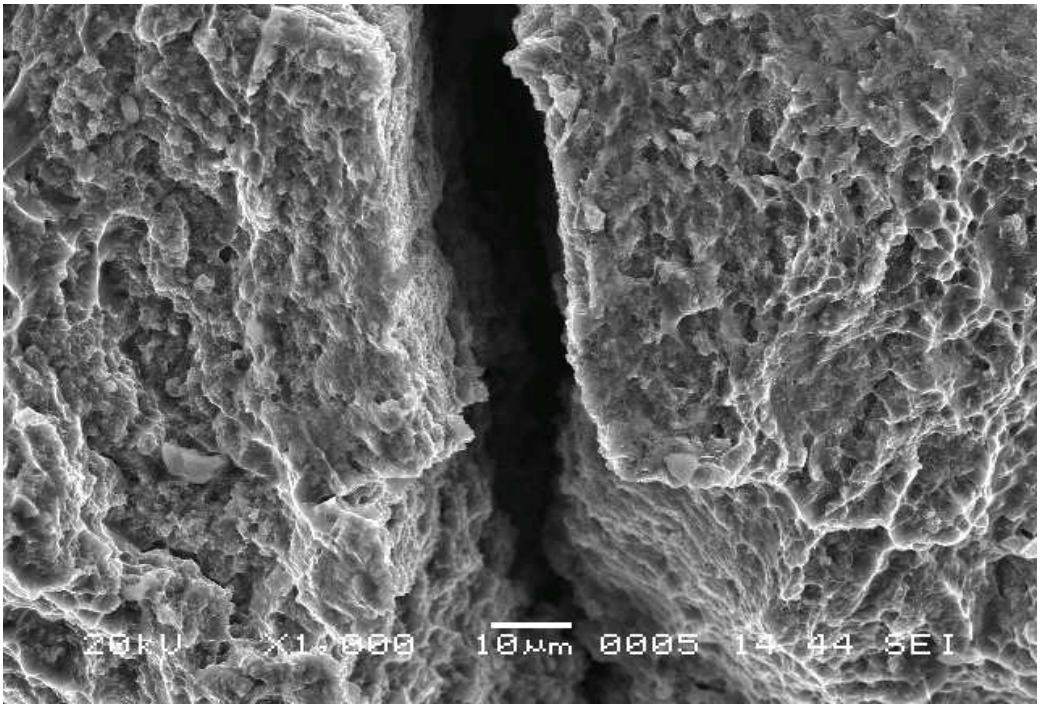

Fig. 4.78: SEM impact fracture surface of 10% v_f Al_2O_3 composite at magnification of 1000X showing crack.

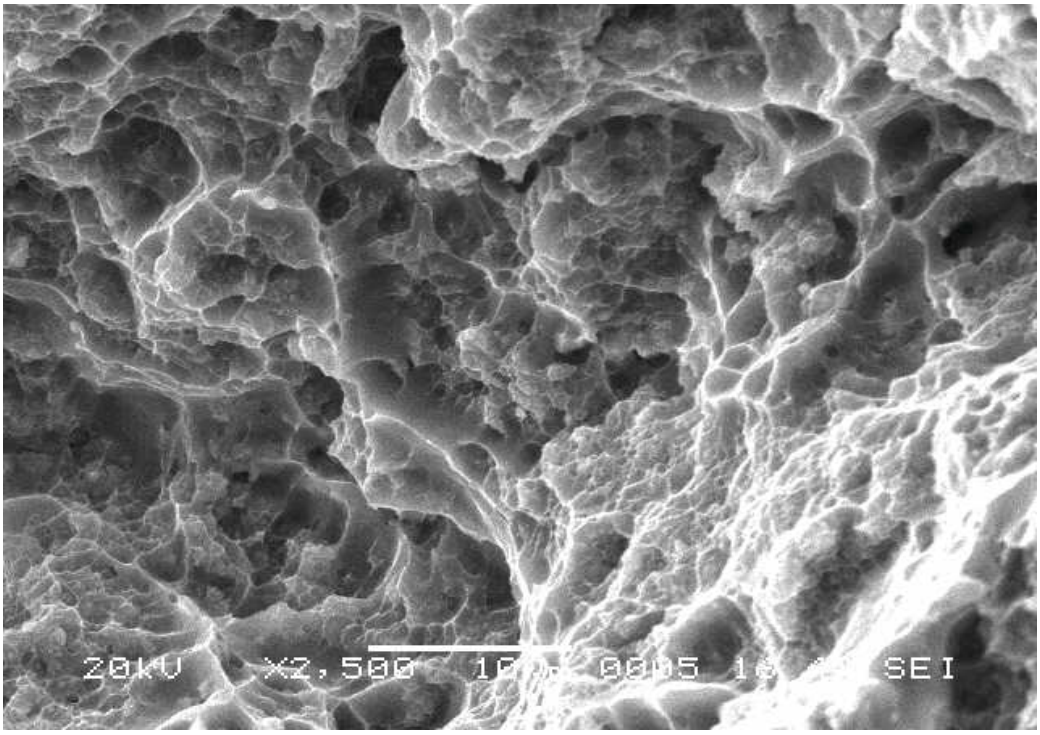

Fig. 4.79: SEM impact fracture surface of 10% v_f Al_2O_3 composite showing dimples at magnification of 2500X.

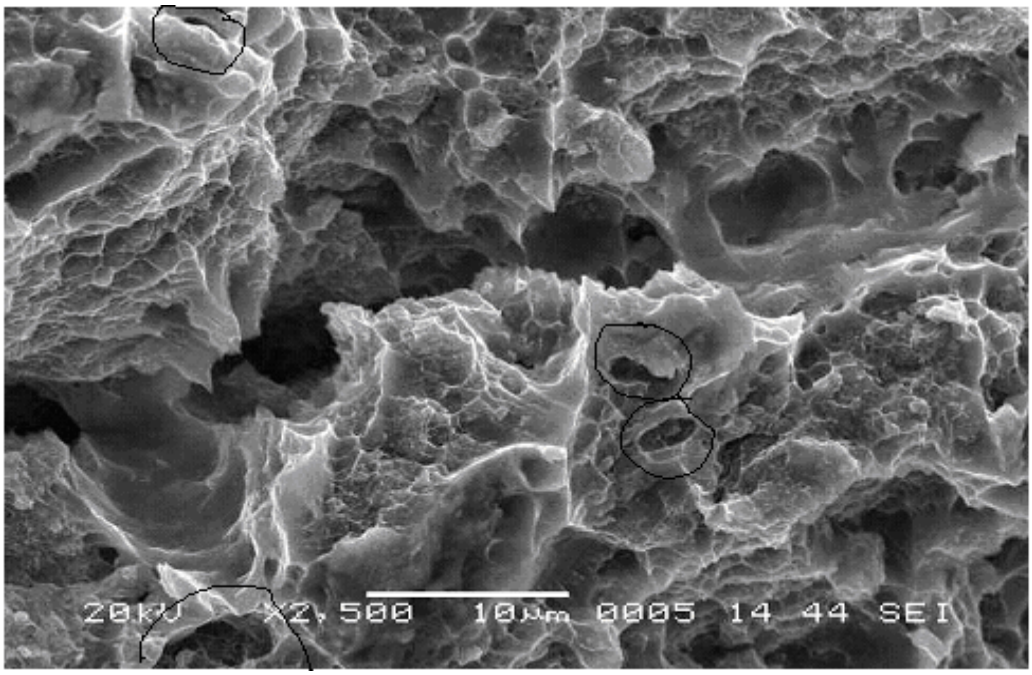

Fig. 4.80: SEM impact fracture surface of 10% $v_f Al_2 0_3$ composite showing dimples with cracks at magnification of 2500X. Circled regions show voids.

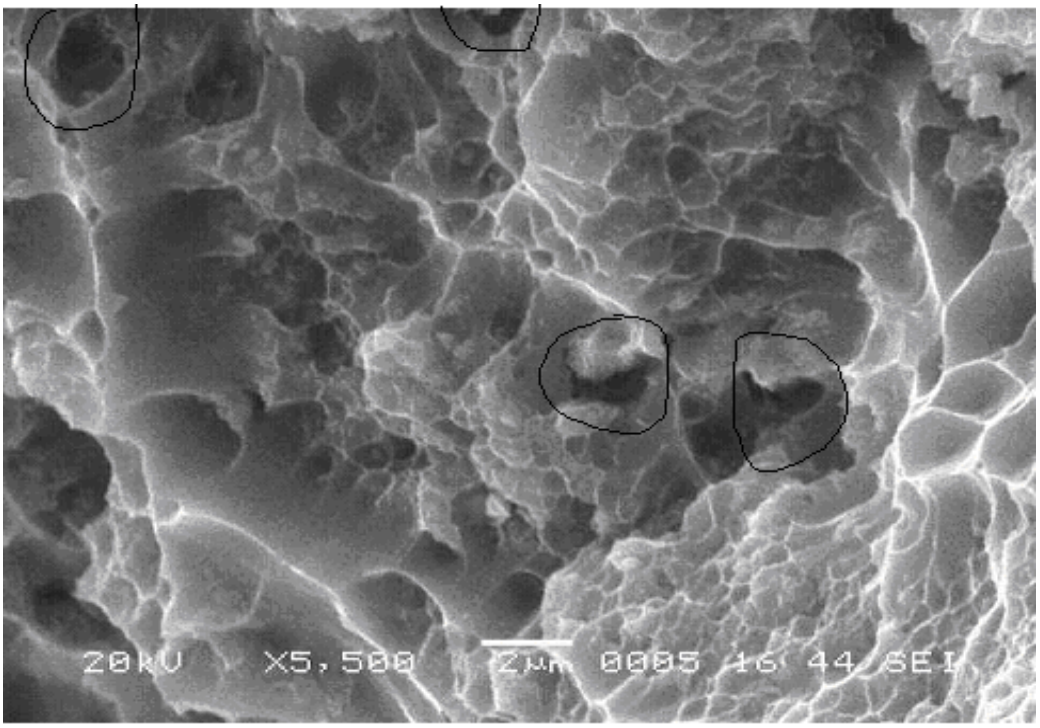

Fig. 4.81: SEM impact fracture surface of 10% $v_f Al_2 0_3$ composite showing matrix- particle decohesion (circled regions) at magnification of 5500X.

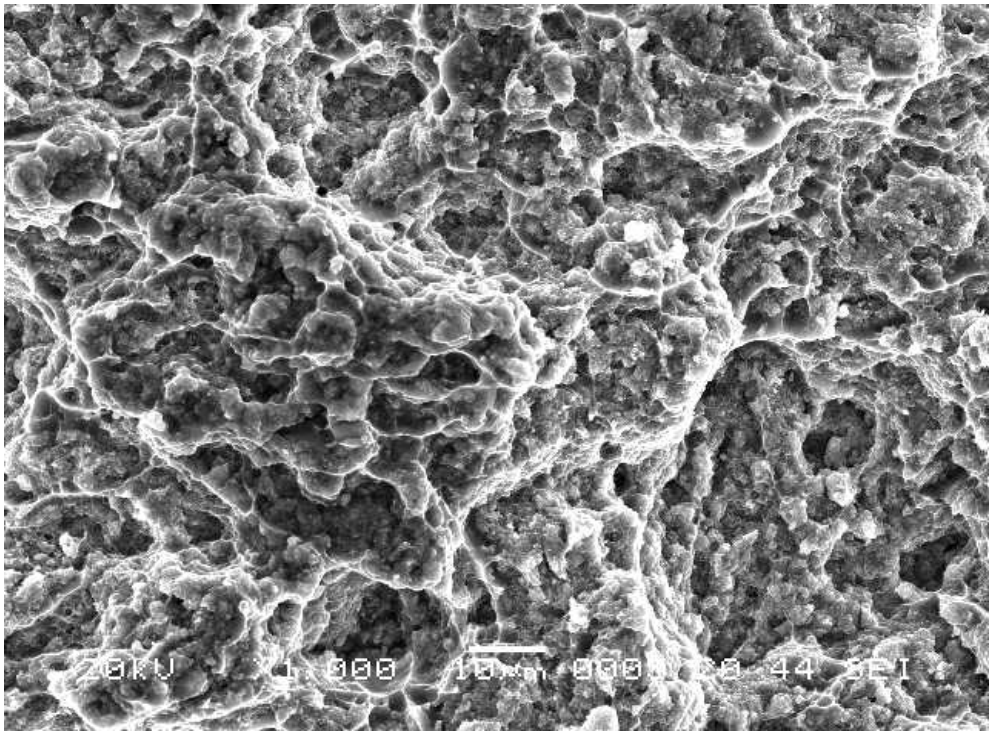

Fig. 4.82: SEM impact fracture surface of 20% $v_f Al_2 0_3$ composite at magnification of 1000X.

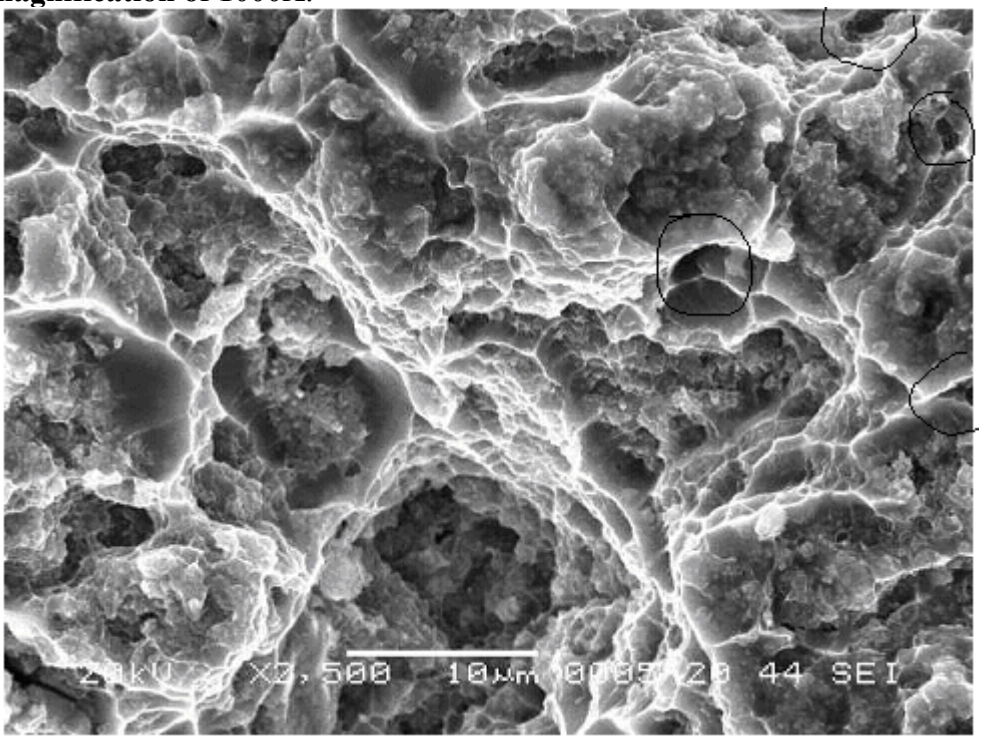

Fig. 4.83: SEM impact fracture surface of 20% $v_f Al_2 0_3$ composite at magnification of 2500X. Circled regions show voids.

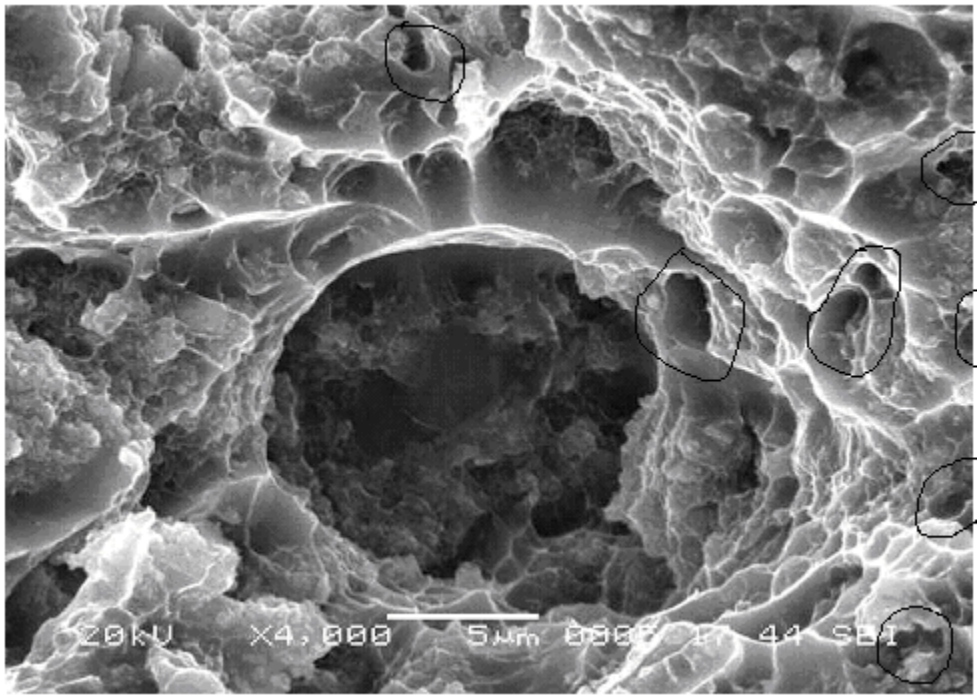

Fig. 4.84: SEM impact fracture surface of 20% v_f Al_2O_3 composite showing dimples at magnification of 4000X. Circled regions show voids.

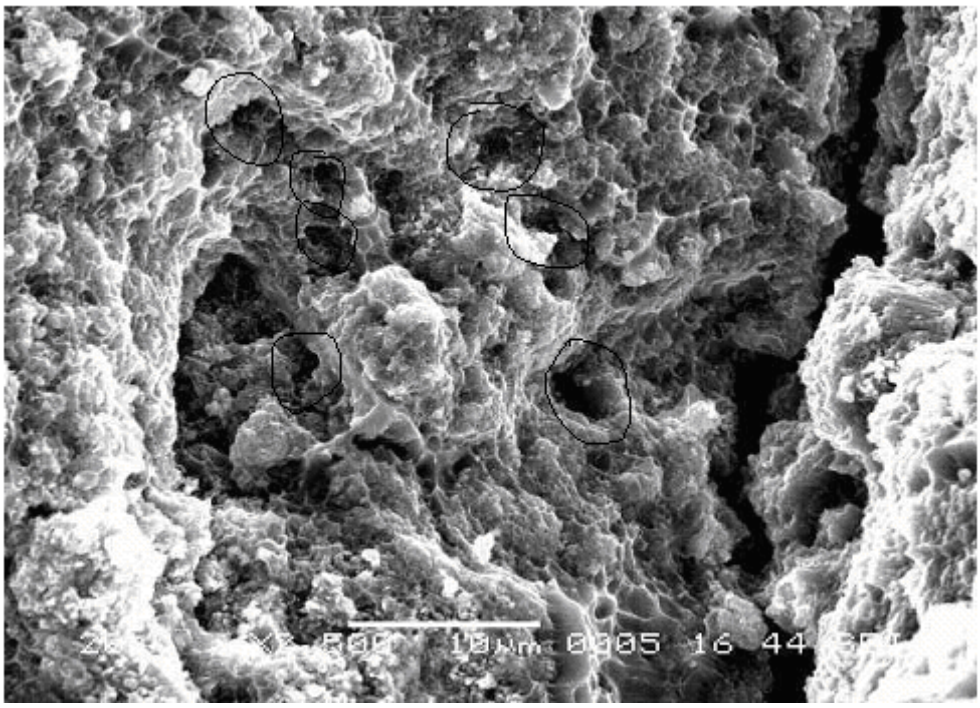

Fig. 4.85: SEM impact fracture surface of 30% v_f Al_2O_3 composite at magnification of 2500X. Circled regions show voids.

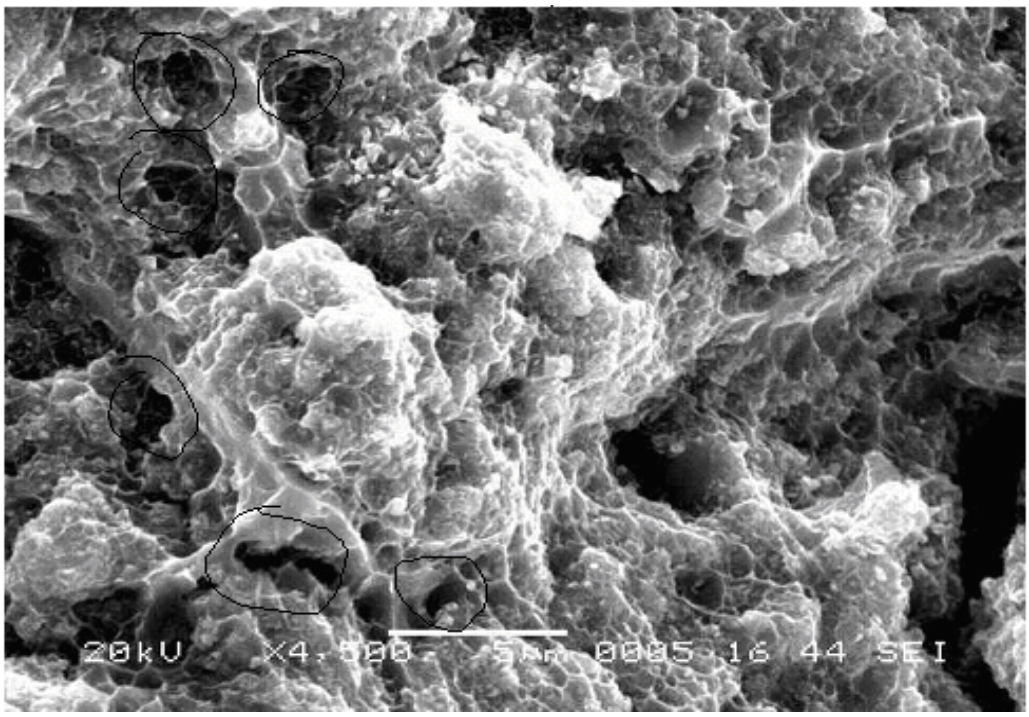

Fig. 4.86: SEM impact fracture surface of 30% v_f Al_2O_3 composite showing dimples at particle free region at magnification of 4500X. Circled regions show voids.

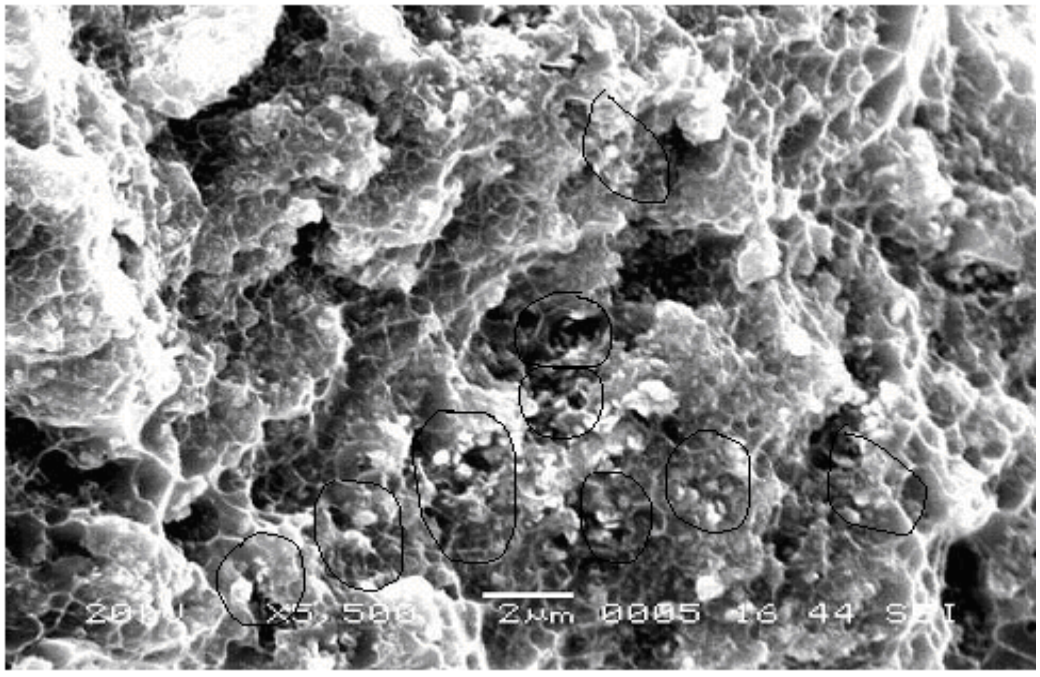

Fig. 4.87: SEM impact fracture surface of 30% v_f Al_2O_3 composite showing matrix-particle decohesion (circled regions) at magnification of 5500X.

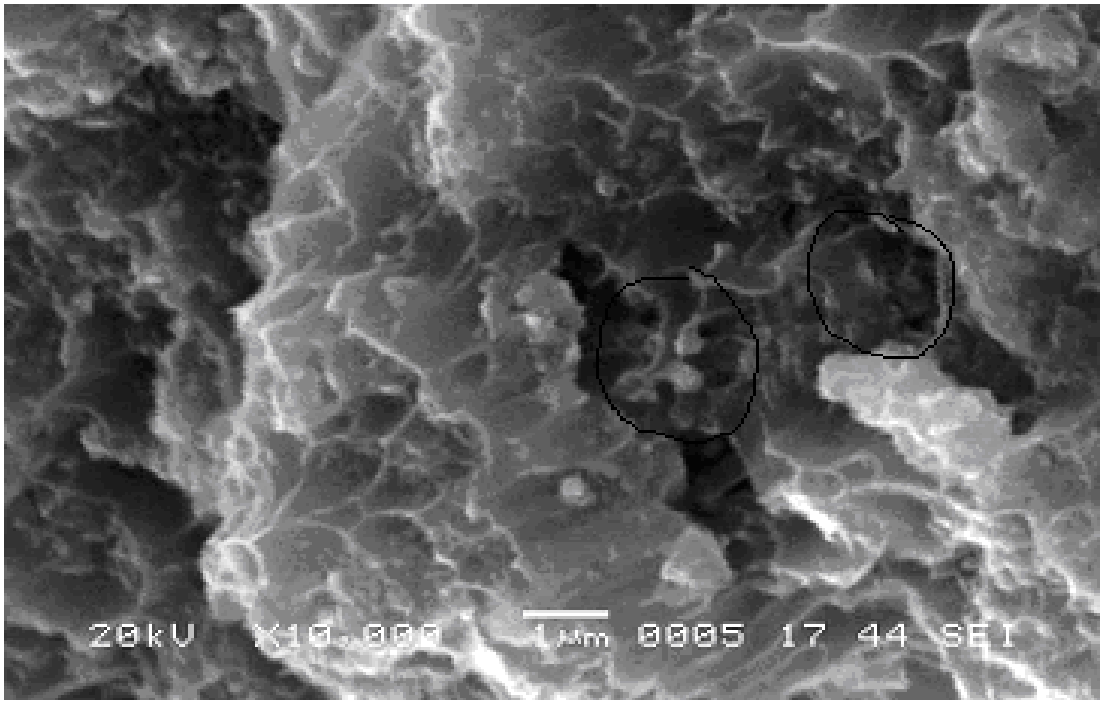

Fig. 4.88: SEM impact fracture surface of 30% v_f $Al_2 0_3$ composite showing matrix-particle decohesion (circled regions) at magnification of 10,000X.

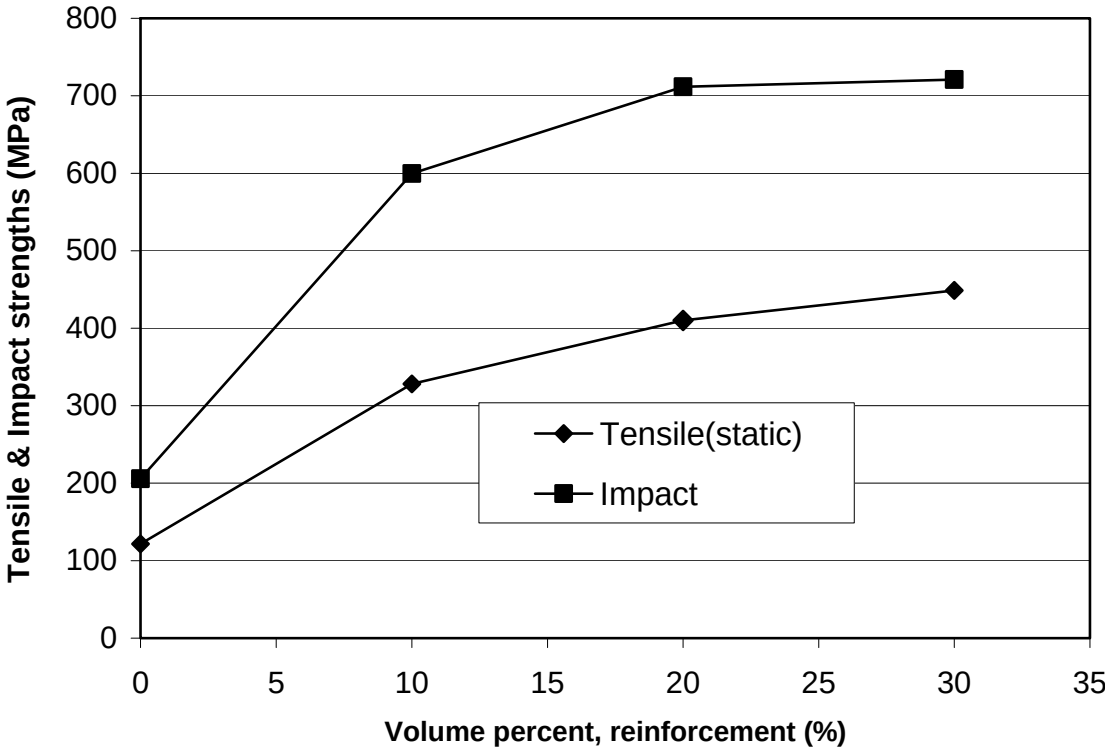

Fig. 4.89: Comparison of low–velocity impact and tensile (static) strengths for Al-based Al_2O_3 PRMMC composites.

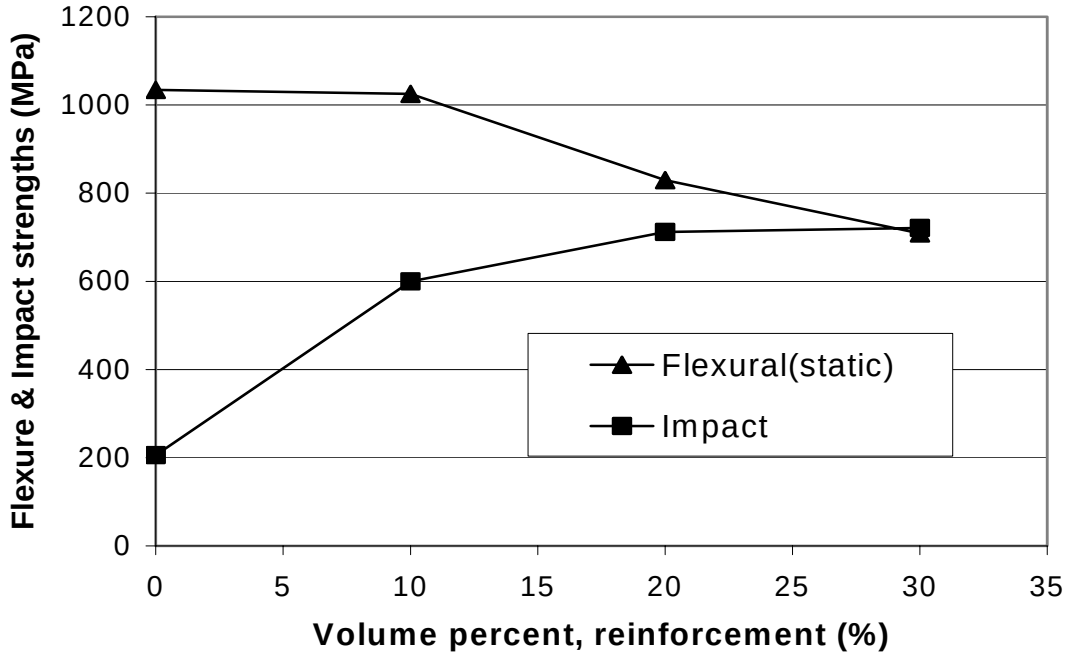

Fig. 4.90: Comparison of low–velocity impact and flexural (static) strengths for Al-based Al_2O_3 PRMMC composites.

CHAPTER 5

NUMERICAL ANALYSIS

5.1 DESCRIPTIONS OF THE FINITE ELEMENT MODEL

The numerical simulation and resulting computations were performed using a finite element analysis with ANSYS software program as a vehicle.

ANSYS is a finite element program with capabilities, ranging from a simple, linear, static analysis to a complex, nonlinear, transient dynamic analysis. For large deformation dynamics, quasi-static problems with large deformations and multiple nonlinearities, and complex contact/impact problems, ANSYS combines with LS-DYNA explicit finite element program with the powerful pre- and post processing capabilities of the ANSYS program.

The explicit method of solution used by LS-DYNA provides fast solutions for short time, large deformation dynamics, quasi-static problems with large deformations and multiple nonlinearities, and complex contact/impact problems. Using this integrated product, one can model the structure in ANSYS, obtain the explicit dynamic solution via LS-DYNA, and review results using the standard ANSYS post processing tools. The procedure for an explicit dynamic analysis is similar to any other analysis that is available

in the ANSYS 8.1 program. A typical finite element analysis on ANSYS/LS-DYNA has three distinct steps: (a) building the Finite Element model, (b) applying loading and obtaining solution, and (c) reviewing the results.

5.2 IDEALIZATION OF THE PROBLEM

In modeling of the impact of a beam full model was employed without using any symmetric condition. The explicit method of solution utilizing LS-DYNA provides fast solutions for short time, large deformation complex contact/impact problems. The procedure for an explicit dynamic analysis is similar to any other analysis that is available in the ANSYS 8.1 program. SOLID164 is used for the 3-D modeling of solid structures. The element is defined by eight nodes having three degrees of freedom at each node: translations in the nodal x, y, and z directions. The element has stress stiffening and large deflection capabilities. Other options are available to suppress the extra displacement shapes and to define the printout locations. The element has various applications, such as for crystals and composites (Fig. 5.1).

- ***Type of problem***: The material behavior for the problem is large deformation and complex contact dynamic problems.
- ***Simplification*:** In the modeling, the full model was employed without using any symmetric condition.

5.3 MODELING

- ***Geometrical model***: Geometrical model with boundary conditions are shown in Fig. 5.2 below.
- ***Material model*:** The problem is Nonlinear, Inelastic, and Bilinear Kinematic Hardening with tangent modulus. The material properties for the impactor and

target object are specified. The impactor (striker) is taken as rigid whereas the material property for Al-based Al_2O_3 PRMMC composites is specified as shown in table 5.1.

- ***Boundary conditions***: The boundary conditions are shown in the Fig. 5.2 where the rectangle block is the sample. The simple supported boundary condition is obtained by applying the constraint of the translation x and z axis to the supporting locations of the beam.
- ***Loading:*** During the free fall stage, the striker is simply accelerating due to gravity. The analysis started at's' mm above the sample and applying an terminal velocity of V_f mm per second to simulate free fall. V_f is an approximation derived using V_f = SQRT (2*g*s) where V_f is the final velocity, g is the acceleration due to gravity, and s is the displacement. Friction from the air is neglected.
- ***Contact pair:*** There are 18 different types of contact can be chosen to accurately represent the physical model; among them the surface to surface (STS) is common in use.

5.4 FINITE ELEMENT MESH

The type of element used is SOLID164. Meshing used is shown in Fig. 5.3. It is refined for more accuracy, because as a general rule, the finer the Finite Element mesh, the more accurate the results. In an explicit solver, such as ANSYS LS-DYNA, the analysis time is highly dependent on the smallest element in the model. Therefore, for efficient results, a uniform element size should be used. The number of elements used in the model was 5059.

5.5 RESULTS

Fig. 5.4-5.11 show the FEM stress (MPa) distribution of Al alloy reinforced with $Al_2 0_3$ PRMMC composites. Fig. 5.4, Fig. 5.6, Fig. 5.8 and Fig. 5.10 show the stress (MPa) distribution whereas Fig. 5.5, Fig. 5.7, Fig. 5.9, and Fig. 5.11 show the magnified views of stress (MPa) distributions for the 0, 10, 20, 30 % v_f $Al_2 0_3$ PRMMC composites, respectively. Low-velocity impact test results (MPa) are compared with the outcome of the FEM results (Fig.5.12). Percent error between the low–velocity impact test results and finite element numerical values for the Al alloy reinforced with $Al_2 0_3$ PRMMC composites are listed in Table 5.2. Percent error between the low–velocity impact test results and FEM numerical values for Al-based Al_2O_3 PRMMC composites increases with increasing volume fraction (v_f) of the particle reinforcement.

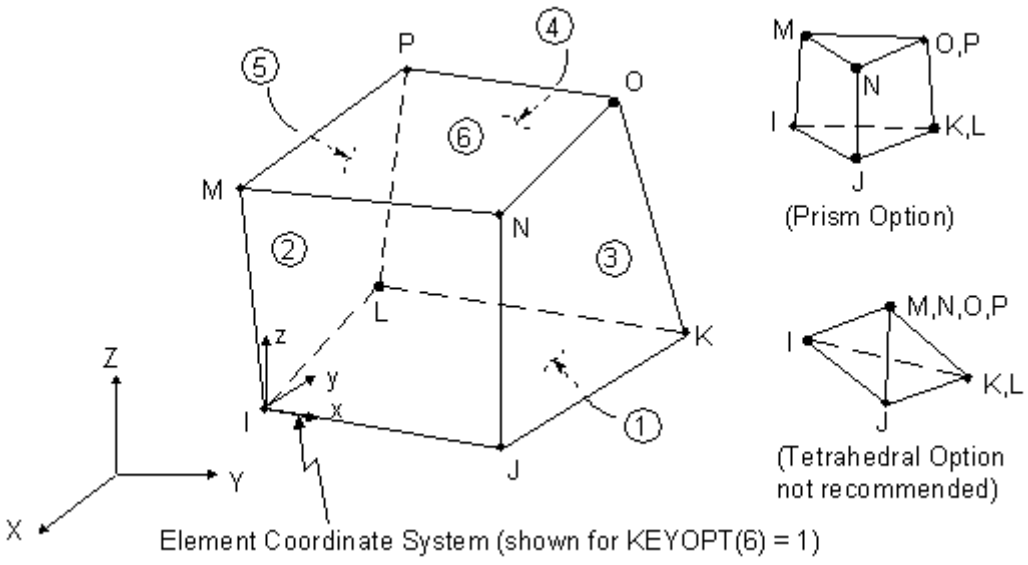

Fig. 5.1: Element SOLID 164

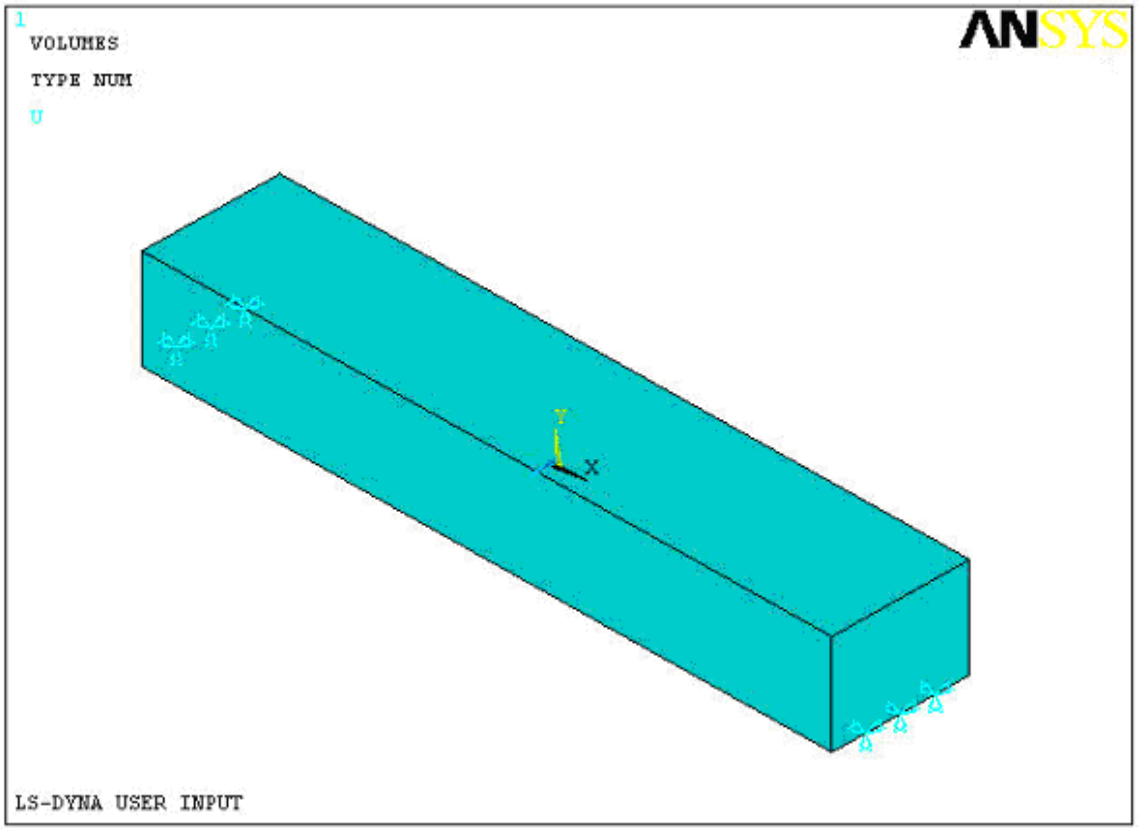

Fig. 5.2: Finite element model with boundary conditions.

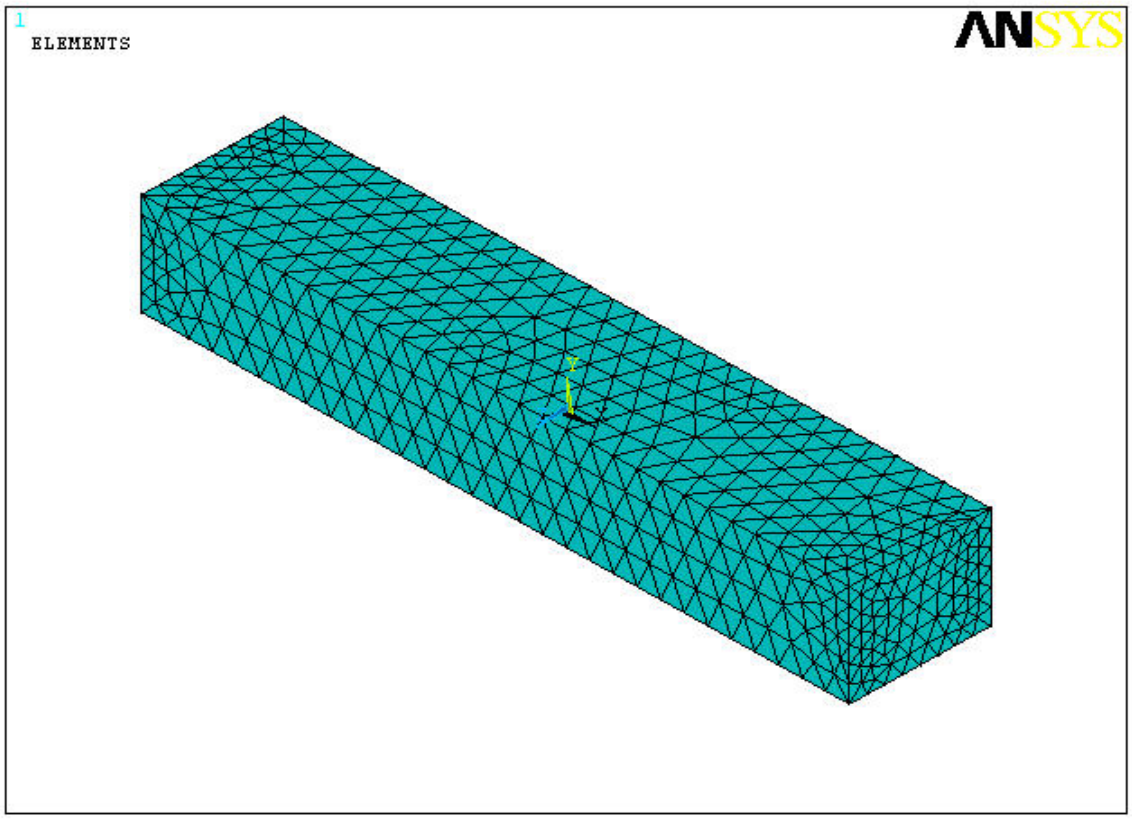

Fig. 5.3: Mesh used in Finite element analysis.

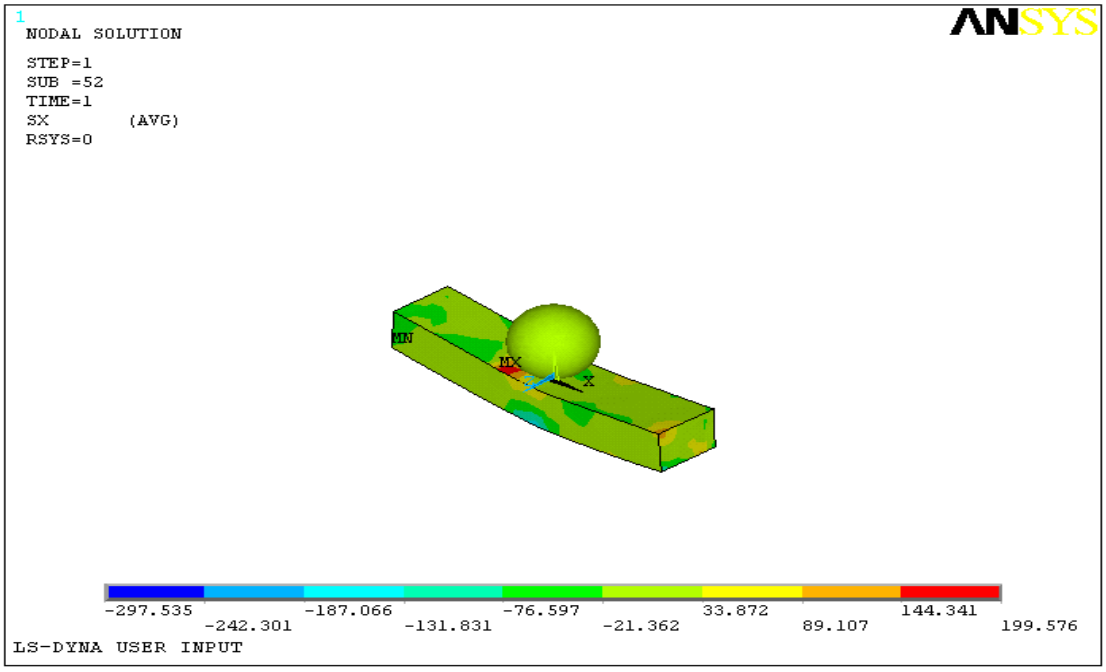

Fig. 5.4: Stress distribution on 6061 alloy (isometric view).

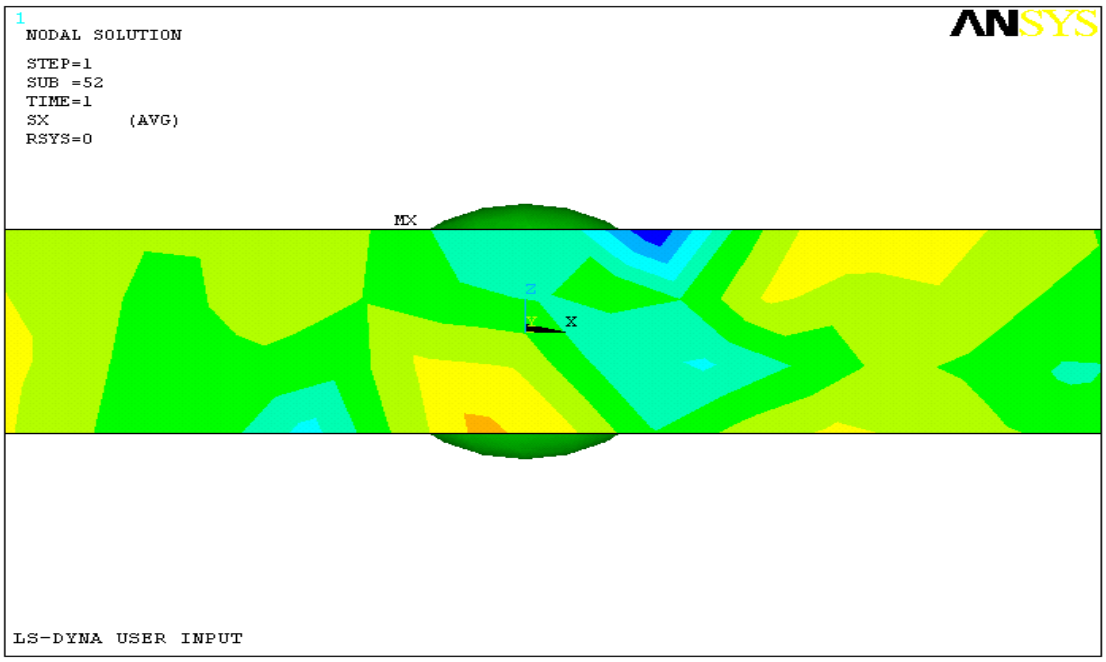

Fig. 5.5: Stress distribution on 6061 alloy (closer view).

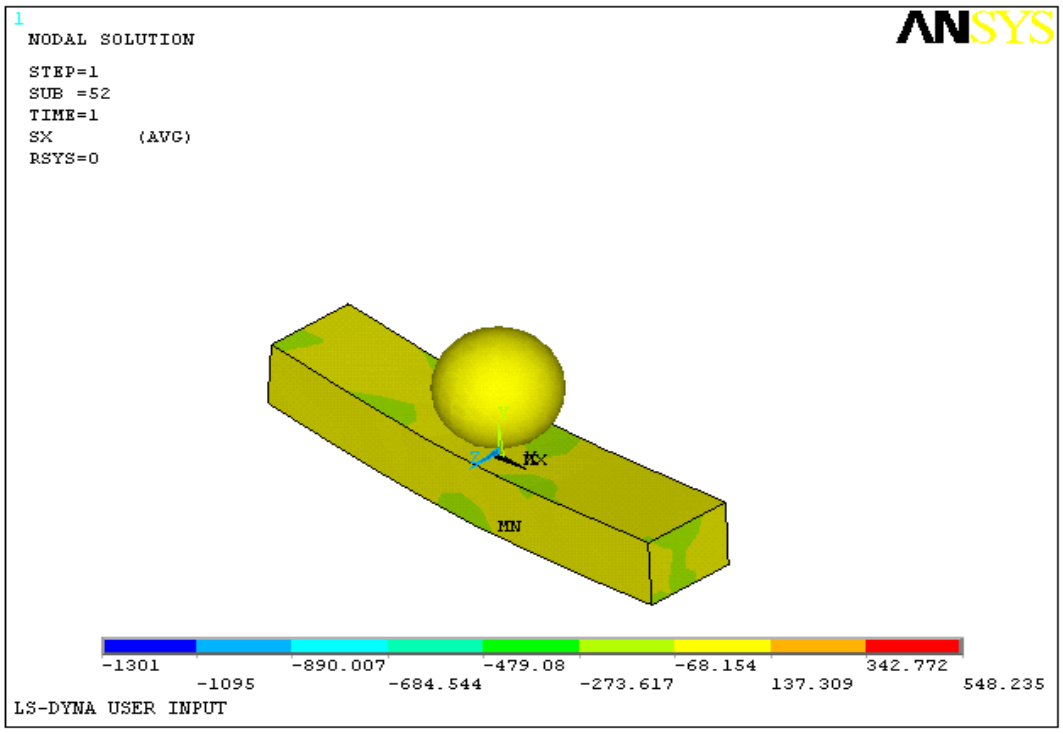

).

Fig. 5.6: Stress distribution on 10% $v_f Al_2 0_3$ composite (isometric view).

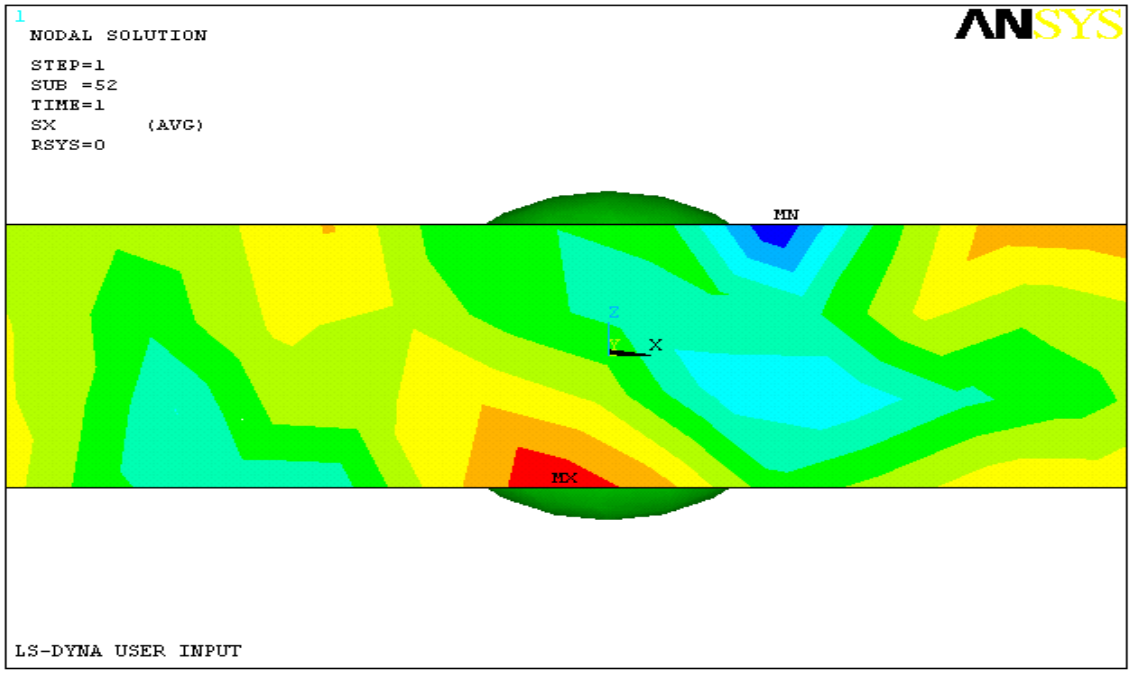

Fig. 5.7: Stress distribution on 10% $v_f Al_2 0_3$ composite (closer view).

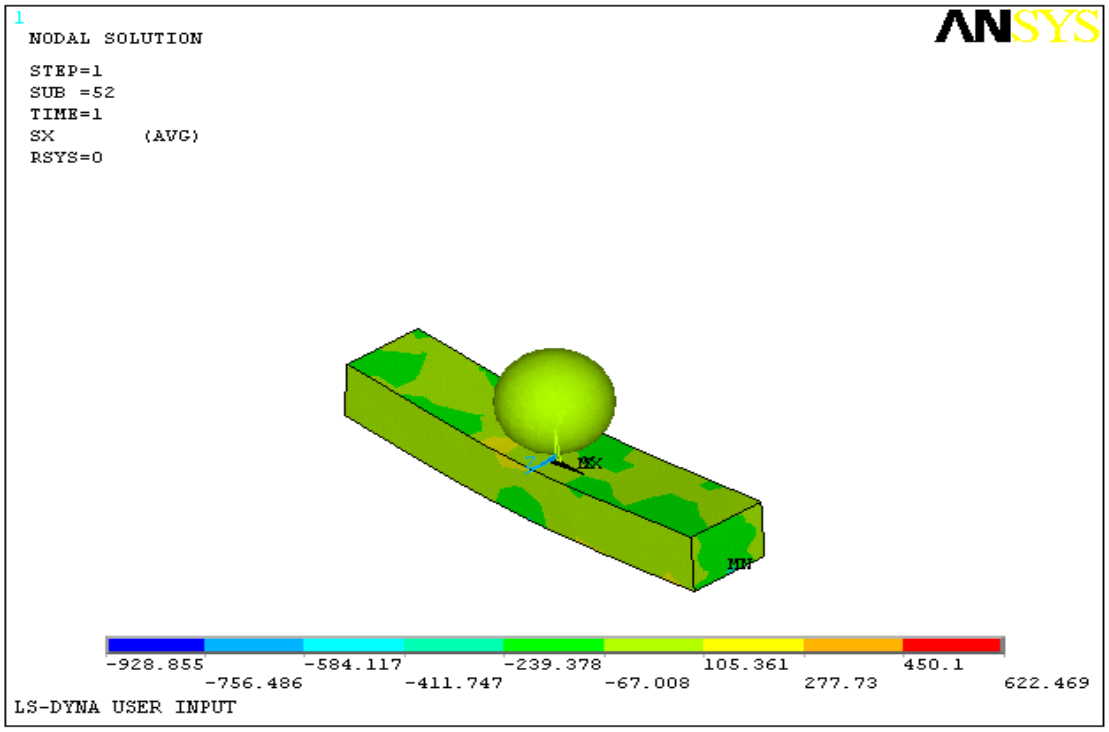

Fig. 5.8: Stress distribution on 20% $v_f Al_2 0_3$ composite (isometric view).

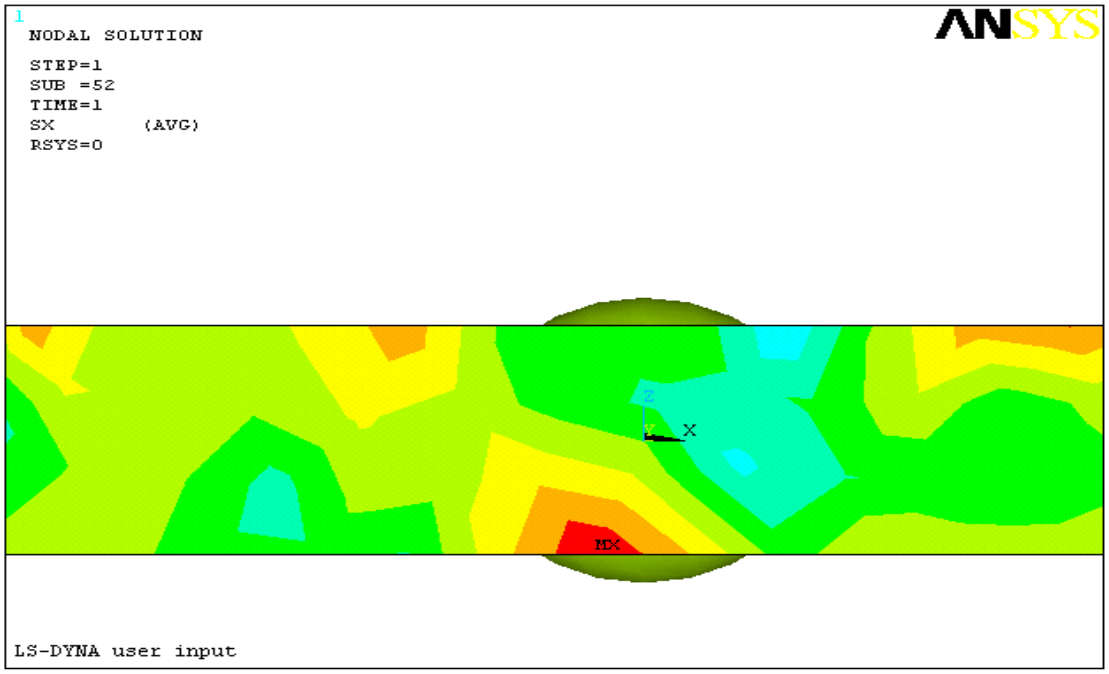

Fig. 5.9: Stress distribution on 20% $v_f Al_2 0_3$ composite (closer view).

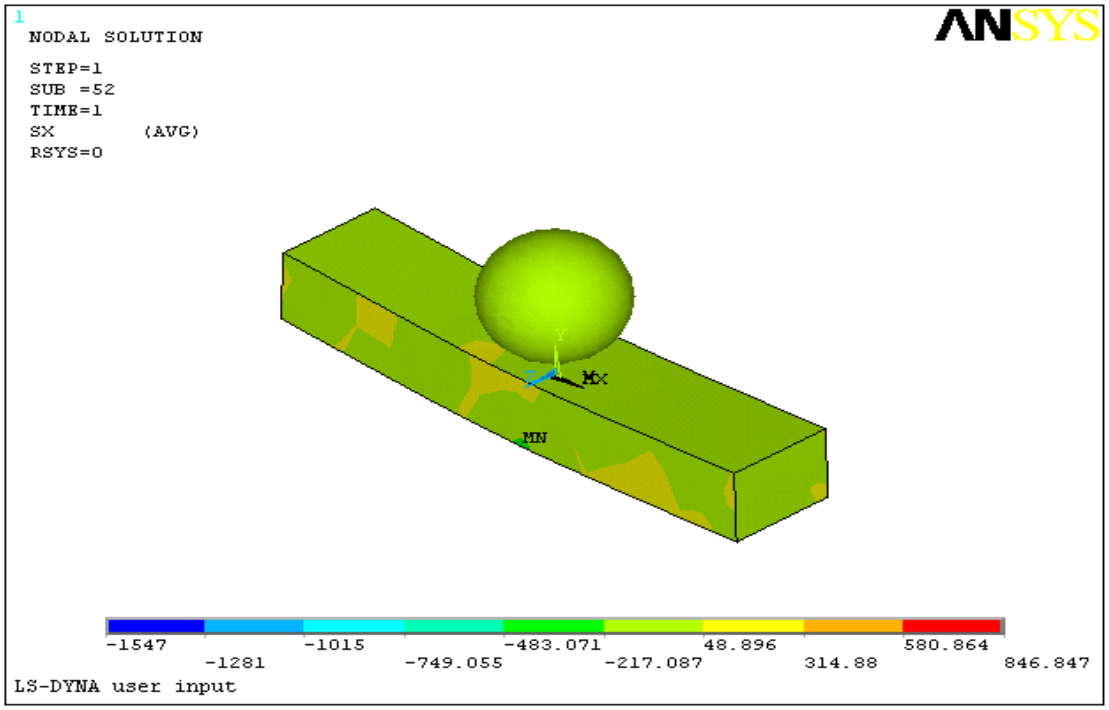

Fig. 5.10: Stress distribution on 30% $v_f Al_2 0_3$ composite (isometric view).

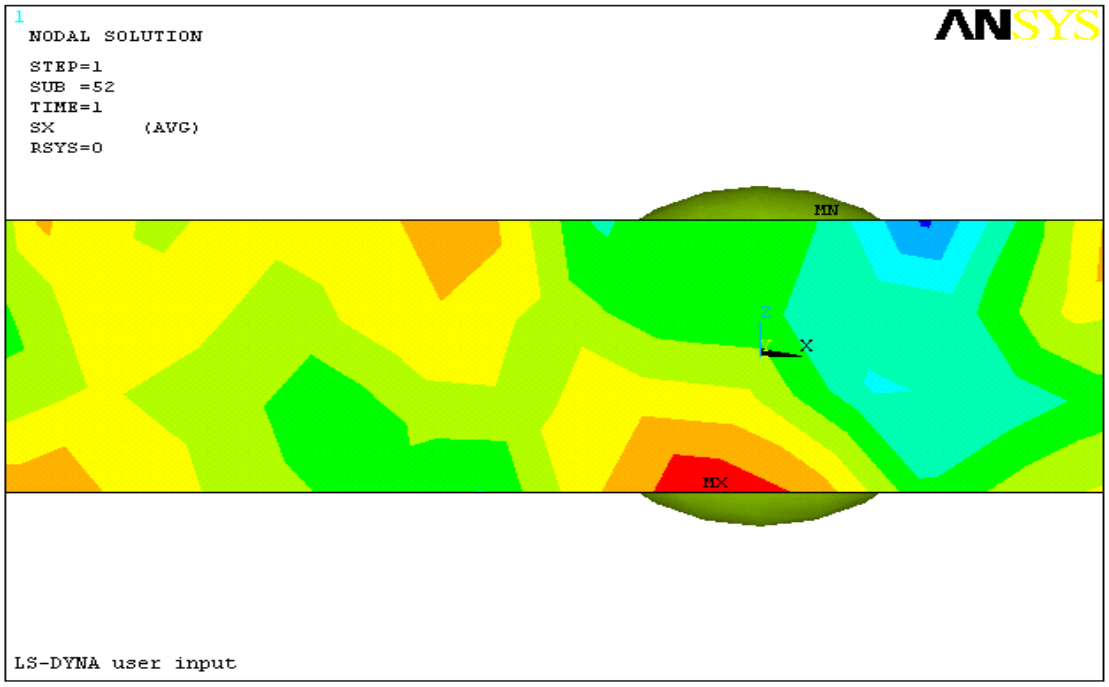

Fig. 5.11: Stress distribution on 30% $v_f Al_20_3$ composite (closer view).

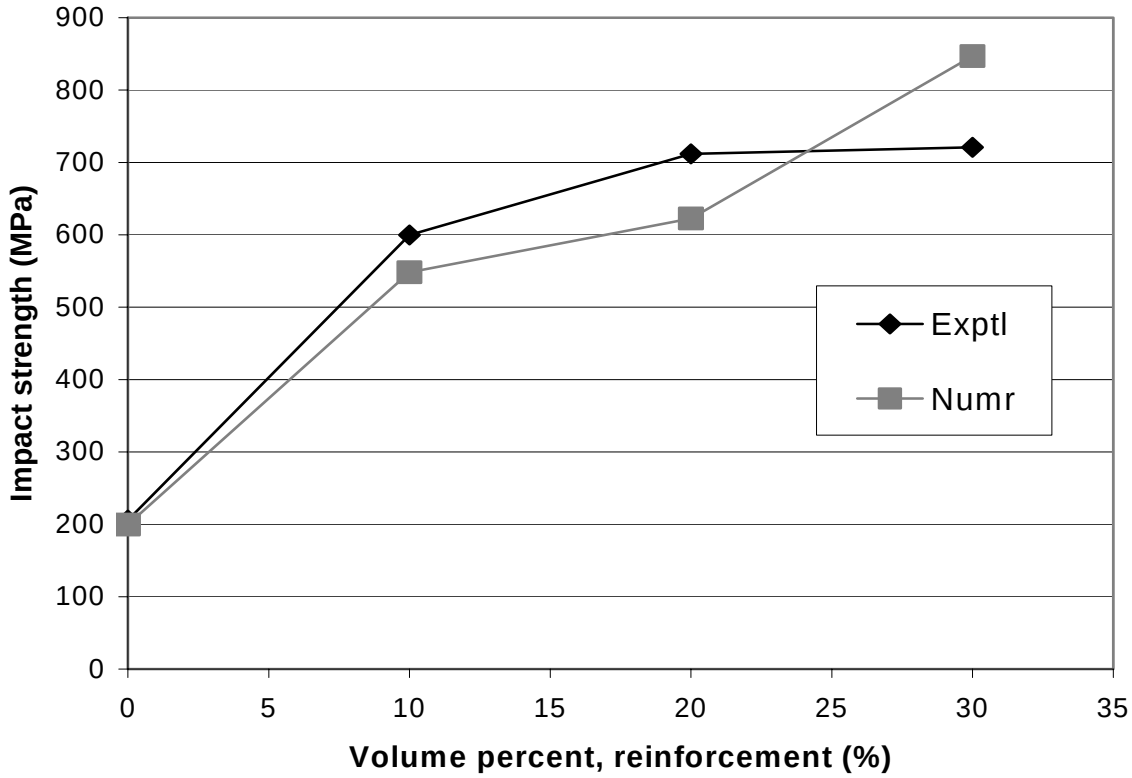

Fig. 5.12: Comparison of low–velocity impact test results and Ansys finite element model for Al-based Al_2O_3 PRMMC composites.

Table 5.1 Material properties of striker and Al reinforced with Al_20_3 PRMMC composites.

	Striker	6061 Alloy	10% v_f Al_20_3 composite	20% v_f Al_20_3 composite	30% v_f Al_20_3 composite
Yield strength (MPa)	417.1	46.5	184.33	297.56	354.67
Modulus of elasticity (GPa)	200	68.03	86.81	104.45	109.90
Tangent modulus (MPa)	-----	214.75	6984.60	9172.70	16347.00
Density (g/cu.cm)	7.865	2.678	2.875	2.956	2.720

Table 5.2: Percent error between the Low–velocity impact test results and Ansys finite element model for Al-based Al_2O_3 PRMMC composites.

vol. % of composite	Experimental Impact strength (MPa)	FEA Impact strength (MPa)	% Error
0	205.85	199.58	3.05
10	599.72	548.24	8.59
20	711.76	622.47	12.55
30	721.03	846.85	17.45

CHAPTER 6

CONCLUSIONS AND RECOMMENDATIONS

6.1 CONCLUSIONS

The main objective of this study is to determine the strengthening mechanisms of Al based Al_20_3 metal matrix composites under both static and dynamic loadings. Several samples of these composites with volume contents (v_f) of 10, 20, and 30 % Al_20_3 were tested and studied. Test results were compared with the outcome of a finite element method model (FEM). In order to understand experimentally the influence of Al_20_3 particle clustering on the deformation characteristics, the fracture surfaces of tested samples were examined under SEM.

The following conclusions are obtained from the outcome of this study.

- The strengthening mechanisms (under both static and impact loadings) are found to be related directly to reinforced particle distribution. Due to the constraints imposed on deformation caused by the presence of the hard and brittle Al_20_3 particles in the soft and ductile 6061 alloy matrix higher applied stress is required to initiate plastic deformation in the matrix. This in turn results in the increase in the tensile strength of the composite.

- The tensile strength of the composite materials studied increases with increasing volume fraction (v_f) of the particle reinforcement. Similar increase is observed for the elastic modulus, but the rate of increase decreases slightly with the increase in volume fraction. The tensile elongation decreases with the increase in reinforcement.
- SEM examination of fracture surfaces of tested PRMMC composites reveals the amount of porosity increases with increasing reinforcement content, especially in the area where particles are clustered (from EDS analysis).
- The presence of the reinforcing particles causes a significant decrease in flexural strength, fracture toughness and fracture impact energy when compared to unreinforced 6061 alloy.
- Analyses of the fracture surfaces using SEM show dimpled structure of the matrix indicating the main fracture mechanism was by void nucleation, growth and linking. The process of failure is by interface decohesion, between the matrix and particles, and its propagation along the particle-matrix interface. In particle rich regions of the matrix fracture propagates rapidly among the reinforcing particle agglomerates. However, in reinforcement-thin regions, the metal matrix aids in retarding the progression and linkage of the damage.
- The fracture surfaces for the 6061 alloy revealed minor difference in the fracture mechanisms under both static and impact testings, which means the effect of rate of loading on fracture mechanisms of 6061 alloy is very small.
- The fracture surfaces for reinforced composites under impact testing show enlarged voids, which are different from those observed under static testing

(tensile & flexural). The impact force causes voids to be enlarged, producing plastic deformation in the matrix. On the other hand, the under static loads stress concentrations at the crack tip most likely cause the fracture.

- The Low-velocity impact test results were compared with the outcome of a finite element model, and percent errors between the results of low–velocity impact tests and ANSYS finite element model (FEM) for Al-based Al_2O_3 PRMMC composites was found to increase with increasing volume fraction (v_f) of the particle reinforcement.

6.2 RECOMMENDATIONS FOR FUTURE WORK

Following are some of the recommendations for any future work to be carried out on submicron Al_20_3 reinforced aluminum PRMMC composites.

- The effect of temperature on the tensile properties of PRMMC composites can be a useful extension to the present work. These results can be used to predict the mechanical behavior at different working environments.

- Fracture toughness is an important material property. The effect of temperature on the fracture toughness can be investigated to explain some of the mechanisms observed here.

- A correlation between the dynamically measured fracture toughness and the fracture energy is also recommended to investigate.

- The effect of heat treatment on the mechanical properties of PRMMC composites may be determined and the results compared to unheat-treated composites.

BIBLIOGRAPHY

1. Clyne T .W; Withers P .J; An introduction to MMCs, Cambridge university press, 1993.
2. Luster, J.W; M.Thumann, and R Baumann; Mechanical Properties of Aluminum Alloy 6061 Al_20_3 Composites, Material science and Technology, vol 9 Oct 1993, pp 853.
3. McDaneals, D.L, Analysis of Stress, Strain, Fracture and Ductility Behavior of Al Matrix Composite Containing Discontinuous SiC Reinforcement, Metallurgical transactions A, Vol 16A, 1985, pp 1105-1115.
4. Ibrahim, I.A; Mohammed, F.A; Lavernia, E.J; Particulate Reinforced Metal Matrix Composites: A Review Journal of material science; 26 mar 1991, pp 1137-1156.
5. Fang, C. -k.; Fang, R.L; Weng, W.P and Chuang, T.H; Applications of Ultrasonic Testing for the Determination of Volume Fraction of Particulates in Alumina Reinforced Al Matrix Composites; Materials characteristics 43, 1999, pp 217-226.
6. A.Mortensen, M.N. Gungor, J.A. Cornie and M.C. Flemings, Microstructures of Cast Metal Matrix Composites, *Journal of Metals*, 38, 30, March 1986.
7. Nair, S. V; Tien, J. K.; Bates, R. C. Silicon carbide-reinforced aluminium metal matrix composites. International Metals Reviews (1985), 30(6), pp 275-90.
8. Nardone, V. C; Prewo, K. M; On the Strength of Discontinuous Silicon Carbide Reinforced Aluminum Composites; Scripta Metallurgica (1986), 20(1), pp 43-8.

9. Stacey, M. H; Production and Characterization of Fibers for Metal Matrix Composites. Materials Science and Technology (1988), 4(3), pp 227-30.
10. Lloyd,D.J; Particle Reinforced Al and Mg Matrix Composites; International Materials reviews, vol 39 No.1, 1994, pp 1-23.
11. Park, B.G; A.G.Crosky and A.K.Hellier, Fracture Behavior and Toughness of an Al 6061 Metal Matrix Composites, Journal of the Australasian ceramic society, 30(1-2), 1994, pp 41-47.
12. Zhou Zhao, Song Zhijia and Xu Yingkun; Effect of Microstructure on the Mechanical Properties of an Al alloy 6061-SiC Particle Composite Materials; Material science and Engineering A 132, 1991, pp 183-188.
13. Delannay, F; Froyen, L and Deruttere, A; The wetting of Solids by Molten Metals and its Relation to the Preparation of Metal Matrix Composites; Journal of materials science, 22, 1987, pp 1-16.
14. Yadav, S; Chichili, D.R and Ramesh, K.T."The Mechanical Response of a 6061-T6 Al/ Al_2O_3 MMC at High Rate of Deformation", Acta metallurgica et materialia, vol 43 No 12, 1995, pp 4453-4464.
15. Divecha, A. P.; Fishman, S. G.; Karmarkar, S. D. Silicon Carbide Reinforced Aluminum - a Formable Composite. Journal of Metals (1981), 33(9), pp 12-17.
16. Hasson, D. F.; Hoover, S. M.; Crowe, C. R. Effect of Thermal Treatment on the Mechanical and Toughness Properties of Extruded SiC whisker/aluminum 6061 Metal Matrix Composite; Journal of Materials Science (1985), 20(11), pp 4147-54.

17. Daehn, Glenn S.; Gonzalez-Doncel, Gaspar. Deformation of whisker-reinforced Metal-Matrix Composites under Changing Temperature Conditions. Metallurgical Transactions A: Physical Metallurgy and Materials Science (1989), 20A (11), pp 2355-68.
18. Arsenault, R. J. The Strengthening of Aluminum Alloy 6061 by Fiber and Platelet Silicon Carbide; Materials Science and Engineering (1984), 64(2), pp 171-81.
19. Roebuck, B; Fractography of a Sic Particulate Reinforced Al MMC; Journal of materials science, 6, 1987, pp1138-1140.
20. Lonsdon, W.A and Liaw, P.K; "Tensile Fracture Toughness and Fatigue Crack Growth Rate Properties of SiC whisker and Particulate Reinforced Al MMCs", Engineering fracture mechanics 24, 1986, pp 37-751.
21. Composites, Machine design, June 1993, 65, 13, pp 727-737.
22. Aghajanian, M. K.; Macmillan, N. H.; Kennedy, C. R.; Luszcz, S. J.; Roy, R. Properties and Microstructures of Lanxide Alumina-Aluminum Ceramic Composite Materials; Journal of Materials Science (1989), 24(2), pp 658-70.
23. David L.Davidson; Tensile Deformation and Fracture Toughness of 2014+15 vol pct SiC Particulate Composite; Metallurgical transactions A, Vol 22A, January 1991, pp 113-123.
24. Vincent C, Nardone, James R.Strife and K.M.Prewo, "Microstructurally Toughened Particulate Reinforced Al Matrix Composites", Metallurgical transactions A, vol 22 A, Jan 1991, pp171-182.

25. Manoharan, M.; Kamat, S. V. On the fracture toughness of particulate reinforced metal-matrix composites. Scripta Metallurgica et Materialia (1991), 25(9), pp 2121-5.

26. Paul S. Gilman, Discontinuously reinforced Aluminum: Ready for the 1990s, Journal of metals, august, 1991, pp 7-15.

27. Zhirui wang and Ruby J. Zhang, mechanical behavior of cast particulate SiC/Al (A 356) MMCs; Metallurgical transactions A, Vol 22A, July 1991, pp 1585-1593.

28. Mummery, P.; Derby, B. The influence of microstructure on the fracture behavior of particulate metal matrix composites. Materials Science & Engineering, A: Structural Materials: Properties, Microstructure and Processing (1991), A135, 1991, pp 221-4.

29. Kim, H.J; Kobayashi, T and Yoon, H.S; "Micromechanical fracture process of SiC particulate reinforced Al alloy 6061-T6 MMCs", Materials science and Engineering, A 154, 1992, pp 35-41.

30. Bhattacharyya, J.D;. Bowis, M.E and Gregory, J.T; "The influence of alumina microsphere reinforcement on the mechanical behavior and weldability of an Al metal matrix composite", Proceedings of the machining composite materials symposium, ASM materials week, Chicago, Illinois, 1-5 Nov 1992, pp 49-56.

31. Chia-Chaw Perng, Jiun-Ren Hwang and Ji-liang Doong, High Strain rate tensile properties of an (Al_20_3 particles)-(Al alloy 6061 T6) metal matrix composites, Materials science and Engineering, A171, 1993, pp 213-221.

32. Pestes, R. H.; Kamat, S. V.; Hirth, J. P. Fracture toughness of Al-4%Mg/Al2Op composites. Materials Science & Engineering, A: Structural Materials: Properties, Microstructure and Processing (1994), A189 (1-2), pp 9-14.
33. Kamat, S. V.; Hirth, J. P.; Mehrabian, R. Mechanical properties of particulate-reinforced aluminum-matrix composites. Acta Metallurgica (1989), 37(9), pp 2395-2402.
34. Manoharan, M.; Lewandowski, J. J.; Hunt, W. H., Jr. Fracture characteristics of an aluminum-silicon-magnesium model composite system. Materials Science & Engineering, A: Structural Materials: Properties, Microstructure and Processing (1993), A172 (1-2), pp 63-9.
35. Hadianfard, M. J; Healy, J;.Mai, Y. –W; ”Fracture characterization of a particle reinforced metal matrix composite”; Journal of materials science, 29,1994, pp 2321-2327.
36. Hadianfard, M. J; Heness, G;.Healy, J.C;.Mai, Y. –W; “Fracture toughness measurements and failure mechanisms of metal matrix composite”; Fatigue fracture engineering, material structure vol 17,No.3, 1994, pp 253-263.
37. Zulfikar H.A.Kassam, Ruby J. Zhang, Zhirui wang, Finite element simulation to investigate interaction between crack and particulate reinforcements in metal matrix composites, Materials science and Engineering, A 203, 1995, pp 286-299.
38. Sriram, S; Daniels, Christopher; Srivatsan, T. S, Influence of Al2O3 particulate reinforcement on tensile fracture of an aluminum alloy metal matrix composite. Metals, Materials and Processes (1995), 7(2), pp 83-92.

39. Srivatsan, T. S. Microstructure, tensile properties and fracture behavior of Al_2O_3 particulate-reinforced aluminum alloy metal matrix composites. Journal of Materials Science (1996), 31(5), pp 1375-88.

40. Shi, N; Song, S.G; Gray III, G.T. and.Roberts, J.A; "Particle shape effects on the fracture of discontinuously reinforced 6061 Al matrix composites", The Johannes weertman symposium, the minerals, metals, and materials society, Feb 4-8, 1996, pp 243-254.

41. Song, S.G; Shi, N; Gray III, G.T. and Roberts, J.A; "Reinforcement shape effects on the fracture behavior and ductility of particulate reinforced 6061-Al matrix composite", Metallurgical and materials transactions A, vol 27 A, Nov 1996, pp 3739-3746.

42. Watt, D. F.; Xu, X. Q.; Lloyd, D. J. Effects of particle morphology and spacing on the strain fields in a plastically deforming matrix. Acta Materialia (1996), 44(2), pp 789-99.

43. Brent V.chambers, Maxim L.Seleznev, James A.Cornie, Shiyu zhang, and mark A. Ryals; The strength and toughness of cast Al composites as a function of composition, heat treatment and particulate.Society of automotive engineers, 1996, pp107-111.

44. Bonollo, F.; Ceschini, L.; Garagnani, G. L. Mechanical and impact behavior of Al2O3)p/2014 and (Al2O3)p/6061 Al metal matrix composites in the 25-200□C range. Applied Composite Materials (1997), 4(3), pp173-185.

45. Davis, L. C.; Andres, C.; Allison, J. E. Microstructure and strengthening of metal matrix composites. Materials Science & Engineering, A: Structural Materials: Properties, Microstructure and Processing (1998), A249 (1-2), pp 40-45.

46. Jian Zhang; Yuqing Wang; Benlian Zhou, The influence of particle size on yield strength of metal matrix composites, transactions of the materials research society of Japan, 24(2), 1999, pp 141-144.

47. Long, S; Beffort, O; Banjour, C; "Microstructure and mechanical properties of a high volume fraction SiC particle reinforced AlCU4MgAg squeeze casting", materials science and engineering A 269, 1999, pp 175-185.

48. Hsu-Shen chu; Kuo-Shung Liu and Jien-Wei Yeh, Study of 6061 Al_2O_{3p} composite produced by reciprocating extrusion, Metallurgical and materials transactions A, Vol 31A, Oct, 2000, pp 2587-2595.

49. Park, B. G.; Crosky, A. G.; Hellier, A. K. Material characterization and mechanical properties of Al2O3-Al metal matrix composites. Journal of Materials Science (2001), 36(10), pp 2417-2426.

50. Qian, Lihe; Kobayashi, Toshiro; Toda, Hiroyuki; Goda, Takashi; Wang, Zhong-Guang. Dynamic Fracture toughness of a 6061 Al composite reinforced with SiC particles. Materials science and engineering A 318, 2001, pp 189-196.

51. Duwel, A.H.C; Mussert, K.M; Janssen, M.; Balkker, A; Van der Zwang, S; "A study on the fracture toughness of Al-based MMCs containing different volume factions Al_20_3", Journal of materials science letters, 20, 2001, pp1147-1150.

52. Xia, X; McQueen, H.J; Zhu, H; Fracture behaviour of particle reinforced metal matrix composites. Materials and processes manufacturing Engineering and design, Applied composite materials, 2002, 9(1), pp 17-31.

53. La Vecchia, G. M.; Badini, C.; Puppo, D.; D'Errico, F. Co-continuous Al/Al2O3 composite produced by liquid displacement reaction: Relationship between microstructure and mechanical behavior, Journal of Materials Science (2003), 38(17), pp 3567-3577.

54. Ceschini, L.; Morri, A.; Cocomazzi, R.; Troiani, E. Room and high temperature tensile tests on the AA6061/10vol.%Al2O3p and AA7005/20vol.%Al2O3p composites. Materialwissenschaft und Werkstofftechnik (2003), 34(4), pp 370-374

55. Prewo, Karl.M; "The impact of fibre and particulate reinforced MMCs, Proceedings conference on mechanical behavior of metal matrix composites", Dallas Texas, 1982, pp 181-194.

56. Vincent C, Nardone and James R.Strife; "NiAl-Based Microstructurally Toughened Composites", Metallurgical transactions A, vol 22 A, Jan 1991, pp183-189.

57. Geiger, A.L and Walker, J.A; Journal of met., 43, 1991, pp 8.

58. Hong, S. J.; Kao, P. W.; Chang, C. P. Microstructural development in aluminum-silicon carbide composites made by resistance sintering of mechanically alloyed powders. Materials Science & Engineering, A: Structural Materials: Properties, Microstructure and Processing (1992), A158 (2), pp 195-202.

59. Arsenault, R.J; Journal of composite technology research, 10, 1988, pp 140-145.

60. Shanker, K; Drew, R.A.L; Mavropoulos, L.T. and Tsantrizos, P.G; Composites, 23, 1992, pp 47.

61. Muscat, D; Shanker, K. and Drew, R.A.L. ; Materials science and technology, vol 8,1992, pp971.

62. Redsten, A.M; Klier; E.M; Brown, A.M; Dunand, D.C; Mechanical properties and microstructure of cast oxide-dispersion-strengthened aluminum, Materials Science & Engineering, A: Structural Materials: Properties, Microstructure and Processing (1995), A201, pp 88-102.

63. Zhou, Z; Peng, H X; Fan, Z; Li, D X; "Metal matrix composites with controlled non-uniform distribution of submicrometer (Al_20_3) particles in 6061 Al alloy matrix", Material selection and Technology, vol 16(7/8) July/Aug 2000, pp 908.

64. Qian, Lihe; Kobayashi, Toshiro; Toda, Hiroyuki; Goda, Takashi; Wang, Zhong-Guang. Fracture toughness of a 6061Al matrix composite reinforced with fine SiC particles. Materials Transactions (2002), 43(11), pp2838-2842.

65. Friend, C.M; "Impact response of short δ-alumina fibre/Al alloy metal matrix composites", Journal of materials science, 23, 1988, pp 1967-1975.

66. Roebuck, B; Gorley, T.A.E; McCartney, L.N; "Mechanical property test procedure for metal matrix composites", Materials science and technology, Feb. vol 1, 1989, pp105-117.

67. ASTM E 8m "Standard Test Methods for Tension Testing of Metallic Materials".

68. C1161-90 "Standard test method for flexural strength of advanced ceramics at ambient temperature".

69. Clyne, T.W; “Comprehensive composite materials, Vol 3, Metal Matrix Composites, 2000.

70. Rajeev kapoor, Kenneth S. Vechhio, Deformation behavior and failure mechanisms in particulate reinforced 6061 Al MMCs, Materials science and Engineering, A 202, 1995, pp 63-75.

71. Surasak Suranuntchai “A review of particulate reinforcement effects on its MMCs Deformation Behavior with Modeling Techniques”, pp 344-354.

72. Chingsten Li, F. Ellyin, Fatigue damage and its localization in particulate reinforcement MMCs, Materials science and Engineering, A 214, 1996, pp 115-121.

73. Evans, Robert David; Damage evolution and micromechanisms in a small-particle metal matrix composite, PhD Thesis, Queen's university at Kingston (Canada), 1999.

74. Al-Dheylan A. Khalid, The low velocity impact loading of Al_20_3/SiC whisker reinforced ceramic composite, Journal of Materials Processing Technology, 155-156, 2004, pp 1986-1994.

VITA

NAME: Syed Hafeez
DATE OF BIRTH: 9, August, 1979
PLACE OF BIRTH: Hyderabad, INDIA.
E-MAIL: syedhafeez_m@rediffmail.com

EDUCATIONAL QUALIFICATION:

M.S *(Mechanical Engineering)*
May 2005
King Fahd University of Petroleum and Minerals
Dhahran, Saudi Arabia.

B.E *(Mechanical Engineering)*
June 2001
Osmania University
Hyderabad, India.